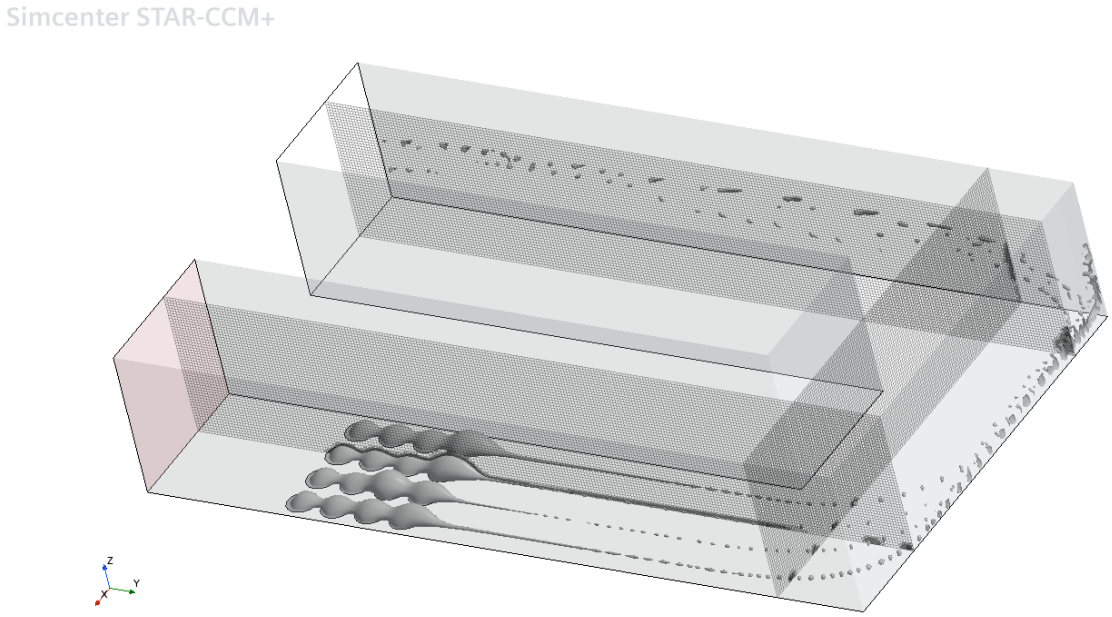

Water management in PEM Fuel Cells

A Numerical CFD Study using Volume-Of-Fluid (VOF) Method

Master's Thesis in Mechanics and Maritime Sciences (MMS)

Charan Kamal Vedula (MPSES)

Department of Mechanics and Maritime Sciences
Chalmers University of Technology
Gothenburg, Sweden

Chalmers University of Technology

MMSX30 Master's Thesis Report

Water management in PEM fuel cells

A Numerical Study

Authors:

Vedula, Charan Kamal
vedula@student.chalmers.se

May, 2024

MMSX30 Master's Thesis Report on Water Management in PEM fuel cells
A numerical study

Master's Thesis for the Master's Programme Sustainable Energy Systems
CHARAN KAMAL VEDULA

Supervisor: Konstantinos Konstantinidis, Department of Fluid Dynamics.
Examiner: Srdjan Sasic, Department of Fluid Dynamics.

Department of Mechanics and Maritime Sciences
M Building
Chalmers University of Technology
SE-412 96 Gothenburg
Telephone: +46 31 772 1000

Cover: Simulation result depicting the water flow pattern in the extended domain - modelled in StarCCM+

Department of Mechanics and Maritime Sciences
Gothenburg, Sweden 2024

Water Management in PEM Fuel cells
A numerical study
CHARAN KAMAL VEDULA
Department of Mechanics and Maritime Sciences
Chalmers University of Technology

Abstract

A fuel cell functions on the electrochemical principle of simultaneous reduction and oxidation (redox) reactions producing an electric current for powering devices. The fuel cell type under focus in this thesis work is of the Proton Exchange Membrane Fuel Cell or Polymer Electrolyte Membrane Fuel Cell (PEMFC) variety. In this type, hydrogen (H_2) is used as fuel with an air/oxygen (O_2) supply to produce electricity and water as products, making it a clean & sustainable source of energy with a plethora of applications.

This thesis work intends to understand the behaviour of the water product as it traverses across the flow channels designed to transport it away and out of the fuel cell by using the same oxygen supply (air) used as fuel. The level of water present in the electrolyte membrane and the bipolar plate flow channels in the fuel cell is extremely important to the performance of the fuel cell. Therefore, this management of the optimum hydration levels is fundamental to the optimal power performance. This region of focus in the study of PEMFC water management is an exciting avenue for research and possible optimization of hydration levels in the PEM fuel cell.

This thesis work utilizes existing literature to provide a valid simulation model as groundwork to elaborate on the same, due to the unpredictable nature of computer simulations. The simulation results from this thesis work is corroborated with the theoretical physical laws to validate the accuracy of the results.

Since the water product formed has to be taken away by air at a suitable to prevent both flooding and drying out of the fuel cell, the dynamics of the flow of the air and water phases in the flow channels assigned are dominated by complex physics. Since, the observation techniques are limiting in understanding the problem, the complexities and behaviour patterns must be studied with numerical simulations which model a flow which incorporates all the relevant factors in the flow of the constituent phases, their interactions, the physics of their interfaces and their movement behaviour in a region with transient flows at changing pressures and temperatures. These challenges can be effectively solved with the help of a CFD simulation. Therefore this thesis work utilizes the Volume Of Fluid (VOF) Method in simulating this two-phase problem for studying the phase interface and the scales of the problem at hand are within the range of this algorithm (both spatially and temporally), additionally investigating the effect of contact angles.

The results from the simulation show that the rate of the water transport across the channels is highly dependent on the inlet velocity of the air phase, the geometry and arrangement of the water inlet - pore size and number, and the relative humidity of the inlet air.

Keywords: Fuel Cells, PEM fuel cell, hydration levels, water management, flow channels, CFD simulations, VOF Method.

Acknowledgement

This thesis work would not be possible without the direct and indirect contributions of several people, towards whom I would like to express my heartfelt gratitude.

I would like to express my immense gratitude to my thesis supervisor, Konstantinos Konstantinidis for his ever present help, constant supervision, guidance and immense patience in times of continuous and innumerable setbacks which made me doubt myself, and without his support, this thesis work would not have come to fruition.

Secondly, I would like to wholeheartedly thank Prof. Srdjan Sasic, for being an exemplary teacher and providing me the opportunity to pursue this thesis which gave me an invaluable insight and knowledge into the workings of a fuel cell.

Next, I would like to profusely thank Chalmers University of Technology for providing the platform to make this project work of mine come to reality. In addition to the support, resources and academic networking, the environment provided by the university has helped tremendously in realizing this goal.

Lastly, I would like to thank my friends and family for being an unwavering pillar of support and motivation without whom I would not have been able to finish this thesis project.

Charan Kamal Vedula, Gothenburg, May 2024.

Preface

In this thesis study, the computer simulation of the multiphase flow of air and water in the flow channels of the bipolar plate in a Polymer Electrolyte Membrane or Proton Exchange Membrane (PEM) fuel cells is undertaken to investigate the factors that exert their influence on the rate of water transport across the flow channels as this is key in optimizing the hydration levels across the PEMFC. This thesis project was carried out with the resources and guidance from the Fluid Dynamics division at the Chalmers University of Technology for the purposes of the master's degree, part of the Department of Space, Earth and Environment (SEE).

This department works to further the understanding the physics behind fluid flow and undertakes research work for the same. The simulation models and their usage in studying the complexities of multiphase flow is one of the key aspects of research undertaken at the department. The results obtained from this thesis study aims to further the understanding and subsequent optimization of the water management in a PEM fuel cell.

Gothenburg, Sweden, May 2024
Charan Kamal Vedula

Contents

Nomenclature / Abbreviations

Abbreviation	Definition	Units
PEMFC	Proton Exchange Membrane Fuel Cell	-
FCEV	Fuel Cell Electric Vehicle	-
MEA	Membrane Electrode Assembly	-
PFSA	Per-fluorinated sulphonic Acid	-
PTFE	Poly-tetra-fluoro-ethylene	-
GDL	Gas Diffusion Layer	-
HOR	Hydrogen Oxidation Reaction	-
ORR	Oxygen Reduction Reaction	-
CFD	Computational Fluid Dynamics	-
MRI	Magnetic Resonance Imaging	-
M^2 model	Multi-phase Mixture model	-
LBM	Lattice Boltzmann Method	-
PNM	Pore-Network Method	-
LS method	Level Set Method	-
VOF	Volume Of Fluid Method	-
γ	Phase Indicator Function	-
α	Volume fraction	-
CFL	Courant Number	-
ρ	Density	kgm^{-3}
u	Velocity of interface	ms^{-1}
T	Stress Tensor	Nm^{-2} or Pa
g	Acceleration due to gravity	ms^{-2}
F_σ	Surface Tension Force	N
$F_{wall\ adhension}$	Wall Adhesion Force	N
σ	Surface Tension	Nm^{-1}
δ	Interface Delta Function	-
k	curvature of the interface	-
$\hat{n}$	normal to the interface	-
HRIC	High Resolution Interface Capturing	-
AMR	Adaptive Mesh Refinement	-
QUICK	Quadratic Upstream Interpolation for Convective Kinematics	-
θ_{CAH}	Contact Angle Hysteresis	$^\circ$
θ_F	Forward Contact Angle	$^\circ$
θ_R	Rear Contact Angle	$^\circ$
θ_C	Static Contact Angle	$^\circ$
ϕ	Relative Humidity	%
P_w	Partial Pressure of Water	Pa
P_{sat}	Saturated vapour pressure of water	Pa

Abbreviation	Definition	Units
V_c	Cell Voltage	V
V_r	Open Circuit Voltage (OCV)	V
$\bar{g}_f$	Gibbs Free Energy	J
F	Faraday constant	$C.mol^{-1}$
R	Universal Gas Constant	$JK^{-1}mol^{-1}$
A	Tafel Equation constant	-
i_o	Current Exchange Density	Am^{-2}
P_e	Power output of the fuel-cell stack	W
P_{exit}	Pressure at the channel exit	Pa
λ	Stoichiometric ratio of air supply	-
ψ	Coefficient relation b/w inlet air pressure and water pressure	-
$\dot{m}$	Mass flow rate	kgs^{-1}
r_{pore}	Pore radius	μm
N_{pore}	Pore number	-
v_a	Air Inlet Velocity	ms^{-1}
v_w	Water Inlet Velocity	ms^{-1}
LPT	Lagrangian Particle Tracking	-
CW	Channel Walls	-
AMI	Adaptive Mesh Interpolation	-
τ_t	Time of water transport	s
D_w	Distance travelled by the water droplet	μm
$v_{wf,avg}$	Average Water Film Velocity	ms^{-1}

List of Figures

List of Tables

Structure of the Thesis

The thesis is structured as follows and the multiple facets of the report addressed in each chapter can be found below:

Chapter 1 - Introduction and Background

This chapter, as the name suggests, introduces the reader to the technical background required to understand the work presented in the subsequent chapters. The aim and scope, along with the research questions has also been presented to provide an idea to the extent to which the problem has been studied.

Chapter 2 - Literature Review

This chapter consists of the previous research done in studying the problem and its various aspects, namely, the emergence of water in the gas channels, the behaviour and the factors affecting said behaviour. Then all of these sub aspects have been summarized to provide a picture as to the phenomenon that will be simulated in the subsequent chapters.

Chapter 3 - Methodology

This chapter focuses on breaking down the complex problem based on the literature reviewed. The assumptions and simplifications that have to be implemented to set up the simulation. The method used - the VOF Method and the sub-models used in setting up the initial and boundary conditions have also been discussed in detail. In addition, the approach in identifying the impact of individual parameters on the water transport has been assessed in a systematic manner to arrive at the results that would be discussed in the following chapter.

Chapter 4 - Results and Discussions

The results obtained from the computer simulations are presented here and the effects of each parameter in the order of significance based on their impact on the water emergence and behaviour are also displayed. The inferences based off of the results have been discussed for each and every parameter studied. Then the results were summarized and conclude. In addition to this, the limitations and the validity of the results have been presented to provide an idea about the validity of this thesis work. The potential for the possible pathways for future research work based on the results obtained has also been touched upon.

1 Introduction & Background

1.1 Fuel Cells

1.1.1 Basics

A fuel cell is an electrochemical device that converts chemical energy of its reactants into usable electricity by undergoing redox (reduction-oxidation) reactions at the electrodes. The most commonly used fuel source and oxidant are hydrogen and oxygen respectively, hence the name, hydrogen fuel cell. The underlying principle of a hydrogen fuel cell is utilizing the electric potential available on oxidation of hydrogen when the reactants are separated over an electrolyte producing a flow of electrons. The attractiveness of this technology lies in its emissions or lack thereof - water vapour. This sustainable energy source can run on several different kinds of electrochemical reactions based on the type of the electrolyte used in the cell. This leads to a plethora of different kinds of fuel cells. Out of all the varieties of electrolytes available today, the most commonly used type is an acid electrolyte. This is due to the fact that it is the simplest and easily commercialized variant of the fuel cell, because it was the first type of fuel cell to be manufactured and innovated to the commercialized version seen today[1] . The main focus of this study and document is the study of a Proton Exchange Membrane Fuel Cell or Polymer Electrolyte Membrane Fuel Cell (PEMFC) (see Figure 1). The explanation of its function is elaborated further in the sections below.

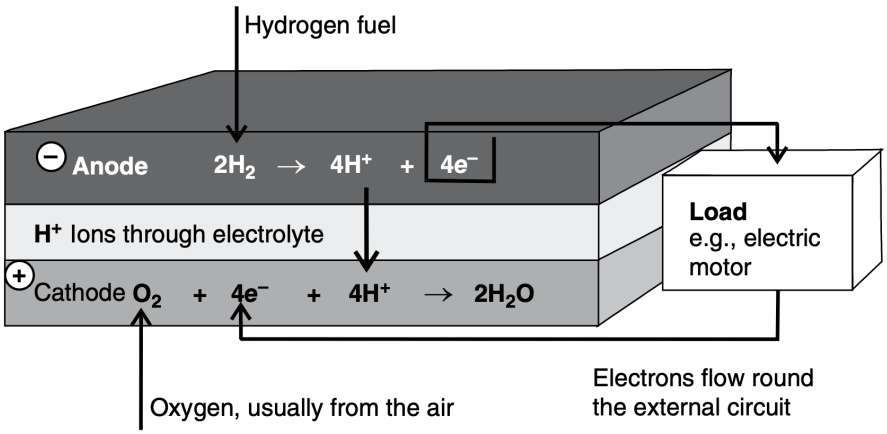

Figure 1: Schematic diagram of a working PEM fuel cell [2]

The redox chemical reaction that occurs in a PEMFC can be explained by demonstrating the oxidation and the reduction reactions that take place at the respective electrodes separately first and then combining them for the overall understanding :

Anode reaction:

At the negative electrode, i.e. the anode, hydrogen gas which is supplied from outside, gets oxidized in an exothermic reaction and releases electrons (e^-) along with hydrogen ions (H^+). The electrons (e^-) flow to the other electrode i.e. the cathode along an external circuit performing electric work. The hydrogen ions (H^+) or protons, flow to the cathode via the acid electrolyte. They form the basis of the electrochemical reaction in the fuel cell and their mobility determines the performance of the same. The equation for the oxidation of hydrogen is given below (see Equation 1):

$$2H_2 \longrightarrow 4H^+ + 4e^- + \Delta \tag{1}$$

Cathode reaction:

The hydrogen ions (H^+) and the electrons (e^-) take two different paths, via the acid electrolyte and the external circuit respectively and reach the cathode. Here, they interact with oxygen supplied either in the form of pure oxygen or from air and reduce the oxygen to form water as seen in the reaction below (see Equation 2):

$$O_2 + 4e^- + 4H^+ \longrightarrow 2H_2O \tag{2}$$

The combined redox electrochemical reaction can be equated as given below is as follows (see Equation 3):

$$2H_2 + O_2 \longrightarrow 2H_2O + \Delta \tag{3}$$

For the cell reaction to take place continuously, the electrons (e^-) and the hydrogen ions (H^+) must reach the cathode without interacting with one another along the way, this necessitates the need for the electrolyte to be electrically insulating but also be proton conducting. This leads to flow of only the hydrogen ions through the cell, facilitating the reduction reaction at the cathode of the cell.

The electrons (e^-) on the other hand, must pass through the external circuit, producing an electric current, due to the potential difference between the electrodes, which in turn, powers the necessary electrical devices.

The acid electrolyte, in addition to being electrically insulating, also has a high availability of free hydrogen ions (H^+). This feature of the electrolyte makes it easy for the hydrogen ions to pass through and reach the cathode where they recombine with the electrodes and the oxygen to complete the reaction and produce water.

However, it is not necessary for the electrolyte to be an acid, certain solid polymer membranes and ceramics can be used to achieve the same effect. They are termed as 'proton exchange membranes' or 'polymer electrolyte membranes' and the fuel cells that include them are called Proton Exchange Membrane Fuel Cells or Polymer Electrolyte Membrane Fuel Cells (PEMFCs).

Electrode Reaction Rates:

The oxidation reaction at the anode releases chemical energy as well as heat. However, the reaction does not proceed spontaneously but requires activation energy to excite the molecules sufficiently to kick-start the reaction. If the energy required for the process to begin is not sufficient, the rate of the reaction is slow. To overcome this, three steps can be undertaken namely:

1. **Utilize catalysts:** This is the most common method of improving reaction rates, however, the most commonly used catalyst in a PEMFC is platinum (Pt), which is expensive. Therefore, the dosage should be carefully monitored to avoid high costs.

2. **Increasing reaction temperature:** This method provides the necessary activation energy for the reaction, however, the operating temperatures play a key role in membrane longevity and fuel cell performance. The thermal integrity of the components should also be considered.

3. **Increasing electrode area:** Increasing the size (area) of the electrodes results in a higher probability of the molecules possessing sufficient energy to start the reaction, however, this method is constrained by the material cost as well as space considerations in transport applications in FCEVs (Fuel Cell Electric Vehicles). To overcome this problem, the electrodes are made porous. This significantly increases their effective surface area required for electrochemical reactions, without necessarily increasing the geometric area.

The Proton Exchange Membrane Fuel cell runs at relatively low temperatures (30 - 100 °C), this implies that the low reaction rates present are improved by the use of catalysts and porous electrodes. Platinum is the most favoured catalyst, although expensive, improvements made in material chemistry has reduced the impact on cost by utilizing minute quantities without affecting performance.

1.1.2 Proton Exchange Membrane Fuel Cells (PEMFCs)

The Proton Exchange Membrane Fuel Cell or Polymer Electrolyte Membrane Fuel Cell is the most successful type of acid fuel cell commercially. The electrolyte used is a hydrogen-ion/proton conducting solid polymer. It is an electric insulator but an ionic conductor and is stable under both strong oxidizing and reducing environments.

The negative electrode - anode - contains an electro-catalyst that is dispersed on a electrically conducting material. It is fabricated in such a fashion that the three-phase boundary of the catalyst, the electrolyte and the fuel (hydrogen gas) come in contact with each other to facilitate the oxidation reaction.

The positive electrode - cathode - is also dispersed with an electro-catalyst, also creates a three-phase boundary at which the incoming oxygen (either pure oxygen or in air) is reduced in the presence of the electrons from the external circuit.

The negative electrode (anode) - the electrolyte (polymer membrane) - the positive electrode (cathode) together are considered to be a singular component called the membrane electrode assembly (MEA). They are considered to be the main component in making up a cell. The voltage output across a single cell is approximately 1.1V (theoretical) and in reality, about 0.7V. This voltage is too little to have viable applications. Therefore, the voltage has to be built up by connecting the cells in series to the required output voltage. The series of the membrane electrode assemblies bound together electrically is called a stack. The stack also includes current-collectors at the two ends connected by end plate assemblies.

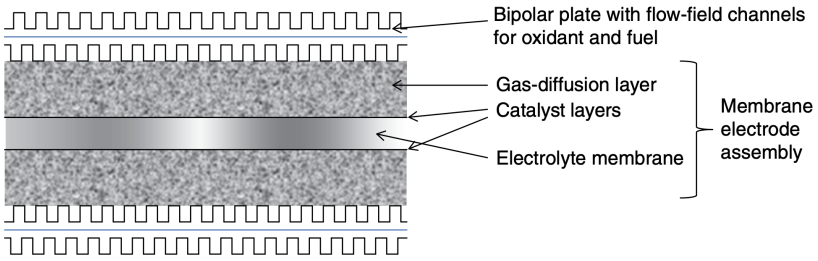

Figure 2: Schematic diagram of the MEA and the bipolar plates [3]

The individual cell assemblies are electrically interconnected via a 'bipolar plate' (see Figure 2). It is an electrically conducting plate the joins the positive electrode (cathode) of one cell to the negative electrode (anode) of the next cell. After the MEA, it is one of the most important components of a fuel cell. It is due to the fact that it also provides a means of providing the reactants to their respective electrodes - hydrogen fuel to the anode and the oxygen gas to the cathode. This is done by using machined or moulded channels on either side of the bipolar plate. The bipolar plate also facilitates the removal of the product water formed at the reduction reaction site on the cathode.

The contact points between the individual cells have to be optimized in order to reduce the electrical resistance between the plates. Therefore, the contact points on the bipolar plates should be large. However, this would hinder adequate gas flow over the electrodes from the channels.

In addition to this, the electrodes must be porous to allow a greater surface area for reaction, there is a strong possibility of gas leakage along the edges of the plates. This is overcome by the use of external manifolds to seal the edges. However, this leads to cooling problems and uneven pressures in the fuel cell.

Therefore, it is a balancing act between maintaining good gas supply and product removal, temperature and pressure maintenance and low electrical resistance. The design of the bipolar plates is therefore of critical importance in the performance of the fuel cell.

The flow behaviour of product water through the flow channels and out of the fuel cell plays a crucial role in the working of a fuel cell and is discussed in the following chapters. The water flow behaviour through the bipolar plate flow channels is the key focus of this study.

1.1.3 Polymer Electrolyte

Proton Exchange Membrane Fuel Cells (PEMFCs) uses a solid sheet of electrolyte that is bound on both sides by catalyzed porous electrodes, forming the Membrane Electrode Assembly (MEA). The main charge carrier in the polymer electrolyte is an $H^(+)$ ion (a proton), and works the same way as an acid would - conducting the $H^(+)$ ions through it. The membrane electrolyte works at near ambient conditions therefore, the water movement through the cell is in liquid form and the water level in the membrane directly affects the proton conductivity.

The industry standard membrane used in PEMFCs, is a certain kind of perfluorinated sulphonic acid (PFSA) called "Nafion®" It is built on the backbone made of polymerized version of polyethylene (see Figure 3).

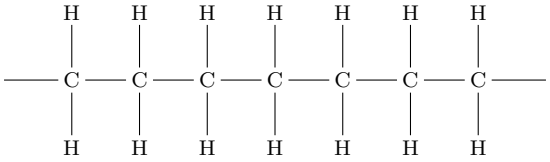

Figure 3: Polyethylene chemical structure [4]

The polyethylene is substituted chemically with fluorine to form poly-tetra-fluoro-ethylene (PTFE) (see Figure 4). This makes the polymer extremely resistant to chemical attack due to the strong bonds between the carbon and fluorine atoms. In addition to this, PTFE is hydrophobic and helps driving the product water out of the electrolyte and prevents flooding. It also adds some mechanical rigidity to the material making it able to withstand mechanical stresses and suitable for use in stacks which are thousands of cells thick.

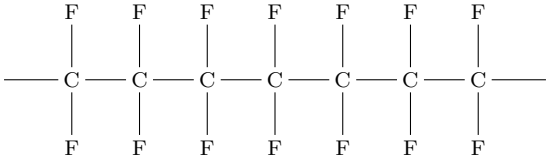

Figure 4: Poly-terta-fluoro-ethylene (PTFE) chemical structure [5]

To make it ion-conducting, the PTFE chain undergoes further chemical modification in the process of sulfonation. In this process the PTFE molecular backbone receives side chains and these side chains to the main PTFE backbone are terminated with sulfonic acid ($-SO_3H$) groups. This compound is now known as perfluoro-sulphonic acid PTFE copolymer (PFSA) (see Figure 5) The acidic form of the $-SO_3H$ ions (after treatment with concentrated sulfuric acid) becomes an (SO_3^-) ion which makes the side chains highly hydrophilic. Therefore, Nafion has a several hydrophilic regions in an overall hydrophobic structure.

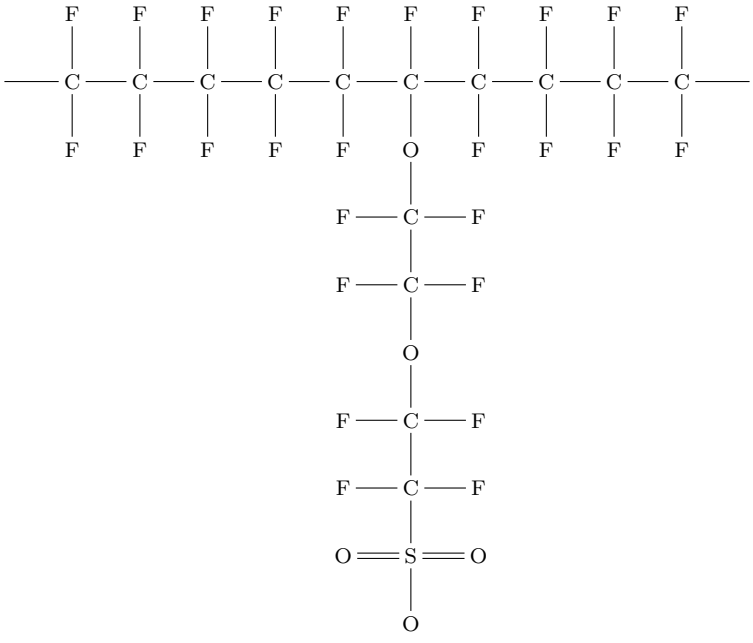

Figure 5: Perfluoro-sulphonic acid PTFE copolymer (PFSA) chemical structure [6]

These hydrophilic regions lead to absorption of significant amount of water providing a platform for the H^+ ions produced on the oxidation reaction at the anode to interact with the SO_3^- ions due to weak mutual attraction, making them mobile and move across the electrolyte via electro-osmotic drag and the Grotthus mechanism.[14]

The ionic conductivity of these H^+ ions depends strongly on the degree of hydration and the concentration of the sulphonic acid sites. Therefore, maintaining the hydration levels is crucial in maintaining the optimum ionic conductivity of the membrane.

1.1.4 Gas Diffusion Layer (Electrodes)

In an electrolyte cell, the other critical component required for it to function is the electrodes - the anode and the cathode. In a PEMFC, they are called the Gas Diffusion Layer, as they are made of porous carbon supports, dispersed with catalyst, usually platinum (Pt). It provides the necessary conditions for the three phase boundary of the reactants, the catalyst and the electrolyte promoting good reaction rates at both the anode and the cathode. The basic structure of both the electrodes in various designs of PEMFCs are very similar, if not identical.

The Gas Diffusion Layer is attached to the bulk of the electrolyte - the polymer membrane in this case, which has carbon supports holding the platinum catalyst. Attached to this carbon support/catalyst layer is the diffusion layer - usually made up of porous carbon fibres. These carbon fibres not only hold the dispersed Pt catalyst particles, they are also good conductors of electricity, allowing for high amounts of current to be drawn.

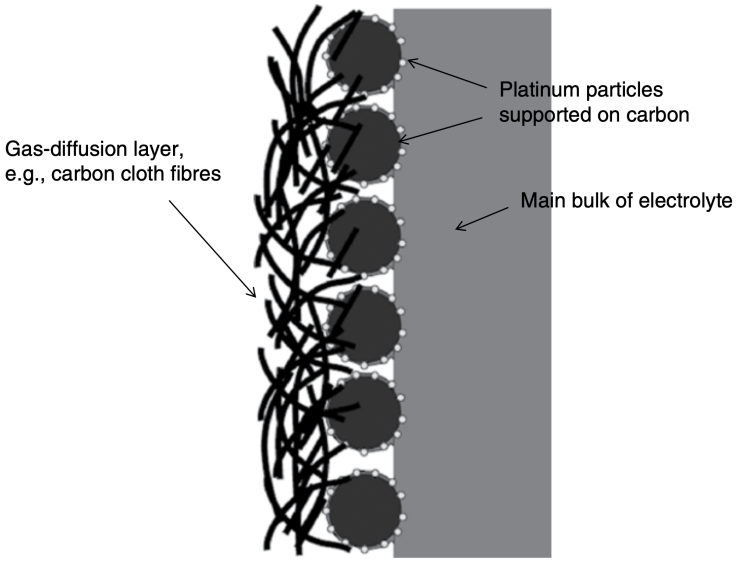

Figure 6: Schematic diagram of the polymer electrode and the GDL [7]

Not only does the GDL provide a platform and reaction sites for the redox reactions, it also is connected to the flow channels on the bipolar plate on the outside, providing a pathway for the fuel (hydrogen) and oxygen to diffuse through and reach the catalyst layers at their respective electrode sites to undergo their respective reactions (see Figure 2).

The GDL also carries the water product away from the membrane electrolyte surface and offers a layer of protection over the thin catalyst layer. The catalyst being supported on the carbon structure, as seen in Figure 6, not only has the electrolyte bulk mass on one side, but also has a thin layer impregnated onto the electrode. This extension of the electrolyte onto the GDL, increases the number of sites where the electrolyte and the catalyst particles meet, improving the number of sites where the three phase boundary can exist, improving the catalyst activity, subsequently improving the reaction rates.

Despite the electrodes having similar structure when it comes to the shape and size of the carbon fibre material, which is used on both sides, the primary difference between the cathode electrode and the anode electrode lie in the amount of catalyst dispersed in the GDL catalyst layer next to the electrolyte membrane. This is due to the fact that the reaction rates for the hydrogen oxidation reaction (HOR) and the oxygen reduction reaction (ORR) are vastly different, with the rate of the oxygen reduction reaction being significantly lower than the rate of the hydrogen oxidation reaction. The exchange-current density, which describes the current that can be generated based on the reaction at the electrodes, and the exchange-current density at the cathode ($10^{-3}\ mA\ cm^{-2}$) (O_2) is about three orders of magnitude lesser than the exchange-current density at the anode ($1\ mA\ cm^{-2}$)(H_2) . In addition to this, the voltage loss at the cathode is one order of magnitude greater than at the anode.

Due to these reasons, the platinum loading at the oxygen electrode (cathode) is significantly higher than at the fuel electrode (anode).

The main focus of this study would be on the cathode side of the reaction - particularly on the removal of the water produced from the gas diffusion layer. From Figure 6, we can see that the platinum catalyst particles attached onto the carbon support adhered to the electrolyte provides a location for the three phase reaction. These are the only sites where the catalyst is in contact with both the electrolyte and the incoming gas. The Gas Diffusion Layer on the cathode side, being hydrophobic causes the water produced from the catalytic reaction to diffuse out. This water will be collected in the channels on the bipolar plate and will be removed at the rate required for optimal cell performance.

1.1.5 Water Management

In a Proton Exchange Membrane Fuel Cell in addition to the design, and the catalyst concentrations in the electrodes, the hydration levels in the electrolyte is of paramount importance. As previously mentioned, the chemistry of the electrolyte polymer membrane is made up of side chains of sulphonic acid groups (SO_3^- added onto a backbone of poly-tetra-fluoro-ethylene (PTFE) making it a perfluorinated sulphonic acid (PFSA) copolymer. This special compound has a specific property of being generally hydrophobic in nature, with the side chains being hydrophilic. These hydrophilic side chains create micro-domains inside the general structure which attract water molecules.

The presence of water inside the polymer electrolyte leads to the formation of hydronium ions (H_3O^+) on combining with the hydrogen ions (H^+) forming a dilute acid. This acidic environment is precisely what is needed for the transport of the hydrogen ions (H^+). This takes place due to the migration of both the hydronium ions (H_3O^+) and via the hopping of the hydrogen ions (H^+) from one water cluster to the other by breaking the weak hydrogen bond from one molecule and forming another weak bond to the next bond. This process is known as the Grotthus mechanism and has been accounted for the

high ionic conductivity of the hydrogen ions (H^+) experimentally. Therefore, the ionic conductivity of the Nafion polymer membrane depends on the level of hydration present in it.

Therefore, the PFSA membranes are very good proton conductors when they are sufficiently hydrated. However, due to the operating temperatures of the PEMFC lie within $80°C$ to 100 $°C$, the liquid water present in the membrane has a tendency to evaporate at these temperatures. If the hydration levels of the membrane are below optimal, i.e. the membrane getting dried out, the ionic conductivity drops, which leads to a severe drop in the performance. So, sufficient hydration levels must be maintained at any cost.

On the other hand, if the hydration levels are above the optimum levels, this leads to the flooding of the membrane with water, which leads to the formation of a two-phase gas-liquid flow with oxygen/air and water that increases the resistance to the transport of the reactants at the active sites, reducing the effectiveness of the catalyst, as the reactants have difficulties reaching the three-boundary reaction sites and therefore, making the electrochemical reactions improbable. This leads to a drastic reduction in the performance of the fuel cell.

So, effective hydration levels in the electrolyte membrane must be maintained at all costs for effective electrochemical redox reactions, to promote good movement of the protons across the electrolyte without hindrances and also to prevent interference of the two-phase flow from interfering with the reactants at their respective reaction sites. Therefore, it is important to maintain the right balance - sufficient enough for good proton conductivity but lower than the level that would cause flooding. Therefore, the water removal rates must be optimal at the GDL on the cathode side.

In an ideally designed PEMFC, the water that forms as the product of the electrochemical reaction (see Equation 3), helps keep the ideal level of hydration throughout the electrolyte. The air that is pumped over the cathode electrode, in addition to supplying the necessary amount of oxygen also carries away the excess water with it. Therefore, the design has to take into account the right amount of oxygen necessary for the optimal reaction rates as well as the water it can remove along with it after the reduction reaction is complete.

The design also should take into the operating temperature of the fuel cell as at temperatures above 60 $°C$, the air flowing through the cathode has a high drying effect which leads to the membrane drying out because the air dries out the water faster than the rate at which it is produced from the oxygen reduction reaction (ORR) at the cathode, this leads to a drop in performance, owing to the membrane drying out. To overcome this, the air flowing into the cathode must be pre-hydrated [37] to reduce the drying effect at high temperatures. This may appear to be counter-productive as it leads to formation of excess water by-product in the cell, but it is necessary to maintain the hydration levels and to improve the performance of the fuel cell.

1.1.6 Water Movement in PEMFCs

As mentioned in the previous section, maintaining the optimum hydration levels in the PEMFC is of utmost importance, if the maximum performance and longevity of the fuel cell is desired. To maintain the ideal water levels in the electrolyte and the surrounding electrodes, the behaviour of the water molecules must be understood. There are several

water movement mechanisms that take place simultaneously in the membrane electrode assembly, essentially the crux of the fuel cell. These water movement mechanisms as seen in Figure 7 can help us identify the problems some of these movements pose to the optimum performance of the fuel cell and the actions taken to optimize said performance.

Firstly, the high availability of hydrogen ions (H^+) present in the electrolyte during the cell operation, drag water molecules along with them from the anode electrode side to the cathode electrode side via a process called electro-osmotic drag. This leads to a higher concentration of water on the cathode side compared to the anode side, which tends to dry out the anode part of the cell during this process. This imbalance provides ionic resistance at the anode and results in a drop in the transport rates of hydrogen ions (H^+) towards the cathode.

Secondly, at temperatures above 60 $^\circ C$, as previously mentioned, the air flowing across the cathode electrode has a high drying capacity and tends to carry away water much faster than that can be replaced by the water formed by the slow reaction rates of the oxygen reduction reaction. This also tends to reduce the hydration levels at the electrolyte, affecting cell performance.

Thirdly, this mechanism is a result of both the electro-osmotic drag and the formation of product water at the cathode. The water content at the cathode is significantly higher due to said mechanisms. Due to concentration imbalances between the cathode and the anode, the water tends to flow back from the cathode towards the anode i.e. from a region of high concentration to a region of low concentration in order to reach equilibrium. This mechanism tends to keep the electrolyte membrane uniformly hydrated.

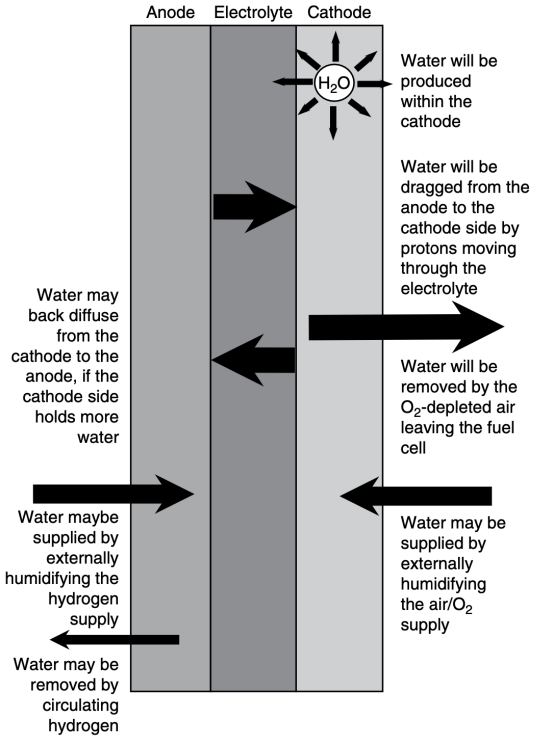

Figure 7: Water movement mechanisms in a PEM fuel cell [8]

To achieve optimum ionic conductivity, the hydration levels in the electrolyte must be

uniform, but due to the all the simultaneous water mechanisms taking place, the hydration levels in the electrolyte is far from uniform.

To improve the uniformity of the hydration levels in the membrane electrode assembly, one or both of the reactants must be pre-hydrated. Due to the effect of the electro-osmotic drag, the anode side of the electrolyte tends to dry out. To avoid this, the hydrogen supplied has to be hydrated to keep the anode side of the electrolyte sufficiently hydrated and to aid the ionic conductivity of the hydrogen ions (H^+).

To counter the drying effect of air at higher temperatures (compared to the air inlet), the water formation at the cathode due to the oxygen reduction reaction is not sufficient, and therefore must be supplemented by additional means, i.e. pre humidification of the incoming oxygen/air. This reduces the drying effect of the incoming air, as the higher humidity levels already present reduce the water holding capacity of the air and therefore not lead to a dry membrane on the cathode side.

These methods help equalize the hydration levels inside the electrolyte across both the cathode and the anode side.

Improper water management in the electrolyte assembly can lead to several negative effects on both the cell performance and the longevity of the fuel cell. Firstly, the differences in hydration levels can lead to swelling in the regions with excess water content, causing additional internal stresses that threaten the structural integrity of the fuel cell assembly can rapidly deteriorate the electrolyte and the catalyst layers, reducing both the performance and the lifetime of the fuel cell.

Secondly, if the water product is not removed out from the stack assembly, this can lead to the accumulation of water-soluble ionic species, like calcium (Ca^{2+}), magnesium (Mg^{2+}), iron (Fe^{2+} or Fe^{3+}). They interfere with the existing electro-chemistry of the cell, creating resistance to the flow of hydrogen ions (H^+) which is absolutely critical to optimum cell performance.

Lastly, the excess water present in the electrolyte membrane, under sub-zero temperatures can freeze and permanently damage the fuel cell stack. So, it is absolutely essential to purge the fuel cell stack of any existing water before shut down to prevent occurences of freeze-out damage.

Therefore, it is important to maintain optimum hydration levels, not just for optimum ionic conductivity and cell performance, but also to prevent the degradation to the membrane electrode assembly. Water generation, management and removal are fundamental to the optimum cell performance and good membrane health of the fuel cell.

There are places in the electrolyte that are dried out, some that are flooded and some possessing the right amount of hydration. This leads to reduced performance of the fuel cell. This is also one of the key problems that needs to be addressed and overcome in order to have optimum hydration levels, and subsequently optimum performance. In this study, the focus would be on the excess water removal mechanism via the bipolar plate channels after exiting from the gas diffusion layers. The effects of the design of the bipolar plate plays a huge role in water removal in PEMFC. The basic designs are described briefly in the next subsection.

1.1.7 Flow field patterns of the bipolar plates

As previously mentioned, the water levels present in the fuel cell must be maintained uniformly throughout the membranes for optimum ionic conductivity, which is directly proportional to the voltage levels across the stack electrodes. The need to ensure proper hydration levels along with the proper flow of reactants to and from the gas diffusion layer (GDL), with minimum pressure drop across the layers, are the main factors inspiring the design of the flow-field plates.

The main types of the flow-field patterns utilized for the bipolar plates are:

1. Parallel groove type
2. Pin or grid type
3. Interdigitated type
4. Serpentine type

The effect of each flow-field on the cell performance is dependent on the type of fluid flow taking place on either side of the membrane electrode assembly (MEA) - either co-flow, cross-flow or counter-flow. The type of flows described, have different flow velocities, which in turn affect the rate of reactant flow towards the GDL, and the rate of the product removal from the GDL. They also have different drops in pressure across the layers. All these factor influence cell performance and to whether involve extra pieces of equipment like compressors to achieve the desired flow conditions. Therefore, the design of the flow-field plates is a deciding factor in the operation of the fuel cell.

The main types of the flow-field arrangements have been illustrated in the figure given below (see Figure 8):

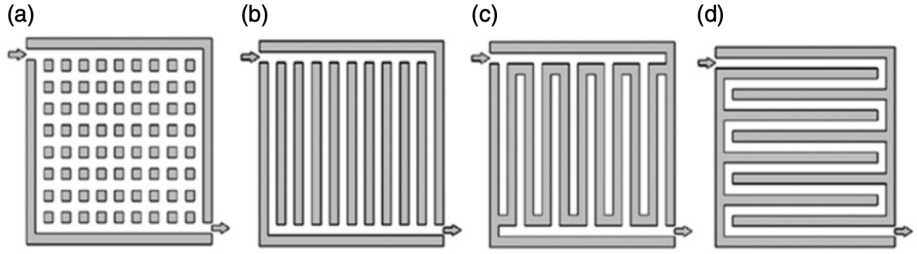

Figure 8: Different arrangements of the flow field channels - (L to R) pin type, parallel, interdigitated, serpentine [9]

The **parallel groove** type flow-field arrangement is used in conditions where there is a minimal likelihood of water droplet formation, due to a higher tendency for accumulation and subsequent blockage, which leads to a poor distribution of the reactants which in turn leads to a poor distribution of electric current through the fuel cell. This can be offset by restricting this flow-field type usage only for applications where high fluid flows are possible, as this minimizes droplet formation.

The **pin or grid** type flow-field arrangement allows for high turbulent flows across the face of the electrode improving the utilization of the fuel and oxygen reactants. Due to this

ability of the pin type flow-field, it is perfectly suited for applications that require high reactant flows and have low fuel (hydrogen) and air (oxygen) utilization rates.

The **interdigitated** type flow-field arrangement features dead-ended channels forcing gases through the gas diffusion layer (GDL). On the anode side, the reactant gas is forced into the GDL layer to interact with the membrane. To ensure the correct amount of fuel (hydrogen) passes into the membrane for the catalyst reaction, the gas diffusion layer (GDL) must be highly porous. On the other end, i.e the cathode side, the water must be drained out of the cathode, for this to take place, the GDL must also possess high hydrophobicity to push the water out of the cell. If these properties of the GDL are not fulfilled, the interdigitated type will pose the threat of becoming a bottle-neck to cell performance. As, the porosity and the hydrophobicity of the gas diffusion layer tends to decrease as the cell ages, this type of flow-field arrangement is not usually preferred.

The **serpentine** type flow-field arrangement is the most commonly used type by PEM fuel cell manufacturers. It strikes a balance between good water removal rates and acceptable pressure drop. The large number of turns in the flow path ensure that the water removal is not too high as to cause dry-outs, and the multiple serpentine passages ensures that the water velocity is maintained so as to have the required pressure drop.

The material used for the bipolar plate channels also plays a crucial role because the hydrophobicity/hydrophilicity of the material dictates the surface tension contact angles and also the tendency of the water produced to form droplets and subsequently, the kind of flow of the two phase water-air mixture in the bipolar plate flow channels. This is extremely important in modelling and studying the water removal process and to find an optimum rate of water removal. There are several more factors that influence water removal via the channels and that would be elaborated in the subsequent sections.

The fluid flow behaviour in the flow-field channels of the bipolar plate is not easy to predict or measure due to the complexity of the two-phase turbulent of water and air. Significant studies using fluid flow finite-element methods have been done to model the fluid flow behaviour and to validate and optimize the design efficacy.

1.2 Computational Fluid Dynamics (CFD) Simulations

The need to understand the physics of water formation and water flow behaviour in the two-phase mixture when exiting the gas diffusion layer (GDL) through the flow-field channels in the bipolar plate is paramount in understanding and furthering the cell performance of a PEM fuel cell. To understand and theorize a complex physical phenomenon, one does it either by observation or via simulation tools and validate the results with experimental data.

In the case of studying the turbulent two-phase flow of the water and air mixture in the flow-field channels, visualization techniques are very limited and therefore do not provide an accurate picture of the physical phenomenon taking place.

In the case of optical visualization, though it provides good accuracy in terms of resolution in both the spatial and temporal dimensions, the PEM fuel cell made for this purpose must be restricted to be constructed out of transparent materials, which for obvious reasons possess vastly different properties in terms of porosity, ionic conductivity, catalyst holding capacity and hydrophobicity/hydrophilicity, structural integrity and such when compared to the PEM fuel cells used in practice.

If the different regions in the electromagnetic spectrum were to be used for observing the phenomenon, such as in the case of X-ray imaging, MRI or neutron imaging, the constraint of constructing a transparent PEM fuel cell is lifted, but they still would have to be fabricated out of materials that are different from the materials used in a working PEM fuel cell. Even, if the material is not as vastly different from the working models as in the case of a transparent PEM fuel cell, the resolution in both the spatial and temporal dimensions is not very accurate to provide a good picture.

In addition to the existing limitations due to the choice of materials in both the optical visualization techniques and in the others, the visualization techniques used do not provide the necessary quantitative information to understand the behaviour completely. For example, the visualization techniques provide no useful information on the volume fraction of the water present in the two-phase mixture or on the coverage ratio of the water in the gas diffusion layer (GDL) both of which determine cell performance.

Due to the inaccuracies resulting from observation (visualization techniques), the behaviour of the two-phase flow can be studied only via simulation. Although the results from experimental results are valid, they do not explain the minutiae of the behaviour processes and the parameters affecting cell performance. So, to understand the fine details like droplet formation, the volume fraction of water, the flow characteristics, regions of laminar flow (if any), the experimental data has to be supplemented with computer simulations. The computational models provide insight into flow characteristics and behaviour in an actual fuel cell, due to no restraints related to material properties and visualization limitations. In addition, simulations also have the ability to test multiple designs to optimize behaviour models.

However, computational models are only as good as the designer's understanding and model choices. Therefore, the experimental verification needs to be done to validate the accuracy of the model. To ensure that the model simulates the physical phenomenon reflecting the actual working of the fuel cell instead of just providing apparently important data which has no basis in reality.

This study focuses on the simulation aspect of the two-phase flow behaviour and dynamics in the flow-field channels of a bipolar plate in a PEM fuel cell, taking in initial conditions that are within the acceptable range of values that have been experimentally verified. The results from the simulation are then compared to actual values that have been established in literature after extensive experimentation to verify the validity of the simulation model. This report only includes the simulation setup, results and post-processing and comparisons with the experimental data found in literature to ascertain its validity in reflecting the physical phenomena in reality.

1.2.1 CFD modelling approach

The two-phase turbulent flow of water and air in the PEM fuel cell bipolar plate flow-field channels is a two-pronged problem with one aspect of it being the concern of the liquid water formation and movement in the gas diffusion layer **before** it reaches the bipolar plate and the second aspect being the transport of the said flow **in** the flow-field channels in the bipolar plate. Historically, the first aspect was under more study and scrutiny while the second has been largely ignored.

The two-phase flow modelling approaches in the early days made use of the multi-phase mixture (M^2) model and the multi-fluid model. The M^2 **model** included the saturation levels of water as a function of the volume fraction of the water present[15]. It did not have two separate phases for water and air, but instead considered them to be a single phase with varying composition of water and air. The multiphase flow was defined on the basis of the mass-averaged velocity of water and air. Simply put, the model converted the two-phase flow into a single phase flow and differentiated the two phases by using mass and volume fraction.

The **multi-fluid model** on the other had, did not simplify the two-phase problem, but instead provided each phase with a complete set of equations based on the laws of conservation of mass, momentum and energy. However, in modelling criteria, this is not sufficient, as the two phases do not exist independent of each other and instead interact with each other. To acknowledge this interaction between the phases, the multi-fluid model utilized a coupling of the saturation state as a parameter to link the two phases.

The two early models described above (M^2 model and the multi-fluid model) had the advantage of predicting the exact amount of the liquid water formed and its location in the fuel cell stack, this led to studying their influence on fuel cell performance. However, these models were not perfect in providing a complete understanding of the water behaviour in as such they had a drawback in their inability to identify the physical state of the water present in the mixture - they could not identify whether the water quantity present was in the form of droplets or a film. These states have vastly different flow behaviour and mass transfer rates. In addition to the absence of concrete data on the physical state of the water, the film layer data was incomplete as in the concentration of the layer and distribution across the gas diffusion layer was unknown. Due to the aforementioned shortcomings, the early models could not describe the initial behaviour of water behaviour and the transport in the gas diffusion layer, leaving the models incomplete and requiring researchers to search for better models for a more complete and accurate understanding.

To overcome these roadblocks on the way to a more understanding of the two-phase problem, the interface between the two phases had to be tracked via algorithms. The identification of the interface of the phases indirectly identifies the size and the shape of

the water present in the gas diffusion layers. By identifying the interface or boundary between the phases gives an accurate outline the water physical state, as only one phase can exist in a given physical space. The algorithms help us visualize the phases based on the location of the interface. This also leads to identifying the flow behaviour accurately as the phases have different flow properties, owing to the differences in their density, mass flow rate and viscosity. Therefore, they are critical to the understanding of the formation and the motion of liquid water in the gas channels.

The availability of multiple tracking algorithms that can be employed for tracking the interface between the phases does not simplify the problem, as there is no one-size-fits-all solution when it comes to employing tracking algorithms. The tracking algorithms used are optimized for the scale of the problem. The scales present are - **microscopic**, **mesoscopic**, and **macroscopic** scales. They are based on the physical and temporal dimensions the flow and its study takes place at. The scale determines whether the particles are considered to be discrete i.e. individual particles or as a part of a continuum i.e. the particles are considered to be members of the "bulk". The properties exhibited by the particles at different scales are different due, to the fundamental definition of what consists a particle. The theories used to describe the behaviour of the particles at different scales are different owing to the predominant forces exerted by the particles at those scales. Quantum mechanics and molecular dynamics describe the particle behaviours at the microscopic scale and the kinetic theory and continuum mechanics at the mesoscopic and the macroscopic scales respectively. Therefore, the need to identify the scale of the flow is important in identifying the level of detail required to model the flow behaviour and its understanding.

The most commonly used algorithms in CFD simulations are the **Lattice Boltzmann Method (LBM)**, the **Pore-Network Method (PN)**, the **Level - Set Method (LS)** and the **Volume of Fluid Method (VOF)**.

Out of these available tracking algorithms, the constraints with the choice of scale of the model under study limits the choices. In this case, the **Lattice Boltzmann Method (LBM)** and the **Pore-Network Method (PN)** cannot be used for the macroscopic scales that the two-phase flow in the channels takes place in. These models are very effective in both the microscopic and the mesoscopic scales but not for the macroscopic scale the flow behaviour and transport takes place in. The Level Set Method (LS) and the Volume Of Fluid Method (VOF) are much more suited to this scale.

The **Level Set Method (LS)** is simpler to implement and manages the complex interfaces between the two different phases in the problem by simplifying it. The problem with simplifying complex behaviour into simple models is the fact that there is always some assumptions to be made and some information being ignored and consequently, lost. The drawback of this simplification in the Level Set Method (LS) is that it leads to mass conservation problems and this leads to a deviation from the laws of natural physics as mass needs to be conserved at all costs. To overcome this additional convoluted and complex corrections are necessary to close the equations and make it reflect and validate the physical phenomenon.

This problem with the conservation of mass does not arise when the **Volume Of Fluid Method (VOF)** is implemented as this model is built on the principles of conservation of mass. This model approaches the problem by not tracking fluid (water) volume directly, but instead tracking the volume fraction of the fluid (α) throughout the entire computational domain. This indirectly gives the model to track and handle complex interfaces

between the phases in terms of the varying levels of volume fraction of the phases. It has the ability to simulate the flow of two immiscible fluids - water and air/oxygen in this case by solving a single set of momentum equations, instead of two because the other phase can be extrapolated by its absence, which can be known by the function of the volume fraction of the other phase. The volume fraction function effectively identifies the interface with the help of the said volume fraction function.

In other words, the volume fraction of a certain phase is defined by a value as either one or zero, and on a computational grid, any value in between describes the area occupied by that defined phase, which in turn helps us reconstruct the interface to an accurate degree. The level of accuracy of the reconstruction depends on other factors such as the size of the computational cell of the model and the computational resource available to process the simulation. It is painfully obvious that the smaller the computational cell is, the behaviour is described with a degree of high resolution and high accuracy. However, due to the size of the small computational cell, the number of the cells in the computational domain increases, and the same equations need to be solved many more times to get the complete picture. This leads to requiring higher processing power and computational demands in order to arrive at a solution from the simulation in a reasonable time.

1.2.2 Volume Of Fluid Method (VOF)

The Volume Of Fluid Method (VOF) is an Eulerian method based tracking algorithm that captures the interface implicitly on a stationary computational grid with the use of a phase indicator function - volume fraction (an Eulerian model tracks the properties of the fluid passing through a control volume).

The presence of the interface determines the shape and the flow of the water particles, therefore the phase interface is critical in understanding the flow behaviour. In the VOF method, the use of a phase indicator function implicitly calculates the interface based on the value of the said function. The phase indicator function indirectly describes the location of the interface based on the amount of volume occupied by the phase. If the value of the phase indicator function (γ) has been chosen to be equal to 1 for a phase 1 (say water), then it means that the control volume is filled only with phase 1, i.e. water. If the control volume is absent of water, i.e. filled completely with phase 2, i.e. air/oxygen, then the phase indicator function (γ) has a value of 0. If the value of the phase indicator function lies between 0 and 1, it means that the volume is not completely filled with water, i.e. an interface of water and air is present. The value of γ showcases the percentage of the control volume that is filled with water (phase 1). As seen in the table below (see Table 1), the phase indicator function reduces the presence of the interface into a single numerical value.

Phase indicator function value (γ)	**Meaning**
$\gamma = 1$	Control volume is filled with only phase 1
$\gamma = 0$	Control volume is absent of phase 1
$0 < \gamma < 1$	Interface between the phases is present

Table 1: Interface identification with the phase indicator function

The phase indicator function is dependent on the volume fraction in the Volume Of Fluid Method (VOF), the Eulerian technique on which it is based on tracks the control volume,

in this case, the control volume of each computational cell and in turn, the whole computational domain. The percentage of the fluid occupied by the phase in the cell, gives us a rough estimate of the interface between the phase, therefore the size of the computational cell is important in order to get a high resolution picture of the interface. In the figure given below, (see Figure 9), the actual interface between the phases is shown in terms of the phase indicator function and the reconstruction of the same interface with discretized computational cells can also been seen to illustrate the processes involved in simulating the interface and subsequent water behaviour. The accuracy of the simulation results hinges on the level of discretization of the interface. The smoother the curve, describing the interface, the better the reconstruction in comparison with the actual interface, and therefore the accurate the results. However, higher levels of discretization requires smaller computational cells, which in turn result in a high number of computational cells over the same computational domain. This results in higher computational resource requirements and long simulation times.

The phase indicator function (γ) is based on a function of the volume fraction (α), which is often used interchangeably to understand the interface boundary between the two phases, possessing vastly different physical properties.

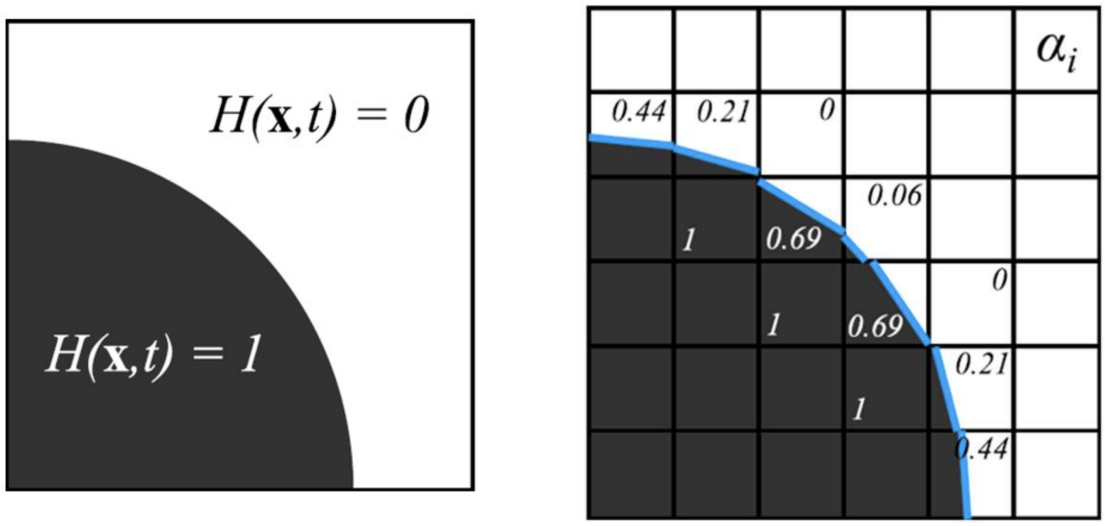

(a) Actual interface between two phases

(b) Discretized interface between two phases

Figure 9: Illustration of the actual and discretized interface between two phases (VOF) [10]

As we can see in the figure above (see Figure 9 (b)), the discretized interface includes regions where the curve connecting the interface is discontinuous and in order for accurate results, effort must be made to connect the end points of the neighbouring computational cells to get a better and smoother curve. To achieve this, additional techniques need to be incorporated to simulate the curve in a much more continuous manner.

The results obtained from the simulation has already been discussed to be dependent on the size of the computational grid. This criterion is dependent on several other subcriteria, such as the physics of the two phase flow, the discretization schemes used on the computational grid, and the interface requirement to be well resolved at every time step of the simulation. To achieve this, adaptive mesh refinement (AMR) is used, as this

reduces the computational load required by just improving the resolution of the mesh only at regions where the interface is located and only during the times when the solution is calculated.

Another aspect that needs to be monitored, is that the when the computational cell size is reduced, the time step of the simulation also must be reduced in order to ensure that the interface must move one computational cell in a single time step for understanding the minutiae of the interface movement through the domain. If the time step is large, then there is a strong possibility of missing out on the behaviour of the interface that take place in between the time step jump. This renders the usage of small computational steps as useless as in such that the resolution of the interface is high enough to visualize the interface accurately, but the continuous behaviour between the time steps is lost. So, if the time steps are large, then one might see a water droplet begin to form, and in the next time step, see it exiting out of the domain. The behaviour occurring in between the steps is lost and the observer has no information on how the water droplet formed, the size of it, the path it took to move across the domain, the forces present on the droplet and if or when it split into different sizes before exiting the domain. Therefore, the time step needs to be within acceptable limits in such, that the interface moves only one computational cell across one time step. This is handled by a non-dimensional number called the Courant number (CFL).

It is based on the equation given below (see Equation 4):

$$CFL = \frac{U\Delta t}{\Delta h} \tag{4}$$

where U represent the velocity or the information travelling across a computational grid of size Δh , in a unit time Δt. The Courant number should be less than 1, in order to visualize the interface information moving only one computational cell in one time step. If the Courant number is greater than 1, as a result from having a higher time step , as seen from Equation 4, the information on the interface between the time steps would be lost. We can visualize this better from the figure given below (see Figure 10).

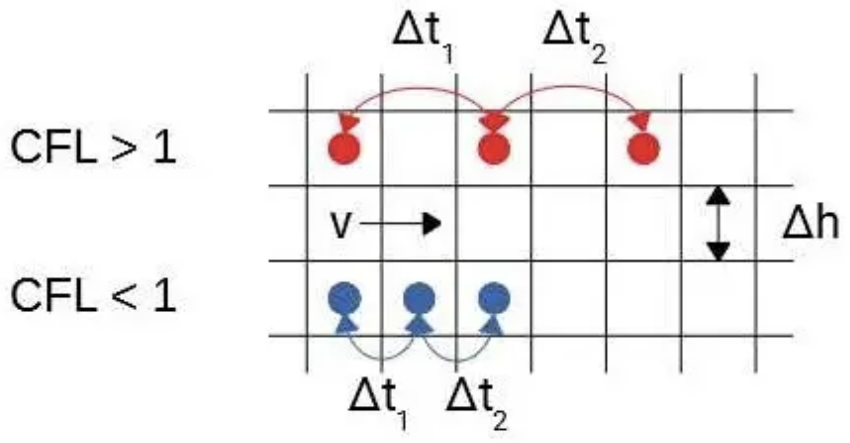

Figure 10: Visualization of the importance of the Courant number [11]

In addition to the sizing of the mesh, the forces of surface tension of the water phase at the walls of the gas diffusion layer flow channels is also to be considered, as this determines the shape of the water particles, and the velocity with which it flows. This surface tension force is originated due to the tendency of the molecules to reach the lowest possible energy state affecting the inter-molecular forces at the interface. However, it is not so easy to incorporate the surface tension force into the VOF Method, as the VOF method is applicable at the macroscopic scale and the surface tension force is present at the mesoscopic level, right before the effects of the continuum take place. There is a conflict of scales with the surface tension force and an additional model has to be supplemented to convert the surface tension force into a form of bulk body force so that it can be included into the VOF Method as a continuum (at the macroscopic scale).

The surface tension force is modelled as a body force spread across the interface and the interface is modelled as a transition region with a certain finite thickness. This results in complex algorithms and calculations - algebraic techniques or geometrical reconstruction techniques to build back the interface after incorporating the surface tension force.

It has to be kept in mind that the interface despite being of finite thickness and a transition region, is not a boundary condition. It is considered to be a part of the solution as it obtained by solving the governing phase indicator function equation.

The final equations for the Volume Of Fluid Method (VOF) are given as follows:

The mass equation is given by the equation below (see Equation 5):

$$\frac{\partial \rho}{\partial t} + \nabla.(\rho \boldsymbol{u}) = 0 \tag{5}$$

where ρ is the density of the phase 1 (water), and $\boldsymbol{u}$ is the velocity of the said phase. This equation describes the conservation of mass of a compressible fluid (the density of the fluid can change over time, due to changes in pressure or temperature in certain regions) in a control volume. It is part of the Navier-Stokes set of equations for the continuity of mass across a control volume. The right hand side (RHS) of equation 5 is equated to zero shows that any amount of fluid entering the control volume, the same amount exits out of the control volume, i.e. no new mass is generated.

The momentum equation is given as follows (see Equation 6):

$$\frac{\partial}{\partial t}(\rho \boldsymbol{u}) + \nabla.(\rho \boldsymbol{u}\boldsymbol{u}) = \nabla.\boldsymbol{T} + \rho \boldsymbol{g} + \boldsymbol{F}_{\sigma} + \boldsymbol{F}_{wall\ adhesion} \tag{6}$$

where $\boldsymbol{T}$ is the stress tensor, $\rho \boldsymbol{g}$ is the body force, the $\boldsymbol{F}_{\sigma}$ is the surface tension force and $\boldsymbol{F}_{wall\ adhesion}$ is the wall adhesion force. This equation describes the forces acting on the fluid passing through the control volume, both on the surface of the fluid - such as viscosity, friction, surface tension and adhesion, and in the body of the fluid - gravity (primarily). This equation is the momentum equation of the Navier - Stokes set of equations for the conservation of momentum across the control volume. This equation (see Equation 6) describes the entirety of the forces acting on the fluid, causing to accelerate or decelerate according to the magnitude and direction of the acting forces. This equation is important as it explains the direction, the velocity and the momentum with which the fluid moves

across the control volume. Therefore, it is critical in explaining the way the fluid behaves across the control volume under study.

In addition to these equations, the interface throughout the domain is tracked by solving the following equation (see Equation 7):

$$\frac{\partial \gamma}{\partial t} + u_j \frac{\partial \gamma}{\partial x_j} = 0 \tag{7}$$

where u_j is the velocity of the phase, γ is the phase indicator function and X_j is the size of the computational cell.

The surface tension force is modeled based on the following equation (see Equation 8):

$$\boldsymbol{F}_\sigma = \sigma \, k \hat{\boldsymbol{n}} \, \delta \tag{8}$$

where δ is an interface delta function defined as seen in the Equation 9, and k is the curvature of the interface as defined in the Equation 10, and $\hat{\boldsymbol{n}}$ is the normal to the interface which is defined in the Equation 11.

$$\delta = |\boldsymbol{n}| \tag{9}$$

$$k = \nabla . \hat{\boldsymbol{n}} = \nabla . \frac{\nabla \gamma}{|\nabla \gamma|} \tag{10}$$

$$\hat{\boldsymbol{n}} = \frac{\boldsymbol{n}}{|\boldsymbol{n}|} = \frac{\nabla \gamma}{|\nabla \gamma|} \tag{11}$$

The curvature of the interface and the normal to the interface are functions of the phase indicator function (volume fraction) as seen in the equations above (Equations 10 and 11). Therefore, the phase indicator function is absolutely important in the processing of the surface tension force and incorporating it into the final VOF equations (see Equation 6).

There are also additional issues when using the Volume Of Fluid Method (VOF). There are issues when solving the advection (transport of fluid) equations of the volume fraction (α). This is handled by utilizing two strategies. In the first one, the equation is solved simultaneously with the other equations utilizing the same time step values, in this case, the equation is free from the Courant number limitations and can incorporate large time steps.

However, this strategy is not preferred, as it does not incorporate the complexities that arise in the regions where the surface tension is a significant parameter. In the other strategy, the time step for solving the volume fraction advection equation is different from the time step used for the other equations. In fact, it is a function of the Courant number and the common time step. This can be seen in the following equation (see Equation 12):

$$\Delta t_\alpha = C \, \Delta t_{fluid} \tag{12}$$

The second strategy is preferred as it provides a better estimation of the curvature of the interface, due to the smaller time step and smaller computational cell size. However, it can lead to tremendous computational requirements.

After the interface has been solved, and calculated, it is reconstructed on the basis of **High Resolution Interface Capturing (HRIC)** technique. This technique mimics the convective transport of the constituent fluid components (phases) resulting in sharp interface tracking between the two immiscible phases. The HRIC technique works in tandem with **Adaptive Mesh Refinement (AMR)** and the **Free Surface Mesh Refinement** criteria to reconstruct the interface between the phases. The AMR refines the computational cells that contain the interface (based on the value of the volume fraction of the primary phase) and the reconstruction based interpolation technique works on the refined cells to build up a sharp interface.

This technique works best when the interface is perpendicular to the direction of the flow, as this reconstruction is based on a downwind scheme. However, in order to overcome the limitations of a downwind scheme, additional correction factors with blending with upwind schemes (in default HRIC) or with QUICK (in modified HRIC) to ensure that the front sharpening aspect of the downwind scheme works in all directions of the interface with respect to the flow direction.

To summarize, due to the macroscopic scale of both the spatial and the temporal dimensions of the two-phase flow problem in the gas diffusion layer flow channels of the PEM fuel cell, the Volume Of Fluid (VOF) method is chosen to be suitable to solve the problem, as it can accurately calculate the amount of water generated, its behaviour across the channel due to its indirect interface tracking and it also incorporates the surface tension forces accurately into the momentum equations despite having continuum scale conflicts, does not produce mass conservation problems and does not require high computational requirements due to tracking the field properties of the fluid across a control volume (instead of tracking individual particles as in Lagrangian systems).

1.3 Aim and Scope

The primary aim of this thesis work is to observe, understand and explain the emergence, transportation and movement of the water particles in a two-phase flow with air in the flow field channels of the bipolar plates in a PEM fuel cell.

The secondary aim of this thesis work is the study and understanding of the factors surrounding the complexity of this multiphase problem, in order to determine their effect on the water emergence and transport behaviour. The observed properties include controllable factors like flow velocity, humidity levels, mass transfer levels, pressure levels, etc. It also includes the significance of factors that cannot be readily changed such as the hydrophobicity or hydrophilicity of the gas diffusion layer and the channel walls, the surface tension contact angles, the porosity of the gas diffusion layers, etc.

The existing literature on the same problem has been used to assess the validity of the simulation model and check if the model explains the physical phenomenon with accuracy. This validation and accurate explanation of the water emergence and transport behaviour would constitute the tertiary aim of this thesis work.

The results of the simulation which is built on conditions and settings based on a heuristic approach based on problem-solving approaches on similar problems with relatable flow conditions. This is to ensure that the simulation model conditions used are reasonable to assess the problem at hand. The results presented, and the understanding derived from them would be the final aim of this thesis work.

The scope involves to the extent to which the problem is studied, and the methodology used and limitations confronted during the simulation and the observation process. They would provide the depth of the complexities involved in simulating and understanding the multiphase flow problem of water and air across a channel with multiple hydrophobic/hydrophilic properties across the channel, which is also subjected to differences in physical conditions such as humidity, variance in operating pressures and temperatures. This may hopefully lead to a better understanding and a breakthrough as to optimizing water movement management in a PEM fuel cell in the future.

1.4 Research Question

There have been many previous attempts at understanding and simulating the multiphase problem of air and water along the flow channels in the bipolar plate of the PEM fuel cell. There have been studies utilizing different CFD algorithms in studying the problem as evidenced by the plethora of techniques utilized which were described briefly in Section 1.2.1 with their respective advantages and drawbacks. This thesis, based on the driving force of the aims it undertakes, condenses them into the following research questions:

1. What are the complexities involved in simulating the multiphase problem of the air and water flow in a bipolar plate flow channel?
2. How does the surface tension of the interface play a role in the behaviour of the water particles as they move across the control volume/computational domain i.e. the channel?
3. How significant of an effect the controllable factors such as air inlet velocity, the pore geometry (size and number) and humidity have on the water emergence and transport behaviour?
4. Can the impact of the aforementioned factors lead to an optimization of water flow without drastic alteration of the flow channel characteristics?

2 Literature Review

This chapter of the thesis work incorporates the previous research done into the phenomenon of the emergence, transport and other ascertaining behaviour of the water-air two phase problem in the flow channels of the bipolar plate. This chapter also includes the different aspects and factors involved in the determining how the water particles produced from the electrochemical reaction emerge, move and exit and out of the flow channels. They also discuss the physical conditions required to maintain an optimum water hydration level across the flow channel and how it affects the behaviour across the fuel cell as a whole.

The following subsections explore the behaviour based on both experimental and simulation observations providing the reader with a better and an in-depth understanding and also being a signpost towards setting up the methodology required to perform the study.

2.1 Emergence of Water in the gas channels

As previously mentioned, the fuel cell is an electrochemical cell with the oxygen/air being supplied externally is reduced with the involvement of protons (flowing through the electrolyte) and electrons (flowing through the external circuit), as seen in Equation 2, which has been reiterated (as Equation 13) here for ease.

$$O_2 + 4e^- + 4H^+ \longrightarrow 2H_2O \tag{13}$$

From the above reaction, water is produced as the product of the reaction and emerges out of the gas diffusion layer because of the moisture carrying capability of the air and also due to the hydrophobic nature of the electrolyte (PTFE is highly hydrophobic). The protons from the electrolyte tend to drag out the water along with them into the flow channels in addition to the air transportation mechanism.

There have been several studies undertaken to consider the rate of water emergence and transport in the gas channels and the factors leading to efficient water transport. It was found by Quan et al.[16] that a secondary flow was induced due to the interaction between the water produced at the cathode and the air supplied in the bend region of the serpentine flow channel type affecting the flow of the water behaviour after emergence. This confirms the two phase problem complexity that has been theorized in previous sections. This complicates the water removal to the extent as to block the air/oxygen from interacting with the other reactants at the reaction sites, reducing the fuel cell performance.

The airflow could get severely blocked despite the channels containing a small quantity of water whether the channel geometry was serpentine or parallel due to the unevenness of the air flow distribution due to the air-water interactions, as found by Jiao et al. [17][18] However, the serpentine flow channel had an unique flow characteristic where the water film would break into droplets at the bends enabling easier removal.

Kim et al.[19] performed a numerical study with the aim of identifying the design guidelines for gas channels based on the effect the surface properties and channel geometry would have on water emergence and transport. Their results showed that a combination of hydrophobic surfaces, round corners and a smaller channel width maximised the water exhaust. This is in line with the theory, as the hydrophobic surfaces would not let any

water particles rest or get stagnated in the channels, and the round corners would provide a smoother curve along which the air can carry out the water without any flow interruptions. Faster velocities, would have a higher water carrying capacity and driving forces, however, it might lead to a larger pressure drop.

To ease the complexities of the serpentine flow, the two-phase flow was usually simulated in a straight channel to study the material properties, i.e. its hydrophobicity or hydrophilicity and their effect on water exhaust in the channels. Cai et al.[20] found out the the wettability (the ability of the material to let water spread across its surface) had a major influence on the water removal rates in the channels - particularly on the water distribution along the channel and also for the time it took for complete discharge out of the channel.

They found out that the best **combination** for water removal is a **Hydrophobic** GDL surface and **Hydrophilic** channel surfaces.

This combination was not only the best way to remove water but was beneficial to the air transportation from the channel to the GDL. This makes sense as the **hydrophobic gas diffusion layer would prevent water from settling on it and blocking the reaction sites**, therefore ensure good reaction rates at the cathode. Since, the water cannot stay latched on the GDL, it must have to be transferred onto the channel walls for the air coming out of the cathode side to carry them away.

This result was corroborated by Zhan et al. [21] where they found out that the more hydrophobic the GDL was, the easier the water was discharged. They also studied the same scenario with different air velocities and found out that higher liquid volume could be discharged with higher air velocities. They also found that the hydrophilic channel wall set up lead to effective removal albeit with a significant increase in pressure drop. It was also observed that the **best design to remove water** was a sharp corner serpentine design , with a negligent drop in pressure as it lead to the accumulation of water in the upper levels of the channel, opening up a larger extent of the GDL surface area for gas (air) transport. The pressure drop was found to increase linearly with an increase in air inlet velocity.

In a later study by Quan et al.[22], they had investigated the effects of the operating pressure drop on the water removal mechanism and found out that on increasing the pressure drop, the water flow regime changed from a combination of corner and slug flow to an intermediate corner flow and then to a shear flow regime which displayed the fastest movement across the channels.

To **summarize** this subsection, based on the above research review, the main factors that are affecting the water emergence and transport and those that that need to be altered to ensure optimum water removal are :

1. A hydrophobic GDL surface for better gas transport and reaction rates at the reaction sites.
2. Hydrophilic channel surface for keeping the water from latching on the GDL surface.
3. High Inlet air velocities to push higher volumes of water out of the fuel cell.
4. Sharp corners for accumulating and dispersing water droplets.

5. High operating pressure drop for faster water movement due to a shear flow mechanism.

2.2 Behaviour of the emerged water

In the research papers mentioned above, the water inlet was assumed to have emerged at the top of the flow channels or had entered as a constant mass flux throughout the uniform GDL surface. However, in reality, and on the basis of experimental observations, this is not the case. The water emerges from the GDL surface through the pores present in the GDL matrix and proceeds to from droplets. These droplets exhibit behaviour which include emergence deformation, detachment and transport which is highly different to that of a constant mass flux previously assumed, and this behaviour plays a very impact aspect in the two-phase flow problem in the gas channels.

Parametric studies investigating water removal rates have shown that the a droplet is easier to sweep away by an air flow with uniform velocity compared to a developing flow that comes from a constant mass flux of liquid water.

The detachment aspect of liquid droplets from the gas diffusion layers (GDLs) used in PEM fuel cells was studied by Theodorakakos et al.[23] and under the influence of a cross flowing air stream, the results obtained were in alignment with the ones obtained from a **transparent** PEM fuel cell. They also observed that a reduction in the values of surface tension resulted in smaller adhesion forces in the channels and faster removal. The droplets were also found to be removed at lower velocities at the side and top surfaces in the channel.

Fluorescence and liquid pressure drop measurements were utilized by Bazylak et al.[24] to investigate the complex liquid water transport in the channels of a PEM fuel cell. They observed that the **water emergence from the GDL surface is restricted to certain favoured locations which offered the least resistance to the droplets** and they had a tendency to change over time. To investigate this, the VOF method was employed to simulate the filling behaviour of water droplets against two competing pathways and the simulations showed that once a preferred pathway was established, the secondary pathways receded which was in line with the experimental results from studies of receding droplets.

Fang et al.[25] analyzed the influence of the contact angle hysteresis (Contact angle hysteresis is the difference between the front (in the direction of the motion) and the rear (opposite to the direction of the motion) contact angles of the droplet) in the micro-channel flow domain using VOF method (see Figure 11. The droplet motion is visualized in Figure 11 with the angles and the contact angle hysteresis (θ_{CAH}), which is given by the relation in Equation 14)

$$\theta_{CAH} = \theta_F - \theta_R \,. \tag{14}$$

They deduced that the **contact angle hysteresis was the reason for drop elongation and post-detachment instability of the droplets**. The model data was corroborated with qualitative experimental observations from droplet and slug dynamic data and was found to be in line with each other across a wide variety of flow conditions. However, the surface properties in relation to the contact angle hysteresis was limited to estimation due to the difficulties present in conducting experimental measurements.

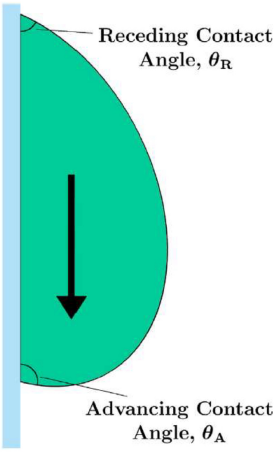

Figure 11: The contact angles on a water droplet on a vertical surface [12]

Contact angle hysteresis results from the difference in the contact angles of the droplet at both the front and rear points of the droplet and is an indicator of the surface tension forces acting on the droplet. This effect of the surface tension forces on the behaviour of the water droplets' adhesion to the cathode GDL surface was numerically studied by Golpaygan and Ashgriz[26][27], firstly in a 2-D simulation and later through 3-D simulations[28] to first identify and then confirm the significance of surface tension forces respectively. They found that surface tension is the most significant factor on the droplet separation and break-up mechanisms out of droplet and gas properties, flow velocity and channel geometry. The impact of the surface tension forces on droplet dynamics was confirmed when they extended their investigation with the 3-D simulations.

Shirani and Masooin[29] used VOF Method and observed that the surface tension prevented the deformation of the droplets while the increase in density, velocity and viscosity in the carrying fluid (i.e. air) led the droplet deform at an accelerated rate. This further proves the importance of the surface tension forces on droplet behaviour and transport.

A 2-D VOF numerical study on the two-phase flow by Zhu et al.[30] investigated the entire behaviour of the water particles from the droplet emergence and formation sequence to their detachment and/or film formation behaviour was studied and it was identified that a hydrophobic GDL resulted in the breaking-up of the droplet, whereas a hydrophilic GDL resulted in a formation of a water film flow after the spread of the original droplets. The inlet air velocity also played a part in the break-up of water droplets and their subsequent conversion to a film flow regime sooner when the velocities were high. In addition to this, the critical air velocity where the droplet detachment would occur was found to decrease with an increase in the hydrophobic nature of the GDL surface meaning an increase in the tendency to form droplets at lower air velocities. This is in line with the previous studies and theory as the water droplets would be unable to coalesce on the GDL layer due to its hydrophobic nature and therefore would be exposed to the air flow far sooner and be carried away much easily. They also investigated the impact of channel geometry, pore size and droplet coalescence on water dynamics in the gas channels of a poly-tetra-fluoro-ethylene treated GDL in a later study[31] and the results showed that the larger dimensions of the flow channels decelerated the rate of droplet deformation and the droplet

coalescence accelerated the same, along with faster water motion.

To obtain a more complete picture of the droplet dynamics in the PEM fuel cell's gas flow channels, Zhu et al., extended their work to 3-D[32] to further analyze the emergence, growth, deformation, detachment, transport and coalescence of the water droplets. In extension to the formation of a film flow regime, they also investigated the water coverage and friction factors of system and showed that the water droplet emergence and its subsequent behaviour (growth, deformation, detachment and removal) was highly cyclic and the frequency depended on the wettability of the GDL and the air velocity. The frequency increased on decreasing the wettability and air velocity. This is line with the theory, low wettability means high hydrophobicity of the GDL layer, ensuring the water droplets would not form a film layer therefore, the droplet growth, deformation and detachment would be accelerated. The air velocity being low would also ensure a more turbulent environment causing surface tension forces to play a major part and resulting in a high frequency droplet cycles.

In a different study[33], they also investigated the significance of the pore location on droplet dynamics and observed that the droplet behaviour depended entirely on the GDL surface wettability when emerged from the longitudinal center-line of the channel, however, when emerged in a location closer to the side walls, the side walls wettability and its effects on the droplet dynamics were far more consequential.

Water droplet movement behaviour in a straight gas channel with varying hydrophilicities and air velocities was investigated Mondal et al.[34] and it was found that the more hydrophilic the channel was (low contact angles), the lower the droplet velocity. In the case of high hydrophobic channels (high contact angles) coupled with high air velocity forced the water droplets to move significantly faster. This result was also substantiated when Raman et al.[35] also observed that a highly hydrophobic channel surface led to lower droplet removal times, in other words, faster water removal rates.

The results from a study led by Kim et al.[36] on the analysis of inter-droplet interactions showed **enhanced water removal rates with coalesced water droplets compared to individual droplets**, among droplets emerging next to hydrophilic channel walls there was an improvement in the gas reactant (air/oxygen) transport. They also observed the clogging up of reaction sites in a hydrophobic channel wall surfaces and with low air velocity.

To **summarize** this subsection, the behaviour of the water droplets **after** their emergence from the gas diffusion layer is determined by the following parameters:

1. Droplet emergence locations from the gas diffusion layer (GDL).
2. Surface tension forces (Contact angle hysteresis).
3. Wettability of the gas diffusion layer (GDL).
4. Dimensions of the channel geometry.
5. Coalescence of water droplets

2.3 Effect of humidity of the incoming air

[37]

The air supplied to the PEM fuel cell is almost always used to remove the water generated as a product from the electrochemical reaction. Due to this reason, the air supplied to the fuel cell is at a higher flow rate than the stoichiometric requirement. If it were supplied at the stoichiometric requirement, the exit air would be devoid of oxygen and the fuel cell would suffer 'concentration losses'[38].

The air flowing through the fuel cell has a tendency to carry away water - in effect, drying out the electrolyte, as previously discussed in Section 1.1.6. In this section, we delve a little deeper into this drying effect and its non-linear relationship with temperature.

It is very important to factor in the drying effect of air as it strongly affects the amount of water vapour it can evaporate and carry with. This drying effect of water is related to the partial pressure of water (P_w) and the the saturated water vapour pressure (P_{sat}). The theory is that at pressures lower than the saturated vapour pressure, the water has a tendency to evaporate, while at pressures higher than the saturated vapour pressure, it condenses. The **lower** the partial pressure of water is, the **faster** the rate of evaporation, as the relative humidity is far lower. The relative humidity of water is the ratio of the partial pressure to the saturated vapour pressure (see Equation below 15). It tells us the quantity of water present in the air at that given temperature. So, the lower the relative humidity, the more water it can evaporate; thus higher the drying effect.

$$\phi = \frac{P_w}{P_{sat}} = \frac{Partial\ pressure\ of\ water}{Saturated\ vapour\ pressure\ of\ water} \tag{15}$$

In addition to this, the **saturated vapour pressure rises exponentially with temperature** (insert reference here). This implies that the air at ambient temperatures (approximately 25 °C) is moderately drying can become extremely drying at operating temperatures of a PEM fuel cell (around 60 - 85 °C). This **can lead to disastrous effects on the polymer electrolyte as they require high water content for good proton conductivity, reducing the cell performance drastically**. The electrolyte membrane is also very thin (thickness in the order of a few microns) which may lead to rapid drying out if exposed to hot non-humidified air.

Therefore, it is absolutely necessary to pre-humidify the incoming air to ensure that the electrolyte membrane is sufficiently hydrated for good proton conductivity, in essence, good cell performance. The alternative to pre-humidifying the incoming air by adjusting the operating conditions of the fuel cell to, in essence, humidify the air **after** it enters the channel can be done via the following methods:

1. Lowering the cell operating temperature, this ensures that the saturation vapour pressure is lower (P_{sat}). However, lower temperatures would result low exchange-current density (i_o), which leads to lower cell voltage at lower temperatures as per the following equations (see Equations 16, 17 and 18).

$$V_C = V_r - A.\ln(\frac{i}{i_o}) \tag{16}$$

where V_r is the open circuit voltage (OCV) given by Equation 17, V_c is the cell voltage, A is the Tafel equation constant given by Equation 18 and i is the cell current density.

$$V_r = \frac{\Delta \bar{g}_f}{2F} \tag{17}$$

$$A = \frac{RT}{2\alpha F} \tag{18}$$

where $\bar{g}_f$ is the Gibbs free energy released in the cell reaction and F is the Faraday constant ($= 9.649 \times 10^4\ C.mol^{-1}$), R is the universal gas constant ($= 8.314 JK^{-1}mol^{-1}$), T is the absolute temperature (in K) and α is the 'charge transfer coefficient' which depends on the amount of electrical energy utilized in altering the electrochemical reaction rate (usually lies between 0.5 and 1). An increase in temperature has a far significant effect in increasing the current exchange density (i_o) than increasing the Tafel equation constant. Therefore, **lower operating temperatures mean lower cell voltages**

2. Lowering the air flow rate would help marginally, however the decrease in cathode performance is not worth the reduction in flow rate. In addition to this, the oxygen reduction rate (ORR) is low to begin with (see Section 1.1.4). So, any **drop in air quantity would lower the cell performance further**.

3. Increasing the air pressure would help significantly, but the **increase in performance should outweigh the cost of compressors required** to increase the air pressure.

The humidity of the air across the PEM fuel cell must be carefully controlled to ensure optimum hydration levels in the electrolyte. The amount of water that must be added to the inlet air can be calculated based on the vapour pressure of the water present. This can be derived using the following equations (see Equations 19 to 26):

Firstly, the relationship between the total air pressure at the exit of the fuel cell and the vapour pressure of water is given by:

$$\frac{P_w}{P_{exit}} = \frac{Number\ of\ water\ molecules}{Total\ number\ of\ molecules} = \frac{\dot{n}_w}{\dot{n}_w + \dot{n}_{O_2} + \dot{n}_{rest}} \tag{19}$$

where $\dot{n}_w$, $\dot{n}_{O_2}$ and $\dot{n}_{rest}$ are the number of moles of water, oxygen and the 'non-oxygen' components of air leaving the fuel cell per second. These quantities can be found using the relations:

$$\dot{n}_w = \frac{P_e}{2V_cF} \tag{20}$$

$$\dot{n}_{O_2} = (Rate\ of\ supply\ of\ O_2) - (Rate\ of\ use\ of\ O_2) = (\lambda - 1)\frac{P_e}{4V_cF} \tag{21}$$

The 'non-oxygen' components of air primarily contains nitrogen and the inlet and the exit flow is the same. By the molar flow rate in comparison to oxygen the multiplication

factor would be $0.79/0.21 = 3.76$ (Nitrogen is 79% by volume in air, compared to oxygen which is 21% by volume in air). This gives:

$$\dot{n}_{rest} = 3.76(\lambda)\frac{P_e}{4V_cF} \tag{22}$$

where P_e is the power output of the fuel-cell stack, V_c is the individual cell voltage and F is the Faraday constant. Substituting them in equation 19, we get:

$$\frac{P_w}{P_{exit}} = \frac{0.42}{0.21 + \lambda} \Rightarrow P_w = \frac{0.42}{0.21 + \lambda}.P_{exit} \tag{23}$$

In the above Equation 23, the inlet air has no water content. The entirety of the water content in the exit air comes from the electrochemical reaction. However, since we must include water in the inlet in order to prevent the obviously disastrous condition of drying out the fuel cell electrolyte, the equation becomes slightly more complicated:

$$P_w = \frac{(0.42 + \psi\lambda)}{(1 + \psi)\lambda + 0.21}.P_{exit} \tag{24}$$

where ψ is a coefficient relating the total inlet air pressure (P_{in}) and the water vapour pressure at the inlet (P_{win}) and is computed by:

$$\psi = \frac{P_{win}}{P_{in} - P_{win}} \tag{25}$$

With the vapour pressure of water (P_w) known, the mass of water that needs to be added at the inlet can be found by the following equation:

$$m_w = 0.622 \times \frac{P_w}{P_{in} - P_w}.m_a \tag{26}$$

where m_a is the mass of dry air supplied to the fuel-cell stack.

As a result, we can see that from Equation 24, the vapour pressure of the water in the fuel cell is dependent on the vapour pressure at the inlet (from the ψ relation in Equation 25). So, **the more the inlet water is hydrated, the higher the vapour pressure of water (P_w) inside the fuel cell**. At the elevated temperatures at which the fuel-cell operates, the drying effect of the air flowing becomes low enough to reach acceptable levels across the flow channels to ensure good hydration levels throughout the fuel cell.

2.4 GDL Microstructure - Pore arrangement and roughness

In the studies performed on droplet behaviour so far, considered only the behavioural dynamics of a single droplet or its interactions between a maximum of two droplets emerging from a **uniform** and **smooth** gas diffusion layer (GDL) surface. This is a case far from what occurs in a working fuel cell. In an actual PEM fuel cell, a multitude of water droplets emerge at multiple random sites from a GDL that is neither smooth nor uniform i.e. porous and rough. As we have seen in the previous section, how the pore location and surface tension play an effect on droplet behaviour, the variation in GDL surface properties from the theoretical assumptions also leads us down a deviated path with the droplet behaviour. In this subsection, the effects of the GDL micro-structure and its influence is showcased to visualize the complexity of simulating a porous GDL.

The results from a study undertaken by Bao et al.[39] showed that the deformation of a GDL had a strong influence on droplet dynamics, in as a highly deformed GDL leads to a slow water removal due to increase in surface contact area between the water droplet and channel surfaces.

A study by Suresh and Jayanti[40] on the effect of air flow on liquid water transport simulated the GDL micro structure in a 2-D computational domain as a **layered structure with circular fibres** and observed the positive effects of a cross flowing air stream for higher water removal rates when serpentine and inter-digitated flow channel varieties were employed.

The GDL micro structure pore simulations employed in VOF simulations so far have extremely long computational times and can be only employed over length scales of very small magnitudes. The pore micro structure is assumed to be repetitive and uniform over the entire GDL surface. This is not true as the pore shape, size and locations are entire random (**anisotropic**) in working PEM fuel cells. So, the challenge for researchers has been to efficiently emulate the intricacies of the GDL micro structure using techniques to simplify the complex micro structure into a model to reduce the computational resources without sacrificing excessive amounts of accuracy when performing simulations on larger spatial and temporal scales.

Out of all the random and irregular features present in a GDL micro structure, the two most impacting features are:

- **Liquid water pore emergence arrangement:** The arrangement of the pores and their geometry is crucial to describe and simulate the droplet emergence behaviour in the gas flow channels in the bipolar plates.
- **GDL surface roughness:** The gas diffusion layer surface roughness affects the droplet movement behaviour owing to the flow resistance provided by the friction and cannot be ignored in the simulation of flows in the micro scales.

Ding et al.[41] focused their study on the GDL micro structure and its effects on the two-phase flow patterns. They simplified the GDL micro structure by representing it with a certain number of pores on its surface to cover all the aspects of droplet formation and movement, which were simulated using the VOF method. The pores selected possessed the same open area and liquid water emergence rate. They concluded that a **four-pore case** to be the absolute minimum number to represent the entire GDL surface as they observed that the flow patterns for **both 4 pores and 64 pores** to be quite similar. They

also concluded that **at least two pores** were required in the channel width dimension to represent the micro structure accurately. This simplification of the GDL micro structure could be scaled to larger dimensions used in actual working PEM fuel cells. They observed three stages in their study of the two-phase flow patterns which are **emergence** and **merging** of liquid water in the GDL surface, **accumulation** in the side walls and the **detachment** from the top walls. Additional observations such as an increase in the liquid water injection rate changed the flow behaviour from a corner droplet flow to a film flow on the top walls leading to annular flow and finally to a slug flow pattern. This change in flow behaviour has been corroborated accurately with observed visualization techniques.

They also observed that**a hydrophobic GDL surface and a hydrophilic channel walls would be beneficial to water removal rates**, which is in line with all the simulation studies undertaken so far.

The analysis of the effects of various water injection methods on the two-phase flow characteristics was undertaken by Du et al.[42]. They studied the liquid behaviour introduced in regions close to the side channel walls, the introduction of continuous liquid along the GDL surface at both uniform and non-uniform flow rates, liquid water introduction with the air phase at the inlet were studied as well using the VOF method. They had observed that the water accumulated was higher when the water was introduced next to the side walls compared to the water introduced at the inlet. They also noticed a lower possibility of slug flow in the channel when the water was introduced in a non-uniform manner and closer to the outlet. For the case of water emergence from the GDL surface and accumulation which lead to a slug flow regime resulted in high pressure drops.

It was also noted that, via parametric studies that the gas (air) flow rate (in directly the velocity of the air flow , as the volume rate remains constant) and the **wettability of the channel walls had pretty determining effects on the water transport behaviour and any change in these parameters would have drastic consequences with the flow patterns**. In addition to the above parameters, the surface tension also changed the slug flow characteristics such as slug length and slug frequency, with the former increasing and the latter decreasing on an increase in the surface tension. This agrees well with the physics, as a stronger surface tension would make the liquid film to adhere to the surface for longer times and to break up less often.

With the aim of finding an optimum water pore arrangement that would lead to a minimum water coverage level on the GDL surface, Hossain et al.[43] lead a study and found that the surface coverage by liquid water on the GDL surface was directly proportional to the pore diameter. This means that lower the pore diameter, the lower the coverage. They also identified other parameters affecting the water coverage, which were the location of the water inlets and the inter-pore distance. They observed that the surface coverage reduced when the inlets were placed near away from the center-line and in regions close to the side wall surfaces and when the inter-pore distance was higher. Based on their results, they conclude that, for an effective water management strategy in the flow channels, a GDL layer with a blend of hydrophilic fibers blended inside the randomly distributed hydrophobic fiber matrix would lead to a strict control of a water pathway and its emergence from the GDL layer.

An investigation into the wall roughness parameter and its influence on the water behaviour was undertaken by He at al.[44] and they factored in the impact of the wettability of the wall surface, the roughness of the elements in comparison to the height of the

channel, the roughness density and type on water droplet behaviour. They found out that the behaviour varied drastically with a change in the relative roughness height (a ratio between the height of the roughness element height (r) and channel height (H) (r/H)) and an increase in this factor resulted in higher water removal rates for a **hydrophilic** wall. For a **hydrophobic** wall, any change in the r/H value was inconsequential and an increase proved disadvantageous for good water removal. For both the hydrophobic and hydrophilic wall cases, the pressure drop increased with higher roughness.

The roughness element geometry also played a role in water removal with a triangular element being more advantageous compared to a rectangular element of the same height. In addition to the geometry, a higher number of the elements was beneficial in a wall which possessed higher hydrophilicity.

A similar result was found by Chen et al.[45] when they studied the liquid water transport mechanism with a rough GDL surface. They determined that **an increase in the roughness expedited the droplet removal and minimized water coverage**. This makes sense as the higher roughness would lead to fewer water droplets adhering onto the GDL and increasing the forces of detachment present on the said droplets. They also, like He et al. (insert reference here) observed an increase in pressured drop with an increase in the roughness of the GDL surface.

The effects of GDL roughness on the dynamic droplet behaviour was also undertaken by Chen et al. [46]. They simulated the micro structures by representing the carbon fibres as 'lathy rectangles' in various orientations. They showed that the rectangles with parallel distributions had higher water droplet detachment rates and a lower possibility of channel flooding compared to their skewed counterparts.

Furthermore, they also presented an analytical model for the force balance which accounted for the surface tension forces on the GDL micro structure and could predict the water droplet detachment size.

To **summarize** this subsection, the GDL micro structure is extremely difficult to simulate to host the same qualities as the GDL in an actual fuel cell due to limited computational resources and impractically long simulation times. Therefore, the region of simulation would be reduced and techniques would be employed to simplify the complexities involved in modelling a working micro structure. In addition to identifying the two most important aspects of the GDL micro structure, namely, the pore arrangement and the GDL surface roughness. their impact on water removal rates was also investigated.

It was concluded that with a large amount of pores were not necessary to simulate the behaviour of the water droplets as there was no appreciable difference between a case with a small number of pores compared to a case with a large number of the same. The inter-pore distance had an inverse relationship with the water coverage ratio. This is understandable, as the larger the distance between the pores, the lesser tendency for them to coalesce together to form a film over the surface.

The roughness of the GDL surface had a major effect on the water removal rate with a higher roughness leading to a higher droplet detachment across the GDL. With higher roughness, the droplet coalescence would be hindered and the hydrophobicity would lead to lowering of the water retention forces and heightening the detachment forces on the droplets. The increase in roughness of the GDL surface also had a drawback of an increase in pressure drop across all the studies undertaken to study the GDL surface roughness.

2.5 Impact of the two-phase flow on the fuel cell performance

In a single-phase computational fluid dynamics (CFD) simulation models, the Navier-Stokes equations for mass, momentum and energy are sufficient to describe the behaviour of the phase in question, with various sub-models required to close the equations for different scales and types of flows.

However, in a multi-phase flow, in addition to the Navier-Stokes equations describing the mass, momentum and energy for each of the phases, the interaction of the phases and the interface between them also has to be modelled. On top of this, the effect of the surface tension forces must also be modelled as well and they are hard to describe numerically due to a discontinuity in particle behaviour across the scales. The differences in the scales of the physical properties also causes complications in modelling of the problem, particularly, in the aspect of resolving the flow field (of a property) around every particle present in the flow.

In the case of the two-phase flow in the bipolar plate flow channels of a fuel cell, there have been studies led to identify the effect of the two-phase flow on cell performance. A complete model for a PEM fuel cell was published by Le and Zhou[47] which consisted of a three-dimensional, unsteady, multi-phase and multi-component model with VOF (Volume Of Fluid) interface tracking technique.

In addition to the aforementioned features, it also considered all the important components of a PEM fuel cell - namely the membrane electrolyte, the catalyst layers, the gas diffusion layer, gas channels and also the current collectors and not only did it coupled the fluid flow properties such as momentum, energy transport along with the species , proton and electron transport, but it also factored in the electrochemical reactions of the reactant species as well.

It also analyzed the two-phase flow behaviour along with the impact of the liquid water on the velocity, pressure and temperature distributions, concentrations of the reactants (hydrogen and oxygen), and the current density produced per unit cell.

The authors had used this general model to study the water behaviour in both serpentine[48] and inter-digitated[49] channels.

The results obtained from this model showed that the liquid water present in the channels led to a higher pressure drop, an increase in the resistance to the mass transfer of the reactants i.e. the liquid water obstructed the reactant flow, and decreased the local cell temperature. This is due to the high heat capacity of water. Additionally, the liquid water presence raised the ionic conductivity of the cathode layers and the electrolyte membrane (providing good proton flow across the electrolytes and the ions needed for the three-phase boundary reaction sites).

The removal rate of the liquid water was found to be higher in serpentine-parallel channels than in a single serpentine channel. With the case of the inter-digitated design, the flow field type necessitated the use of forced convection to achieve reasonable water removal rates. Due to the forced convection, there was a risk of dragging away the water vapour inside the porous media of the GDL, which could lead to lower cell performance due to drop in the ionic conductivity.

Despite the model results being validated with experimental verification, there was a drawback with this model, as it introduced the water droplets into the gas channels in the

regions located on the side walls instead of them emerging from the GDL surface as it so happens in working fuel cell. This simplification of the model restricts its application.

To **summarize** this sub section, there have been many models that would simulate the flow of a single phase fluid, but for a multi-phase problem, there are further complex features that need to be modelled (both relevant forces and irrelevant forces), along with phase interactions and interfaces, necessitating the use of complex and convoluted corrections to cover every aspect of the multiphase behaviour. The addition of certain spatial and temporal scales would further complicate the model with restrictions arising for certain interface tracking algorithms. Despite all these complexities and difficulties, a general model has been established to simulate the two-phase flow with reasonable accuracy with results that are in accordance with experimental data.

2.6 Summary of the Literature Review

In the aspect of the **emergence of water** from the gas diffusion layers, for faster water removal without hindering the cell performance, the GDL surface must be hydrophobic to ensure better reactant transport in reaching the reaction sites. The channel surface material must be hydrophilic to reduce the adherence of the water droplet on the GDL surface and keeping them flowing away from their origin in the gas channels. Higher inlet air velocities to improve reaction rates and carry away larger quantities of water out of the fuel cell.

In addition to the water emergence, the **behaviour of the water inside the gas channels** is determined by several factors and they must be optimized to get good water removal rates. The droplet emergence locations play a crucial role in the droplet behaviour due to the effect of various forces varies with location in the gas channels. The surface tension forces is one of the most important parameters in determining the mobility of the water droplets across the channels. In addition to the surface tension forces, the wettability of the GDL also determines the surface coverage ratio of the liquid and the time it is adhered to the surface. The channel geometry also dictate the droplet deformation and transfer rates with larger dimensions slowing down the transfer rates. The coalescence of water droplets affects the water removal rate by increasing it when the droplets combine together than when they were separated.

When it comes to **the effect of the incoming air**, the operating temperature of the air tends to increase the drying effect of air. If the air is not pre-humidified, the extremely low relative humidity (RH) of the exiting air can lead to extreme drying out and causing irreversible damage to the electrolyte and the fuel cell. So, it makes sense to hydrate the air supplied to the fuel cell, the amount of water that needs to be added to the fuel cell is given by Equation 26 which shows that the water that needs to be added to the fuel cell is dependent on the vapour pressure of the water at that temperature. So, to overcome the drying effect of the hot air flowing across the flow channels, the air supplied must be pre-humidified to ensure optimum hydration levels throughout the cell.

The **effect of the GDL micro structure** is pretty significant to the water droplet formation, growth and subsequent detachment behaviour in the gas channels. However, problems tend to arise when simulating the GDL micro structure as is, due to computational limitations. Therefore, simplification models have been utilized to simulate the GDL micro structure without sacrificing accuracy. On simulating the GDL micro structure and its roughness, it has been found that the water removal rate was affected in cases with high roughness. The high roughness lead to a higher water droplet detachment but also lead to low droplet coalescence. Therefore, the removal rate depends on which effect dominates the other. The pressure drop increased with increase in GDL roughness in all the studies observed. The location of the pores also played an important part in the water removal rate, with higher inter-pore leading to lower water-coverage ratio, and better removal rates due to the feature of drops to be easily swept away compared to the film layers.

The **two-phase aspect of the flow** in the gas channels has a tendency to complicate the simulation models needed to describe the water behaviour in the gas channels of the fuel cell. However, the presence of liquid water present in the flow channels reduced the reactant transport rates but increased the ionic conductivity in the catalyst layers and in the membrane electrolytes. There was also an increase in pressure drop and a drop in cell

temperature due to the presence of liquid water. The model used to completely describe the water behaviour in the fuel cell flow channel had results that obeyed the physical laws and could be corroborated experimentally. However, it had a small drawback due to the simplification used to introduce water droplets into the membrane.

In short, the literature review section considered all the relevant factors that produced a consequential impact to the removal of the water produced in the cathode layer and how each of them affected the water removal rate and why. This provides the user with an idea on the factors needed to be optimized to produce optimal water removal rates to ensure good hydration levels in the fuel cell, and subsequently good water management strategies.

2.7 Simplifications drawn on the basis of the Literature Review

For the simulations undertaken to study the two-phase flow behaviour in the bipolar plate flow channels in the fuel cell, the numerical VOF method analysis can be categorized based on the different stages and computational aspects used (as follows):

1. **For the initial water distribution simplification:** In an actual working fuel cell, the water droplets emerge from the entire surface of the GDL at random favoured locations based on the underlying pathways of least resistance at random flow rates. However, along the course of operation, the preferential pathways tend to change due to the changes in the operating conditions, leading to formation of new pathways that provide less resistance than the already existing pathways due to a plethora of interconnected factors. However, in a simulation scenario, this process cannot be replicated as is due to the strain on the computational resources and therefore necessitates shortcuts to be taken to simplify this complex behaviour by researchers. Some prefer to introduce the entire liquid water distributions at once, while others prefer the water emergence to be gradual at uniform flow rates. Both of which are simplification that do not reflect reality, but tend to give a good understanding of the water droplet behaviour once emerged.

2. **For representing the GDL surface:** A GDL micro structure is a maze of carbon fibres with intertwined catalyst layer embedded in between to produce a maximized surface area for the reactants to reach and interact with one other to produce the necessary products at a good reaction rates. In the case of the cathode side, the gas diffusion layer provides a platform for the protons from the electrolyte, the electrons from the external circuit, the platinum catalyst and the oxygen supplied from the outside to diffuse and interact with each other at several sites to interact with each other and complete the reduction reaction and also provide a pathway for the water to exit. Therefore, the fibre matrix is extremely porous to achieve a high surface area. This means that the fibre matrix is extremely non-uniform with a variety of pore sizes and overlapping fibres with no rhyme or reason. This cannot be possibly be simulated exactly to scale on a computer without a long and tedious process. So, researchers tend to simplify this for computer simulations by either considering the entire GDL to be a smooth surface or take into account a limited view of the micro structure with a limited uniform pore sizes, or the roughness element to be of a particular geometrical shape. They are oversimplified versions of the GDL with the use of contact angles to simulate the hydrophobicity or the hydrophilicity, but it cannot be avoided as simulating the entire GDL with an accurate rendering is a daunting task.

3. **For the computational domain:** Since, the turbulent two-phase flow tends to exacerbate the complexities by creating the need for complex and convoluted corrections to model each and every aspect of behaviour of the phases, their interactions and the movement of their interface, researchers tend to simplify the computational domain by taking only a small section of the gas channels to simulate. If the entire PEM fuel cell would be studied, several simplifications must be drawn to reduce simulation times and reduce the strain on the computational resources. Some even reduce the model to just two dimensional simulations to reduce the simulation times, while some proceed with three dimensional simulations and ignore parameters that do not necessitate the extra processing requirements.

4. **The need for VOF simulations:** The VOF method simulation results are important in complementing the experimental results by providing a further understanding in the terms of quantitative information and detailed behavioural data on the two-phase flows in the PEM fuel cells.

Summarizing the two-phase flow: The liquid water which is formed as a product in the catalyst layers due to the electro-chemical oxygen reduction reaction (ORR) is transported through the catalyst layers and the pores present in the gas diffusion layer and emerges from the gas diffusion layer into the bipolar plate flow channels at preferential locations instead of emerging across the GDL uniformly at every location, tends to form droplets and grow larger until they detach from the surface and move downstream in the form of individual droplets or coalesce into larger droplets to form either a film flow or a slug flow based on the inlet air velocities.

The said behaviour is heavily influenced by the material properties, cell geometry, flow channel type, operating conditions, catalyst layer and GDL design properties. Each of these properties affect the water droplet behaviour and removal rate. They must be optimized individually to obtain the optimal water removal rate. This is one of the key challenges when it comes to simulating and subsequent validation due to the limitations posed by each.

3 Methods and Configuration

3.1 Overview

The focus on the study of water behaviour of the emerging water from the gas diffusion layer and the flow behaviour and characteristics across the flow channels of the bipolar plates is the primary aim of this thesis work. This, in accordance with previous discussions, is difficult to observe experimentally due to the limitations imposed by the present generation of visualization techniques - the observation technology is not advanced enough to visualize behaviour on actual working cells, and the ones where the behaviour can be visualized, the cell material used possessed entirely different properties that would affect the behaviour of the two-phase water air flow. As seen from the previous sections, the effect of the micro structure of the GDL and the channel walls played a markedly important role in the water droplet formation, growth, coalescence and detachment behaviours.

Therefore, the burden of understanding and providing a pathway to the optimization of the removal of product water from the fuel cell bipolar plate flow channels falls squarely on the accuracy and the validity of the CFD simulations used. The experimental verification of the simulation models to ensure that if obeys the theory behind the two-phase flow is also important.

The problem associated with most CFD models is the accuracy and the validity of the simulation undertaken as it is not foolproof. After executing the simulations, the model would produce results that on the surface would appear to be impressive owing to the advances made in the field of graphics of the designed flow simulation. However, it is prone to visualize results that make sense numerically but do not obey the laws of physics. Therefore, the conditions for setting up the simulation must be scrutinized to minimize the risk for erroneous results and the results obtained from the computational simulation must be corroborated and verified to be in accordance with both the behaviour observed experimentally and the theory behind it.

To perform this verification and to ensure the simulation has produced meaningful and accurate results, a CFD simulation model with a simplified domain from an already published research paper was used a reference for the observation, explanation and for the accuracy corroboration of the simulation set up used for this thesis study. This ensures that the simulation model set up conditions are valid and it produces results that are grounded in reality. Based on this sure footing of the simulation model, certain factors of the set up have been varied to provide an understanding to their impact into the two-phase water/air flow across the channels. The changes made were done so as to obtain results that would provide us with a direction leading to the optimal management of the hydration levels in a typical functioning PEM fuel cell.

The following sub chapters would, in detail, describe the methods to capture the water behaviour in the flow channels (especially the generation and the drainage aspects), the VOF method - how it has been adapted to this specific problem and the simulation conditions, with all the parameters required to set them up and how they have been tailored to effectively simulate this problem.

3.2 Water behaviour in the Flow Field channels

In this section, the emergence of the water at the inlet of the pores is described with the help of images from the simulations run and also the water transport behaviour after the emergence is described with the help of the theory and previously researched literature to give an idea on the complexities involved in this study.

The section is split into sub-sections, to describe the emergence behaviour and the transport behaviour.

Emergence of water at the inlet:

The rate at which the water emerges out of the inlet depends on two things, the mass flow rate ($\dot{m}$) and the radius of the pore (r_{pore}). These factors determine the velocity of the water flowing into the domain as can be seen by the Equation 27. These two are interlinked in the sense that, the velocity conserves the water flow rate with the size of the pore area. Therefore, larger the pore area, smaller the velocity.

The velocity of the water at the inlet is **not a major factor to be considered with respect to the flow of the water film in comparison to the air inlet velocity**. As this factor is more than 20 times the water inlet velocity ($v_w = 0.495 ms^{-1}$ for a r_{pore} of 25 μm).

However, the water inlet velocity is important in determining the profile of the water accumulating at the inlet pores **before** the effects of the air inlet velocity takes hold of the water particles. The profile of the water emerging from the pore is dependent on this inlet velocity and this will be one of the behaviour characteristics that would be studied. In addition to the profile formation, the height of the profile, the shape of the profile, the formation of the film before flow will also be investigated to see the effects that this has on the rate of water transport across the water channel. The effect of surface tension forces in determining the shape of the water layer profile will also be an interesting avenue to investigate further.

Flow of water after emergence:

The formation of the film layer after the water is under the influence of the air inlet velocity will be investigated in depth in this study. The behaviour of the water film, in particularly, the width of the water film formed due to the surface tension forces and air inlet velocity will be studied. Further water flow behaviour phenomenon such as droplet detachment, coalescence and formation will also be studied, with the focus being on the identification of the parameters influencing these behaviours. This would help in identifying whether the droplet behaviour is advantageous or detrimental to the water transport rates across the bipolar plate flow channels.

Finally, the effect of the width of the water film , i.e. the water coverage ratio on the GDL surface and its correlation to water removal rates (or average water film velocity) will also be looked into in order to assess all possible factors influencing the water transport behaviour after emergence.

3.3 Lagrangian Particle Tracking (LPT):

In this type of model for solving fluid dynamics problems, instead of monitoring the volume/mass of fluid entering a body and tracking the vector fields across the body, the focus is on the particle and the variation of its properties as it moves through the body. Due to the finite number of droplets being generated in the model, the LPT model is feasible to analyze the droplets as it moves across the domain.

The Eulerian blobs i.e. the unresolved droplets of water that could not be refined due to their small size are better simulated by transitioning them to Lagrangian particles. This is done in a very straight forward manner.

First, the system is defined in terms of two Eulerian phases - air and water. However, we cannot use these to simulate the droplets, as they have to be simulated separately. To do this, we define a new **Lagrangian phase** that would include the water droplets that need to be resolved and prevent instabilities in the domain. Then, the particles need to be defined as either mass-less or material particles. Since, the water droplets present have a finite size and therefore, finite weight and exert their influence on the momentum and the velocity terms, they must be treated as material particles with finite mass and density.

After defining the type of particles the water droplets are going to be, there must be a source for this droplets to exist from. It is not possible for the droplets to exist in the domain without having originated from somewhere, since the water inlet does not create Lagrangian particles and they evolve downstream, **the entire region of the domain is considered to be the point of origin for said Lagrangian particles**.

Then, which Eulerian blobs should be considered as Lagrangian particles and which should be left to be resolved by the VOF method must be defined. This done by setting up criteria that the blob must satisfy in order to be considered as a particle. This is done by fixing the **Blob Diameter Criterion**, the **Blob Shape Criterion** and the **Minimum Blob Volume Fraction Criterion**. With the help of the afore-mentioned criteria, the **Resolved Eulerian - Lagrangian Transition Model** can then determine which Eulerian blobs need to be converted to particles and which should be left as is.

In addition to the Resolved Eulerian - Lagrangian Transition Model, a simulation solver must also be included to account for the momentum and energy interactions between the droplet particles (dispersed phase) and the air (continuous phase). Since both exert influence on each other, the **Two Way Coupling Model** is utilized.

Now, in the Two Way Coupling Model, to differentiate between the particles and an interface existing in the small computational cell, a limit on the **Maximum Volume Fraction** is set to differentiate the phase and the droplets as the effect of the dispersed phase would be accounted for twice - once by VOF and the second time by the LPT model, leading to an over representation of momentum and energy interactions of the dispersed phase in the simulation.

If the Volume fraction (α) of the phase in the cell after transitioning to a Lagrangian Particle is below the maximum specified volume fraction limit, then the blob is converted into a particle and would be handled as a particle. If this limit is broken, this means that the entire cell is filled with the phase and therefore does not need to be resolved by both VOF and LPT. Therefore, the Eulerian blob would be resolved as a VOF phase.

3.4 Static Contact Angle (θ_C):

The static contact angle (θ_C) is a parameter that indicates the level of affinity a certain surface has toward the liquid attached to it. It determines the level of adhesiveness and the amount of the surface is covered by said liquid.

In the context of a water droplet, the static contact angle, indicates whether the surface on which the water flows tends to repel it (hydrophobic) or attracts it (hydrophilic). This can be illustrated with the help of the figure given (Figure 12):

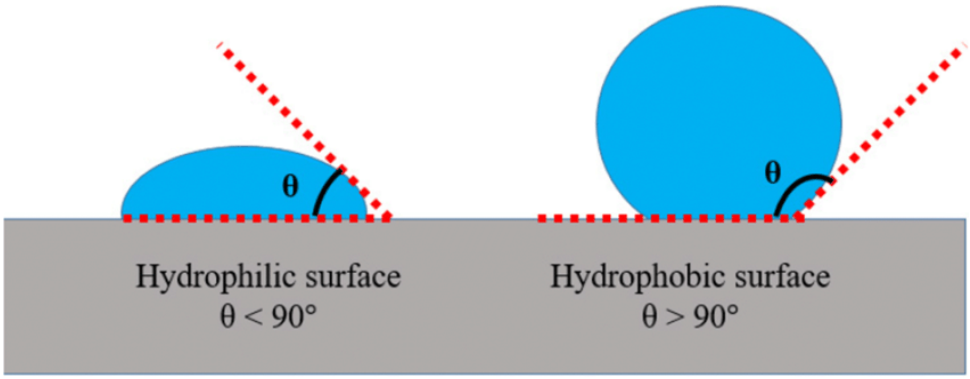

Figure 12: Static contact angle θ_C for different materials [13]

As it can be seen in the figure above, the amount of area occupied by the water droplet is determined by the value of the static contact angle (θ_C) and this determines the amount of surface tension forces acting on the droplet. This further indicates the velocity with which the droplet can move. If the droplet is on a hydrophobic surface, since a smaller area of the droplet is in contact with the surface, the less resistance the rough surface offers to the motion of the droplet.

Similarly, the stronger the hydrophilicity, more force would be required to get the droplet moving at the same velocity due to higher affinity for the water to stick to the surface.

Therefore, the levels of hydrophobicity and hydrophilicity have to be attuned to the level that favours rapid removal of water from the channel.

3.5 Numerical setup

In the following sub-sections, the setting up of the VOF method for simulating the water droplet, emergence, transport and exit will be discussed in detail, with the reasons for choosing various sub-models, simulation parameters and decisions taken for each and every parameter would be explained with reasoning to show that every step has been taken with careful reasoning and logic.

3.5.1 Setting up of the domain

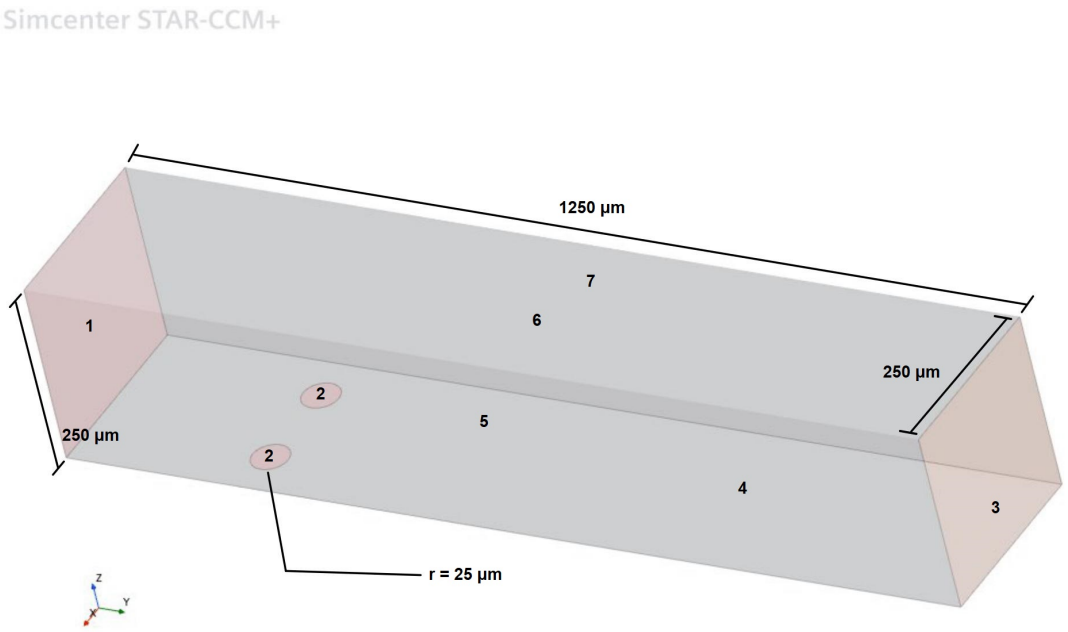

Figure 13: Computational domain with characteristic feature regions

The dimensions and the characteristic feature regions of the domain are summarized in the table for ease (see Table 2):

Domain feature	**Value**	**Units**
Length (Y axis)	1250	μm
Width (X axis)	250	μm
Height (Z axis)	250	μm
Pore radius	25	μm
Dist. of pore center from inlet	250	μm
Region 1	Air inlet	-
Region 2	Water inlet	-
Region 3	Outlet	-
Region 4	Gas Diffusion Layer (GDL)	-
Regions 5,6 & 7	Channel Walls (CW)	-

Table 2: Domain dimensions and features nomenclature

When building the domain, certain parameters should be considered to produce a frame-

work to operate from. These include the dimensions of the domain, the design of the inlets and the exits of the fluid in and out of the domain to provide a starting point towards analyzing the behaviour of the system[41]. These reasons have been identified to give as follows:

1. **Dimensions:** The dimensions for the domain were chosen based on the commonly used channel dimensions in an actual fuel cell. The part to be simulated has been chosen to be a small section emulating the straight section of the bipolar plate flow channel to ease computational requirements and perform a wide variety of simulations with shorter simulation times to assess the factors on their impact on water droplet behaviour and transport. The dimensions and the characteristic regions of the domain are given in the figure (see Figure 13) and summarized in the table (Table 2) above.

2. **Air inlet velocity:** The air inlet velocity has been chosen to be **10** ms^{-1} as this is in the range of air inlet velocities used in a fuel cell. This velocity includes the stoichiometric air required for the oxygen reduction reaction at the cathode. In addition to this, the air needs to carry away the water emanating from the water pore inlet. So, a high velocity of air is required at the inlet.

3. **Water mass flow rate:** The water mass flow rate had been chosen to be **7** gh^{-1}[41] as this expedites the water droplet formation and reduces the simulation times. In actuality, the water mass flow rate for a 800 $mAcm^{-2}$ current density fuel cell is approximately around 0.20 gh^{-1}. The simulation having a mass flow rate an order of magnitude higher does not make a significant difference due to the large flow rate of the air at the air inlet.

4. **Pore size:** Based on the given dimensional geometry, a pore size of **radius 25** μm is taken to ensure a large velocity of the water at the inlet can be obtained with the mass flow rate due to the mass being conserved. The radius of the pores are varied in subsequent simulation with an increase in 50% and 100% to evaluate the effect of the pore size on water behaviour.

5. **Pore location:** The pore location is chosen to be near the air inlet as it is the worst case scenario for water transport, as it has to travel the longest distance to reach the exit. However, it was also decided to not be placed right at the air inlet channel entrance to allow the air flow to be steady before it reaches the air inlet. The reason for the long travel time is to assess the possibility for drop detachment and evolution of the boundary layer flow. This requires a certain length to unravel, and is not possible if the pore inlet was placed near the exit of the channel domain.

6. **Pore number:** The pore number was chosen to be in the base case simulation because the water emergence behaviour has to be studied without the interference of the water emanating from the pores located downstream. This would be simulated in the later simulations, but for initial understanding of the water emergence and transport behaviour, it is ideal to start with as many factors that could be controlled and with which there is no threat of interference.

7. **Contact angles:** In an actual working fuel cell, the bottom channel wall i.e. the GDL layer is hydrophobic to push out water from the fuel cell membrane electrode assembly into the channel walls for removal, and therefore, this is simulated using static contact angle indicating the level of **hydrophobicity**. The value of **140°** is

chosen for this purpose as this is the value of the hydrophobicity of PTFE used in working fuel cells. Similarly, the **hydrophilicity** of the remaining of the channel walls is simulated using a static contact angle of **45°**. This also replicates the hydrophilicity of the material used in working fuel cells.

3.5.2 Mesh Generation

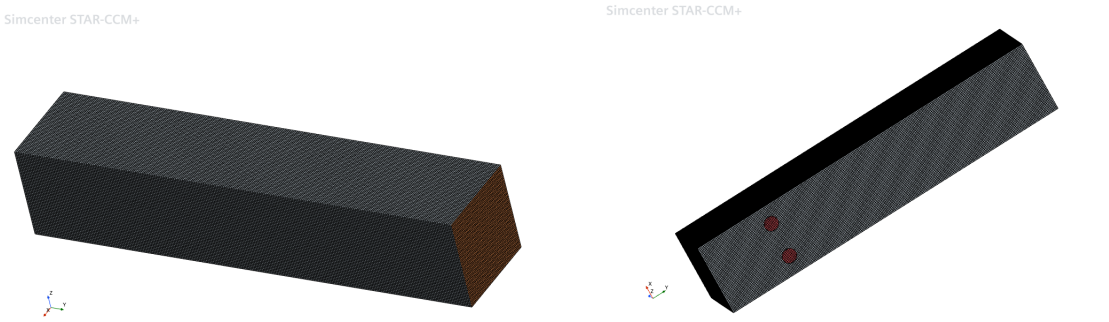

(a) 3D view of the mesh

(b) 3D view of the mesh with the pores included

Figure 14: 3D mesh of the base case computational domain

Mesh Characteristic	Value
Cell Number	881,802
Cell Faces	2,648,891
Cell Vertices	966,289

Table 3: Mesh Characteristics

The mesh characteristics of the given constructed mesh have been given above in Table 3.

One of the most important factors that affect the accuracy of the simulation results, and were a cause of problems for this study, is the quality of the mesh. A poor quality mesh can lead to simulations with inaccurate results due to the mesh elements being unable to capture the flow behaviour properly. The mesh elements maybe too oversized to capture the changes in the flow taking place every time step leading to erroneous flow behaviour analysis and prediction. Sometimes the mesh quality being poor **can lead to a divergent solution**, in other words, the equations being solved numerically tend not to approach zero, or converge to a stable state. Instead, they diverge, meaning the simulation would not arrive at a steady solution, which requires addition of sub-models to solve the set of linear equations. Often, the simulation converges, but the converged **solution may not obey the laws of physics**. In either case, it lacks utility in understanding flow behaviour.

Since the poor mesh quality leads to a situation where the mesh elements cannot capture the intricate details of the fluid film and therefore would need additional refinement, which invariably leads to higher computational costs with additional memory requirements and frustratingly long simulation times. In channel flows, the mesh is usually refined near the solid walls due to the prevalence of strong viscous forces. In a mesh with poor quality,

these forces cannot be refined accurately which leads to simulations being nonsensical. The mesh being of poor quality **often has distorted mesh elements which obviously lead to distorted results**, in other words, a straight vector obtained on a curved or distorted mesh element would actually be a curve in reality. This leads to a distorted boundary layer for example, showing inaccurate results.

In addition to this, the Adaptive Mesh Refinement is a technique that relies on finer mesh in places where there is a lot of fluid activity. It produces a finer mesh in regions where the fluid behaviour is more active and has more flow features to be analyzed. It is reliant on the base level mesh quality on which the refinements are added on. **If the original mesh quality itself, is inaccurate, the applicability of AMR becomes very limited and the information on the multitude of flow features is lost.**

With these reasons in mind, the mesh quality of the simulation has to be carefully monitored. In the table below (see Table 4), the mesh quality markers of the simulation and the optimum guideline values have been compared to show the quality of the mesh obtained.

Mesh characteristic	**Value obtained**	**Recommended value**
Skewness	7.116161e+01	less than 85°
Max. Volume change	4.706523e-02	0.01 or less
Min. Volume Change	1.000000e+00	0.01 or less
Face validity	1.000000e+00	Between 0.5 and 1
Cell quality	0.982475	As close to 1 as possible

Table 4: Comparison of mesh characteristics with recommended values

The maximum skewness angle occurs in the region of the water pore inlet due to the object being circular in shape. Despite this, the mesh skewness angle is still within range of the guideline and as can be seen in the table above (see Table 4), the mesh constructed lies within all the quality guidelines, and can be termed a **good quality mesh**.

3.5.3 Setting up of the boundary conditions

After creating and setting the mesh quality markers to be in accordance with the guidelines used in the industry. The next step is to set up the boundary conditions in the respective regions in the simulation and specify limitations and incorporate methods to simulate these regions as relevant as possible to the actual working fuel cells.

We begin by setting the conditions and limitations of each region as per the nomenclature introduced in the Figure 13.

1. **Air Inlet:** This region is set to **Velocity Inlet** type, with the turbulence specification monitored by the Turbulent Viscosity Ratio and this value is set to be a constant of 0.0 to indicate that the air produced at the inlet is non-turbulent at the **velocity magnitude of 10.0** ms^{-1} (This value is changed for subsequent simulations as can be seen in Table 5). The **volume fraction of the inlet is set to be [1.0, 0.0]** indicating the fluid flow is completely filled with air (This value can be changed on introduction of water through humidification).
2. **Water Inlet:** This region is also set to **Velocity Inlet** type, with the same turbulence specifications as in the Air Inlet region. This is due to the extremely low water inlet

velocities in the region. The **water inlet velocity is set at 0.495** ms^{-1} **for the pore radius of 25** μm and it will be further decreased for the increased pore sizes in the subsequent simulations due to law of mass conservation. The **volume fraction of this inlet is set to be [0.0, 1.0]** indicating that the phase prevalent in this region is only water.

3. **Outlet:** This region is set to the type **Pressure Outlet**. This is to ensure that the fluids exiting out of the domain, via this region is subjected only to pressure monitoring for the purpose of calculating the pressure drop across the channel. Additionally, the back-flow characteristic of this region is set to environmental to simulate that the channel opens to the atmosphere as in a working fuel cell. The **volume fraction is set to be [1.0, 0.0] to track the pressure drop of the air** flowing through the channel as the water passing through would be in liquid form.

4. **Gas Diffusion Layer (GDL):** This region is set to be of the **Wall** type as this region does not allow mass to flow across it other than from the water inlet region, which has been characterized as a separate boundary region. This region also is platform for the phase interactions due to the surface tension forces between the water and air flowing across its surface. Therefore, the **hydrophobicity** of the surface has to be simulated by using the angle that the PTFE material in actual fuel cells has in this regard. The **static contact angle** (θ_C) is set to be 90° in the base simulation to assess the other factors, but will be **changed to 140°** as in an actual fuel cell in the following simulations. The GDL layer also exhibits the **No-slip** property to account for the friction for when the water layer travels across it. The surface property is first set to be **Smooth** and later changed to **Rough** for analyzing its effect. The wall also utilizes the $\kappa - \epsilon$ **blended wall function with default values set at 0.42 and 9.0** respectively.

5. **Channel Walls (CW):** This region is also set to the **Wall** type, similar to the GDL layer. Since the surface of this region is also used for transport of the fluid, the phase interactions between them due to surface tension forces has to be accounted for. This is done with the static contact angle , just as with the GDL. However, since this region is commonly **hydrophilic**, the initial **static contact angle** (θ_C) is set to be 90°, it is later to **changed to 45°** to account for the hydrophilicity of the material used in working fuel cells. This region also possess the **No-slip** condition and the wall is set to be **Smooth** initially, and then later changed to **Rough** to get as close of a simulated model to reality as possible. The model also uses the **same values for the** $\kappa - \epsilon$ **wall function as the GDL**.

3.5.4 Multi-phase Model parameters

In this sub-section, the sub-models used to enhance the accuracy of the simulation results have been discussed with a brief description of their working along with the reason for their use. The sub-models chosen here are the features present in Simcenter STAR-CCM+. They may be different in other commercial CFD modelling software.

1. **Time Discretization Scheme - Implicit Unsteady:** This discretization scheme is used to solve flows that are unsteady, i.e. flow properties vary with time. This is an obvious choice, as the velocities of both air and water, the pressure of the air flowing all vary in regions near the pore inlet, and therefore an unsteady solver is needed to solve an unsteady flow. The implicit variety involves solving the equations

accounting for the solution obtained in the previous time steps as well as the current time step. This scheme is the most commonly used temporal discretization scheme as it can handle a wide variety of flow conditions and domain geometries and also lead to faster solution convergence.

2. **Convection model - HRIC & AMI (Sharp Reconstruction):** Firstly, with HRIC (High Resolution Interface Capturing) is a technique used to track the interface between two immiscible fluids - air and water, in this case. This scheme is designed to mimic the convective transport model between two immiscible fluid components. This scheme includes several sub options dedicated to providing a sharp interface between the two phases. This interface modelling is one of the key advantages that the VOF model possess over other algorithms. This interface capturing scheme, uses the angle between the normal to the interface and the cell-face surface vectors and is corrected with the local Courant number to ensure that the interface produced is always sharp. Since this scheme, is based on the local Courant number and the availability criterion (the amount of fluid that is received by a cell cannot be more than the amount of fluid sent from the donor cell). This criterion ensures that for every time step, the interface produced remains sharp without any diffusion.

   Secondly, The AMI (Adaptive Mesh Interpolation) is a technique that works in collaboration with the Adaptive Mesh Refinement (AMR) to map the volume fraction fields when the AMR process refines the cells from coarse to fine in the vicinity of the interface. This leads to a sharp reconstruction of the volume field, therefore a sharper interface between the phases.

   The sharper the interface is, the more accurately, the surface tension effects of the multi-phase mixture can be studied. This leads to a better and accurate simulation solution.

3. **Free Surface Mesh Refinement:** This technique is used in tandem with HRIC and AMR to refine or coarsen cells in the volume mesh to improve the spatial resolution in the vicinity of the interface between the phases. The algorithm ensures that a sharp interface is maintained but also reduces the unnecessary refinement in regions where high spatial resolution is not required. It does so, by not refining the cells that presently containing the interface, but by marking the cells present downstream of the interface and to ensure that the high level is continued when the interface eventually reaches the marked cells. Since the AMI is set to Sharp Reconstruction, it also marks the interface cells necessary to be refined as well.

   The above two algorithms ensure that the interface between the two phases is always maintained to be sharp and highly resolved. The usual value of refinement is set to the level 2. This value dictates the number of times a cell can be refined. In the refinement process, the parent cell splits into child cells which are exactly half of the original size. Therefore, a higher refinement level would result in a ridiculously large number of cells, exacerbating the strain on computational resources and memory requirements.

4. **Surface Tension Force - Semi-Implicit Surface Tension Force model:** Surface Tension is usually introduce unwanted complexities into the simulation model, making it prone to inaccuracies. This is partly due to the rapid jump (discontinuity) of pressure across the phases, requiring additional handling. Secondly, since the interface

is defined on the basis of volume fraction, and this is reconstructed based on cell face gradients, it is discontinuous, therefore, evaluating the curvature of the interface is difficult. This means that the contact angles that impact the surface tension force cannot be accurately defined. These discontinuities are inevitable when using discretization techniques for interface reconstruction. These complexities create parasitic currents that tend destabilize the simulation.

To overcome this and improve stability, the momentum source term due to the surface tension force has to be defined in a semi-implicit manner. This is done by introducing temporal linearization. This stabilization term counteracts the parasitic current by acting as an artificial stress acting tangentially to the free surface. This factor can be scaled as needed with time steps and surface tension forces.

5. **Segregated VOF Solver - Explicit Multi-Stepping:** To get a sharp interface, the Courant number of the simulation is kept low. This ensures that the cell size is small enough to ensure that the flow features are captured accurately. The Courant number is usually limited to 1 (see Figure 10). But, this limitation has a drawback as in it does not fully utilize the computational capacity of the VOF free surface simulation. If the Courant number is raised, the accuracy of the interface is lost. To overcome this conundrum, Explicit Multi-Stepping is used. This removes the limitation on the Courant number by introducing smaller time-steps within the original time step. This reduces the run-time of the simulation without compromising on the quality of the simulation by producing smaller time steps at the free surface calculations, while allowing larger time steps elsewhere. This lets us use larger global time-steps, so faster convergence can be achieved. The regions at the interface will still be using smaller time-steps so that the interface information is not lost due to low temporal resolution.

3.5.5 Simulation Configuration

In this sub-section, the parameters that affect the formation and flow of water droplets across the channels are varied and the changes to the water flow is analyzed. The factors that would be varied are as follows:

1. Velocity of the inlet air and the inlet water.
2. The contact angles (static - θ_C) of the GDL and the channel walls to simulate the effect of hydrophobicity and hydrophilicity respectively.
3. The wall roughness of the GDL and the channel walls to analyze the effect on water film spread and velocity.
4. The size of the simulated pore on the effect of the water film and its behaviour. The position of the pore on the Y axis is not relevant due to the obvious reasoning, that farther the pore is away from the exit, the more the transport time, and vice versa. So, in a way, calculating the transport time with the pore near the air inlet is analyzing the worst case scenario, in regards to the time taken.
5. The number of pores to simulate the GDL porosity as accurately as possible.
6. The effect of humidity on the droplet formation, momentum and spread across the channel.

7. The effect of geometrical features present in the computational domain after including turns.

The amount of influence the aforementioned factors on the water particles' behaviour is the foundation for setting up the simulation condition. The impact these factors have on the amount of water that is carried away when a fixed mass flow of water is introduced into the domain is analyzed on the basis of the time it takes for the water to reach the domain exit is calculated. This indirectly gives us the rate through which the water moves through the domain and which parameters have a higher impact on water transport rate across the channel than the others.

After setting up the domain, with the base case with just two pores with a radius of 25 μm as seen in the figure below. The mass flow rate of the water inlet is taken to be $7gh^{-1}$ to expedite the water flow rate instead of using the flow rate of 0.2 gh^{-1} that occurs in a working fluid cell, the reason for this expedition is (use the reference from the paper here).

Based on the water inlet flow rate, the velocity of the water entering into the domain is calculated based on the total area of the pores. This can be seen in the equation below (see Equation 27):

$$v = \frac{\dot{m}}{\rho\, A} = \frac{\dot{m}}{\rho\,(N \times \pi r_{pore}^2)} \tag{27}$$

where v is the velocity of the inlet water (in ms^{-1}), $\dot{m}$ is the mass flow rate in (kgs^{-1}), ρ is the density of the fluid (water in this case)(in kgm^{-3}) and A is the total pore inlet area(in m^2), which is simplified further, where N is the number of pores and r is the radius of the said pore.

For, two pores of radius of $25\mu m$, and with the mass flow rate of $7gh^{-1}$ (which is $1.9444 \times 10^{-6}\ kgs^{-1}$), the velocity of the water at the inlet, based on equation above (see Equation 27), is calculated to be:

$$v_{w1} = \frac{1.9444 \times 10^{-6}}{10^3 \times 2\pi \times (25 \times 10^{-6})^2} = 0.495\ ms^{-1} \tag{28}$$

Now, with the velocity of the water kept **constant** at 0.495 ms^{-1}, the velocity of the air at the inlet is set first at 10 ms^{-1}, then lowered to 5 ms^{-1} to study the effect of the air velocity of the water behaviour. In both of these simulations, the static contact angle θ_C at the walls and the GDL is kept **neutral** (neither hydrophobic or hydrophilic) at 90°. The walls and the GDL layer are both assumed to be smooth in this case. This is to isolate the effect of the air inlet velocity on the water transport.

Then, the static contact angle θ_C of the GDL and the channel walls are changed to factor in their hydrophobicity and hydrophilicity respectively by setting them to be 140° and 45° respectively. These values are set based on the **material properties** of the GDL layer and channel walls used in working fuel cells. Values of the static contact angle θ_C above 90° indicate hydrophobicity and values below 90° indicate hydrophilicity. The velocity of the air inlet is set at 10 ms^{-1} as in the first simulation.

Simulation number	Fixed Factor	Factor observed
1	Pore radius ($r_{pore,1}$) = 25 μm, Water inlet velocity (v_{w1}) = 0.495 ms^{-1}, Static contact angle ($\theta_C = 90°$), Wall surface = Smooth	**Air inlet velocity ($v_{a,x}$)** v_{a1} = 10 ms^{-1} v_{a2} = 5 ms^{-1}
2	Pore radius ($r_{pore,1}$) = 25 μm, Water inlet velocity (v_{w1}) = 0.495 ms^{-1}, Air inlet velocity (V_{a1}) = 10 ms^{-1}, Wall surface = Smooth	**Static Contact angle (θ_C)** GDL angle ($\theta_{C,GDL}$) = 140° CW angle ($\theta_{C,CW}$) = 45°
3	Pore radius ($r_{pore,1}$) = 25 μm, Water inlet velocity (v_{w1}) = 0.495 ms^{-1}, Air inlet velocity (V_{a1}) = 10 ms^{-1}, GDL contact angle ($\theta_{C,GDL}$) = 140°, CW contact angle ($\theta_{C,CW}$) = 45°	**Wall roughness** Wall surface = Rough
4	Air inlet velocity V_{a1} = 10 ms^{-1}, GDL contact angle $\theta_{C,GDL}$ = 140°, CW contact angle $\theta_{C,CW}$ = 45°, Wall surface = Rough	**Pore radius ($r_{pore,x}$)** $r_{pore,1}$ = 25 μm, v_{w1}(28) $r_{pore,2}$ = 37.5 μm, v_{w2}(29) $r_{pore,3}$ = 50 μm, v_{w3}(30)

Table 5: Simulation configuration with the factor under observation

After assessing the effect of the hydrophobicity and the hydrophilicity of the GDL and the channel walls, the walls are changed from **smooth** to **rough** to see how this parameter affects water behaviour.

This set of simulations is repeated with different pore sizes of **radius 37.5 μm - an increase in pore size by 50%, and with the radius of 50 μm - an increase in pore size by 100%**, with lower velocities compared to the velocity found in Equation 28, due to conserve the mass flow rate. This can also be seen plainly from Equation 27, where the velocity is inversely proportional to the inlet pore area provided the other terms are constant - the mass flow rate ($\dot{m}$ is constant at 1.9444 $\times 10^{-6}$ kgs^{-1}) and the density (ρ is constant at 1000 kgm^{-3}). **So, to conserve the mass flow rate, the velocities of the larger pores would be lower**. From the Equation 27, we get the velocities for the altered pore sizes to be:

$$v_{w2} = \frac{1.9444 \times 10^{-6}}{10^3 \times 2\pi \times (37.5 \times 10^{-6})^2} = 0.2201\ ms^{-1} \tag{29}$$

$$v_{w3} = \frac{1.9444 \times 10^{-6}}{10^3 \times 2\pi \times (50 \times 10^{-6})^2} = 0.1238\ ms^{-1} \tag{30}$$

In analyzing the different inlet pore radii, with all the other settings being the same, i.e., the static contact angle and the type of surface roughness, we would see which factor would play a major role in the transport of the water - the inlet pore size or the velocity of the water flowing into the domain.

The simulations can be visualized with the varying parameters to understand the methodology as follows (see Table 5):

After running the simulations, the best case with the fastest water transport is calculated based on the amount of time it takes for the water droplet to reach the outlet of the domain is identified. This is done with the help of the variable introduced called the **time of water transport** (τ_t , measured in seconds). This variable tells us the time taken for the water transport to reach the exit from the beginning of the simulation time. This can be visualized in the formula as follows (see Equation 31):

$$\tau_t = (t_{time\ step}) \times (N_{time\ step}) \tag{31}$$

where $t_{time\ step}$ is the time step of the solver and $N_{time\ step}$ is the number of time steps it took for the first layer (surface) of the water to reach the outlet. After we calculate the time taken for the water to transport, we must calculate the average velocity of the water flowing through the channel. This can be done via, calculating the distance travelled by the water (D_w) in the transport time (τ_t).

The distance travelled by the water can be calculated as follows (see Equation 32):

$$D_w = L - D_2 = L - (D_1 + r_{pore}) = 1250\,\mu m - (250 + 25)\,\mu m = 975\,\mu m \tag{32}$$

where D_w is the distance travelled by the water, D_1 is the distance of the center of the pore from the channel inlet (Region 1) (see Figure 13) , D_2 is the distance that needs to be omitted from the channel length to calculate the distance travelled.

Based on the distance travelled by the water (D_w) and the time taken for the transport (τ_t), the average velocity of the water flow ($v_{wf,avg}$) can be calculated. This velocity will be lesser than the air inlet velocity, but will be strongly dependent on it, as this velocity is the driving force behind the water being carried off.

Based on the time of water transport (τ_t), the simulation conditions for analyzing the pore radii for the fastest water transport is chosen. This radii is then chosen to analyze the effect of the number of pores on the water droplet transport behaviour. The pores are then multiplied by a factor of two at each level, i.e. the base case being 2 pores, the next case being 4, then 8 and finally 16. These pores are then uniformly distributed and simulated to calculate the difference in the flow behaviour based on the number of pore inlets.

In the next simulation, the effect of humidity on water transport rate in a sixteen pore domain is calculated by using a multi-component Eulerian gas phase with varying levels of relative humidity (from 1% to 100%) of the air instead of a single-phased air as in the previous simulations. In this case, the mass fraction of the air inlet would include water vapour phase along with air as the inlet phase. The mass fraction of the multi-component gas would be used to determine the relative humidity of the air at the inlet.

In the final simulation, the effect of the humidity is not included, but instead the computational domain would be extended to replicate the serpentine channel pattern to study the effects of turns in the domain on the water droplet behaviour. This is to prevent exceedingly high simulation times due to the extended domain involving turns requiring fine mesh with constant refinement.

4 Results and Discussions

4.1 Effects of the parameters

4.1.1 Velocity of the inlet air and the inlet water:

- The velocity of the inlet air and the inlet water have an impact on both the profile of the water droplet at the emergence and when it flows through the channel. First, the impact of the **inlet water velocity** will be discussed with the help of the images obtained from the simulation 4 (Table 5), with the mass flow rate being kept constant at the inlet, and the velocity being changed owing to the radius of the pore (r_{pore}).

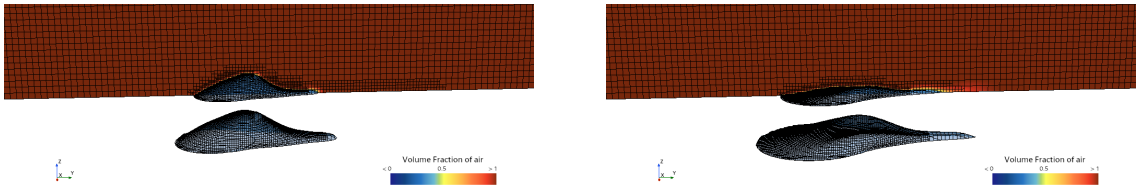

(a) Water droplet profile at higher velocity

(b) Water droplet profile at lower velocity

Figure 15: Droplet profiles at water inlet velocity - 0.495 ms^{-1} (L) ; 0.1238 ms^{-1} (R)

As seen from the figure above (see Figure 15), we can see the differences present in the shape of the profile due to different water velocities. The water droplet with the higher velocity has a convex profile with a higher peak compared to the other profile, which has two concave peaks but at a lower height. Due to the lower water inlet velocity, the water droplets do not rise to a peak before being sheared across the domain by the flowing air.

Due to the higher peak of the water droplet due to higher inlet water velocity, the water droplet tends to accumulate until the surface tension forces cannot compete against the shear stress introduced by the air velocity, which then begins the flow.

- The water inlet velocity has an effect beyond the emergence at the pores. Due to lower volume flowing from the peak, the cross section area of the stream flowing from the pore is **narrower**, since the cross section of the stream is lower, due to the shear force exhibited by the inlet air, the water stream elongates. Now, due to the elongation of the narrow stream, the stream becomes unstable - a phenomenon called **Rayleigh instability**. At this stage, the surface tension of the water droplet cannot keep the stream intact, leading to the stream breaking up into droplets. This can be observed in the figure (see Figure 16) given below.

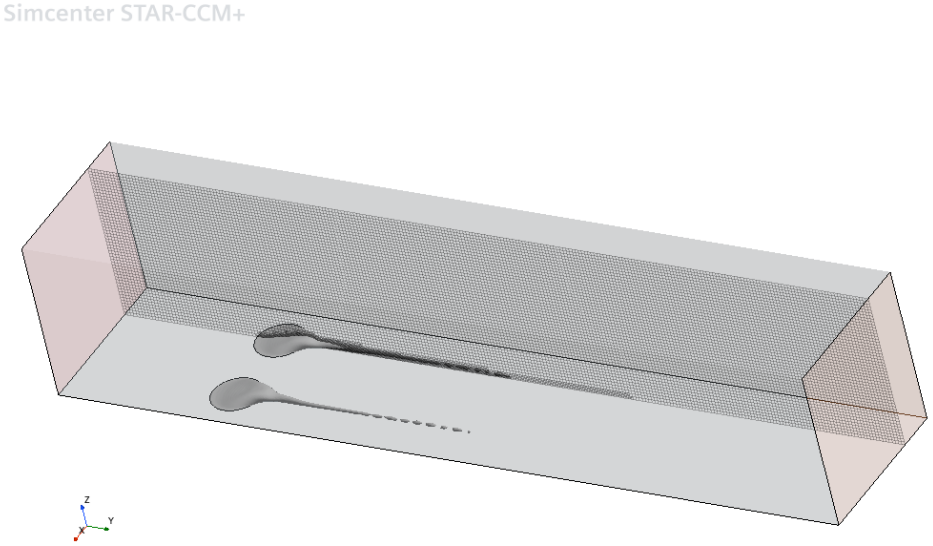

Figure 16: Droplet detachment downstream of the pore inlet

This physical phenomenon is captured accurately by the simulation.

- Secondly, the effect of the **air inlet velocity** has a much higher impact on the rate of the water being transported across the domain than the water inlet velocity. The rate of the water being transported has been assessed as per the simulation conditions set in simulation 1 (Table 5). In this case, the velocity of the air inlet (v_a) has been varied with v_{a1} at 10 ms^{-1} and v_{a2} at 5 ms^{-1}, then the amount of time to reach the exit of the domain (τ_t) is calculated, based on Equation 31. After this value is calculated, we can determine the average velocity of the water flow ($v_{wf,avg}$). This data has been tabulated below (see Table 6):

Air inlet velocity ($v_{a,x}$)	**Transport time** (τ_t)	**Avg. water velocity** ($v_{wf,avg}$)
10 ms^{-1}	1.194375×10^{-4} s	8.163265 ms^{-1}
5 ms^{-1}	2.218125×10^{-4} s	4.395604 ms^{-1}

Table 6: Impact of the air inlet velocity on the average water flow velocity

As seen from the table above (Table 6), the average flow velocity of water across the channel is strongly dependent on the air inlet velocity - and is higher ($v_{wf,avg} = 8.163265\ ms^{-1}$ when the $v_a = 10\ ms^{-1}$). This can be seen in the standard deviation between the two simulation conditions - **1.8838305**. However, when comparing the average water flow velocity relative to the air inlet velocity, the standard deviation is calculated to be **0.313972**.

Since the rate of the water transport is directly proportional to the velocity by which it flows, it is therefore, important to have a high inlet air velocity to transport water as fast as possible.

4.1.2 Static Contact angles (θ_C):

From the settings described for simulation 2 (Table 5), the static contact angle of the channel walls and the GDL have been altered to be more in accordance with the values demonstrated by the materials used in the actual working fuel cells.

In accordance with simulating the hydrophilic and the hydrophobic properties of the channel walls (CW) and the gas diffusion layer (GDL), the static contact angle has been set to 45° and 140° respectively. The effect of these angles has been compared with a neutral contact angle of 90° for both the channel walls and the GDL. Note that, this for illustrating the effect of the contact angle on the water transport rate and a neutral contact angle of 90° cannot be manufactured for actual working fuel cells. The flow pattern in the channel has been compared (see Figure 17) and the effect of the factor on the average water flow velocity ($v_{wf,avg}$) has also been tabulated below (see Table 7)for ease of understanding.

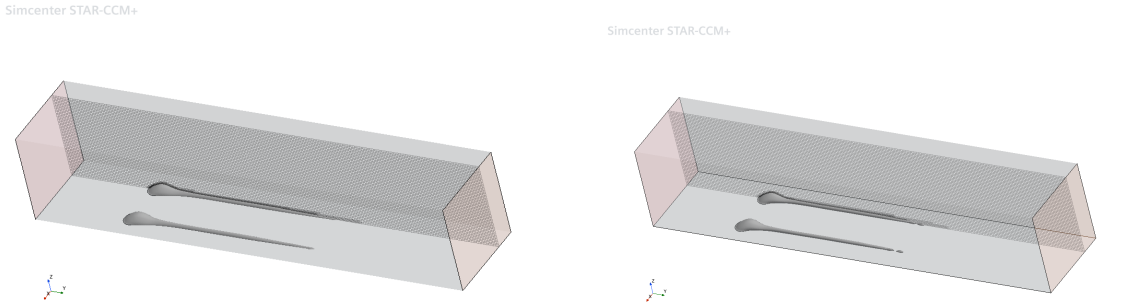

(a) Water flow profile with neutral contact angles

(b) Water flow profile with realistic contact angles

Figure 17: Flow profiles with different contact angles - 90°, 90° (L) ; 140°, 45° (R)

Contact angles ($\theta_{C,GDL}$, $\theta_{C,CW}$)	**Transport time (τ_t)**	**Avg. water velocity ($v_{wf,avg}$)**
90°, 90°	1.194375×10^{-4} s	8.163265 ms^{-1}
140°, 45°	1.218750×10^{-4} s	8.000000 ms^{-1}

Table 7: Impact of the static contact angle (θ_C) on the average water flow velocity

From Table 7 and Figure 17, it can be seen that the impact of the average water flow velocity is not significant - a standard deviation of only **0.081633**, however, the cross section area of the water stream is different due to the contact angle changes made. From the figure (see Figure 17), we can see that the water stream cross section area is wider with the neutral contact angles of 90° for both the channel walls and the GDL. This shows that the **water coverage area on the GDL is higher for the neutral contact angles**. This is not ideal in an actual working fuel cells, as it blocks the air and water mixture being diffused out of the pores after the oxygen reduction reaction (ORR) is completed. This is in accordance with the theory depicting the contact angle and the cross-section area of the drop on the surface (see Figure 12).

In addition to the disadvantage with the coverage area, static contact angles of 90° is not feasible to construct and replicate in an actual working fuel cell.

4.1.3 Wall roughness of the GDL & Channel Walls:

As per the simulation settings in simulation 3 (Table 5), with all the factors being kept constant, the roughness of the GDL and the channel walls has been changed to depict the reality of the porous and rough surfaced materials used in actual working fuel cells. The effect of this difference in wall roughness is straightforward (see Table 8):

Wall roughness	**Transport time (τ_t)**	**Avg. water velocity ($v_{wf,avg}$)**
Smooth	1.194375×10^{-4} s	8.163265 ms^{-1}
Rough	1.243125×10^{-4} s	7.843137 ms^{-1}

Table 8: Impact of the wall roughness on the average water flow velocity

From the Table 8, we can see that the roughness of the GDL and the Channel Walls plays a major role in reducing the average velocity of the water film due to friction - with a standard deviation of **0.160064**, and therefore, the **roughness of the walls leads to slower removal of water from the channel**, and subsequently lesser volume of water being transported out.

Despite, the friction reducing the rate of water transport, this simulation setting will be proceeded with because, in reality, the surface of the walls and the GDL in the channel would be rough.

4.1.4 Pore size:

The size of the pore of the inlet is varied as per the conditions in simulation 4 (Table 5) to gauge the effect of the pore size on the water removal rates. The pore sizes used for this simulation are $r_{pore,1} = 25\ \mu m$, $r_{pore,2} = 37.5\ \mu m$ and $r_{pore,3} = 50\ \mu m$. The mass flow rate is conserved in this configuration. So, to account for the change in area of the pores, the velocity of the pores is altered (see Equations 29 and 30).

Pore size (r_{pore})	**Transport time (τ_t)**	**Avg. water velocity ($v_{wf,avg}$)**
25 μm	1.243125×10^{-4} s	7.843137 ms^{-1}
37.5 μm	1.297400×10^{-4} s	7.515000 ms^{-1}
50 μm	1.418730×10^{-4} s	6.872340 ms^{-1}

Table 9: Impact of the pore size on the average water flow velocity

Since the water inlet velocity is reduced with an increase in pore size, this is reflected in the average water flow velocity (see Table 9). The **increase in pore size lowers the average water flow velocity**. However, if the velocity of the water inlet is kept constant despite the change in the pore size, i.e. the mass flow rate is not conserved, then, the impact of the pore size on the water flow velocity can be understood more clearly. This can be seen in the table below (see Table 10):

Pore size (r_{pore})	**Transport time** (τ_t)	**Avg. water velocity** ($v_{wf,avg}$)
25 μm	1.243125×10^{-4} s	7.843137 ms^{-1}
37.5 μm	1.270000×10^{-4} s	7.677165 ms^{-1}
50 μm	1.245000×10^{-4} s	7.831325 ms^{-1}

Table 10: Impact of the pore size on the water flow velocity when mass is not conserved

It can be seen that there is **no significant variation in the average water flow velocity** when the mass flow rate of water is **not conserved**.

In addition to this, the pore size impacts the flow behaviour of the water droplets across the channels. These can be seen in the figure below (see Figure 18), where **there is a higher and faster tendency for droplet formation with an increase in the pore size**. It can also been seen that for the same time step, the water flow profile is much further down stream for the domain with 25 μm pore radius (see Table 9). This is partly due to the higher water inlet velocity, which prevents the formation of water droplets.

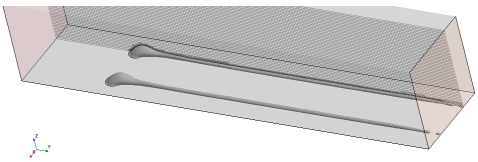

(a) Water flow profile with 25 μm radius

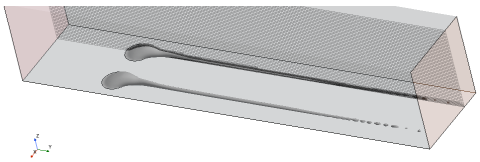

(b) Water flow profile with 37.5 μm radius

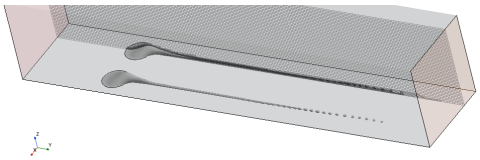

(c) Water flow profile with 50 μm radius

Figure 18: Flow profiles with different pore radii - 25 μm (LU); 50μm (RU); 37.5 μm (C)

In addition to this, the pore size impacts the flow behaviour of the water droplets across the channels. These can be seen in the figure above (see Figure 18), where **there is a higher and faster tendency for droplet formation with an increase in the pore size**. It can also been seen that for the same time step, the water flow profile is much further down stream for the domain with 25 μm pore radius (see Table 9 and Figure 18). This is partly due to the higher water inlet velocity, which prevents the formation of water droplets.

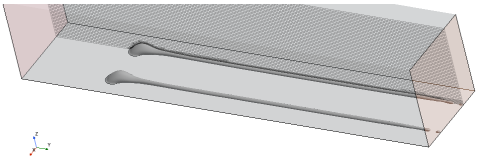

(a) Water flow profile with 25 μm radius

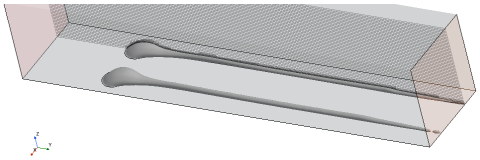

(b) Water flow profile with 37.5 μm radius

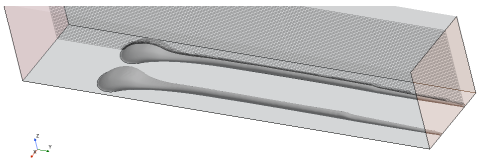

(c) Water flow profile with 50 μm radius

Figure 19: Flow profiles with different pore radii - 25 μm (LU); 50μm (RU); 37.5 μm (C) with unconserved mass flow rate

When the water inlet velocity was kept constant and the pore radius was varied (mass flow rate was not conserved), the droplet formation process was diminished and the average velocities of the water flow became very similar across all the pore radii variations (see Figure 19).

With this observation we can confirm that the velocity of the water inlet (v_w) plays a bigger role compared to the pore size r_{pore}. The average velocity of the water film ($v_{wf,avg}$) was similar with a standard deviation of only **0.075609** when the mass flow rate was not conserved. However, when the water inlet velocity was varied in accordance to the conservation of the mass flow rate, the standard deviation was **0.403200**.

The comparison between different water film velocities of the same pore size but for different inlet water velocities shows that the standard deviation is maximum for the 50 μm pore radius at **0.479493**. However, since the mass flow rates into the domain from the pore inlet is fixed by the rate of the oxygen reduction reaction and the current density of the fuel cell, the standard deviation for the impact of the pore size on average water film velocity will be considered only for the mass conserved case i.e. **0.403200**.

Based on this observation, the simulation configuration for the next simulations analyzing the effect of the number of pores would be based on the smallest pore radius used i.e. $r_{pore} = 25\ \mu m$.

4.1.5 Pore number:

In this section, the effect of the number of pores on the water transport behaviour will be discussed and an assessment regarding the impact of the factor is made with the pore radius (r_{pore}) would be kept at 25 μm and the number of the pores would be increased exponentially to 4, then 8 and then 16 pores. The arrangement of the pores would be as shown in the figure below (see Figures 20 and 21)

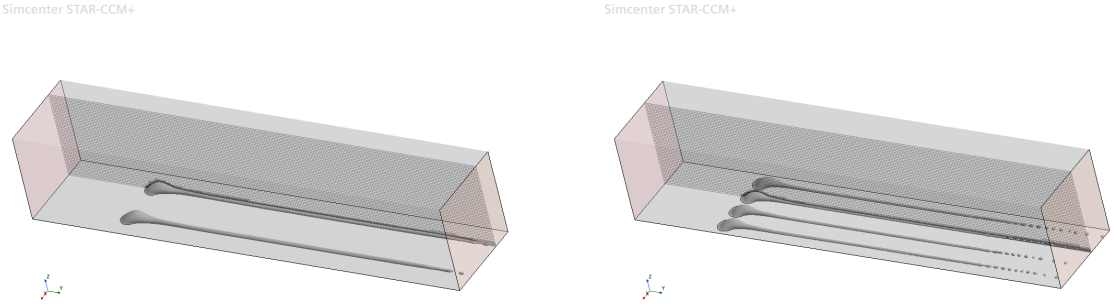

(a) Water flow profile for 2 pores

(b) Water flow profile for 4 pores

Figure 20: Flow profiles with different pore numbers - 2 pores (L) ; 4 pores (R)

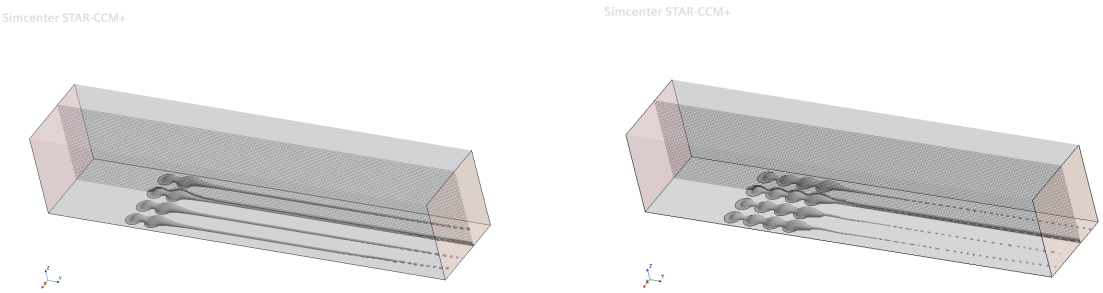

(a) Water flow profile for 8 pores

(b) Water flow profile for 16 pores

Figure 21: Flow profiles with different pore numbers - 8 pores (L) ; 16 pores (R)

The average water film velocity of the different pore simulation configuration has been calculated and shown in a tabular form below (see Table 11):

Pore number	**Transport time (τ_t)**	**Avg. water velocity ($v_{wf,avg}$)**
2	1.243125×10^{-4} s	7.843137 ms^{-1}
4	1.271690×10^{-4} s	7.666900 ms^{-1}
8	1.421610×10^{-4} s	6.436360 ms^{-1}
16	1.720000×10^{-4} s	4.622093 ms^{-1}

Table 11: Impact of the pore number on the water flow velocity

It can be seen that the despite the shorter distance to travel for the last row of pores to reach the end of the channel, the average flow velocity of the water layer is lower with an increase in the number of pores with a standard deviation of **1.286027**. This is due to the larger influence of the water inlet velocity.

In addition to the slower transport of water across the flow channel, there is a higher tendency to from droplets when the number of pores increases with the highest number of droplets being formed in the domain with 16 pores.

Note: Due to the low inlet water velocity (v_w), the cross section area of the stream was extremely narrow in the simulation with 8 pores. Due to this, the size of the water droplets

being formed was extremely small. Due to the small droplet size, the cells downstream of the interface were not refined by the adaptive mesh with the proceeding time step leading to the droplets furthest downstream to freeze in place. This lead to the droplets following to collide with the first droplet, creating a back-flow in a region with no physical reason for it to exist. Due to the sharp interface reconstruction of the AMR based HRIC model, the small sized droplets were not resolved properly leading to the emergence of non-physical shaped particles, further exacerbating the back-flow. So, the back flow and collision based instability lead to the residuals of the simulation to become unnaturally high (see Figure 22).

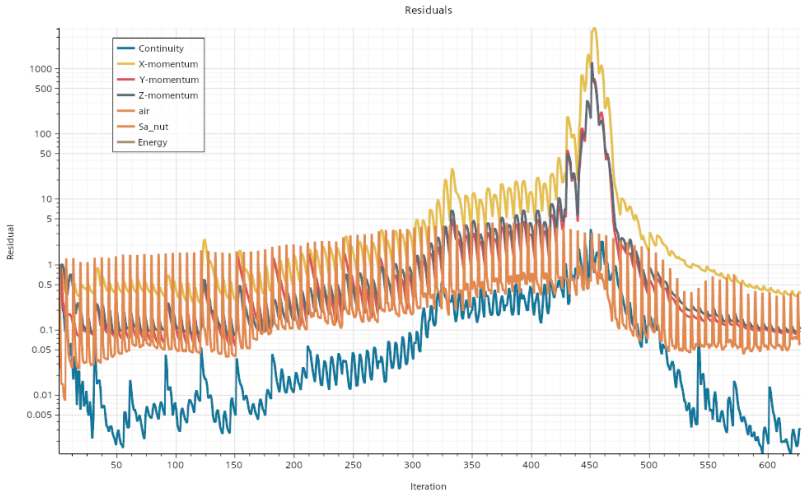

Figure 22: AMR instability due to small sized water blobs resulting in high residuals

To overcome this, the blobs of the Eulerian water phase was transitioned to Lagrangian particles instead of reducing the cell size further to save computational costs. In the Eulerian Blob to Lagrangian particle transition model, the mesh size would remain coarse instead of being finely refined to keep the simulation time low. With the help of the LPT model, the residuals were brought down significantly (see Figure 23).

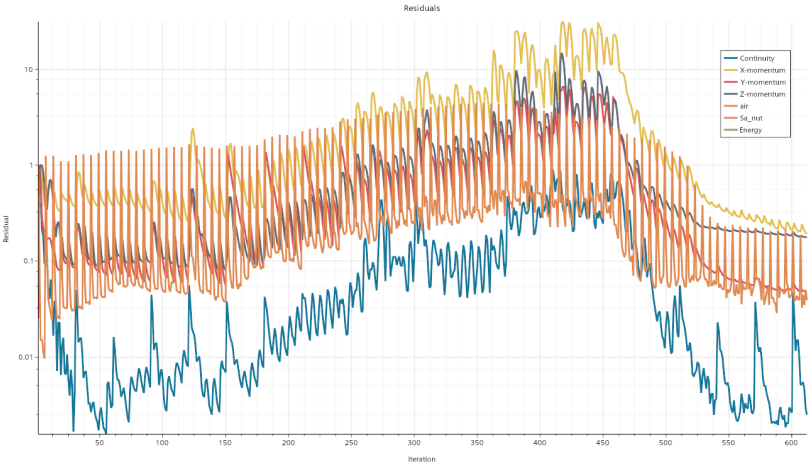

Figure 23: Residuals after incorporating Lagrangian Particle Tracking into the VOF model

4.1.6 Humidity:

For the humidity calculation, the operating temperature of the fuel cell must be taken into account to calculate the relative humidity, as the pressure of the dry air and the vapour pressure of water are highly reliant of the temperature. So, the general operating temperature of PEM fuel cell of 85°C was taken for the calculation.

With the operating temperature of 85°C (358 K), the properties of dry air, saturated water vapour pressure, density were calculated from literature and shown below:

Property	Value
Air density (ρ_{air})	0.98549 kgm^{-3}
Dry air pressure ($P_{dry,air}$)	101.325 kPa
Saturated water pressure ($P_{sat,w}$)	57.867 kPa

Table 12: Air and water properties at 85°C (358 K)

From the air properties given in Table 12, the mass flow rate of the air supplied is calculated as follows:

$$\dot{m_a} = \rho_{air} \times A_{inlet} \times v_a = 0.986 \times (250 \times 10^{-6})^2 \times 10 = 6.1625 \times 10^{-7} kg/s \tag{33}$$

where A is the area of the inlet at the domain (250 μm × 250 μm) and v_a is the air inlet velocity of 10 ms^{-1}.

The mass flow rate of the water to be added to the air to humidify it is calculated based on the Equation 26. On substituting the values from Table 12 and Equation 33, which gives:

$$\dot{m_w} = 0.622 \times \frac{P_w}{P_{in} - P_w} \times \dot{m_a} = 3.782951 \times 10^{-9} \times P_w \tag{34}$$

To obtain the required level of humidity, the amount of water that needs to be added to the air inlet is dependent on the vapour pressure of water (P_w). Equation 34 is an adaptation of Equation 26 to convert the mass of water to be added ($\dot{m_w}$) to be a **function** of the vapour pressure of water (P_w). The denominator in Equation 34 is reduced to ($P_{in} - P_w = P_{dry,air}$). Since the terms ($P_{dry,air}$, $\dot{m_a}$) are known, the equation is simplified such that the mass of water to be added at the air inlet ($\dot{m_w}$) to be just a function of the vapour pressure of water (P_w).

Based on the values from Equations 33 and 34, the mass fractions of the humidified air can be calculated using the equation below (see Equation 35):

$$m_i = \frac{m_i}{\Sigma(m_i)} \tag{35}$$

Where the suffix i denotes the components present. This gives the values of the mass fraction of air and water (from Equation 35) to be denoted in the form [m_a, m_w].

Based on the mass fractions of air and water, the multi-component gas at the air inlet can be used to simulate the effect of various levels of relative humidity have on the mass transfer rates of the water across the channel domain.

Humidity (RH) (ϕ)	**Transport time (τ_t)**	**Avg. water velocity ($v_{wf,avg}$)**
1% RH	2.7225×10^{-4} s	2.920110 ms^{-1}
10% RH	2.6375×10^{-4} s	3.014218 ms^{-1}
20% RH	2.4625×10^{-4} s	3.228426 ms^{-1}
40% RH	2.6625×10^{-4} s	2.985915 ms^{-1}
60% RH	2.6750×10^{-4} s	2.971963 ms^{-1}
80% RH	2.8250×10^{-4} s	2.814159 ms^{-1}
100% RH	3.2375×10^{-4} s	2.455598 ms^{-1}

Table 13: Impact of humidity on the average water flow velocity

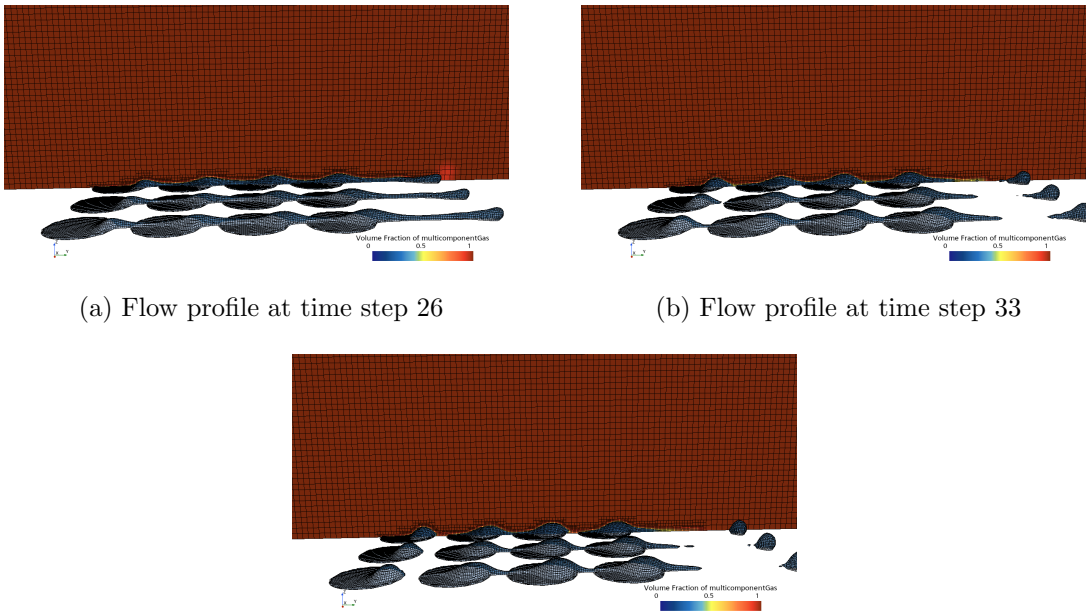

(a) Flow profile at time step 26

(b) Flow profile at time step 33

(c) Flow profile at time step 36

Figure 24: Flow profiles at 20% RH at time steps - 26 (LU); 33 (RU); 36 (C)

From Table 13, it can be seen that the average water film velocity ($v_{wf,avg}$) has a maximum velocity at a relative humidity of 20% RH. The drop in velocity from this region is due to the slower transport of water droplets due to coalescence. The smaller droplets on collision and subsequent collision tend to move at an angle to the Y axis, causing them to take a longer path and time to reach the exit. For the pores located near the walls, the droplets tend to collide with the wall and continue propagating along the channel walls until they reach the exit. Since the walls are hydrophilic, they tend to reduce the water droplet velocity when flowing across their surface.

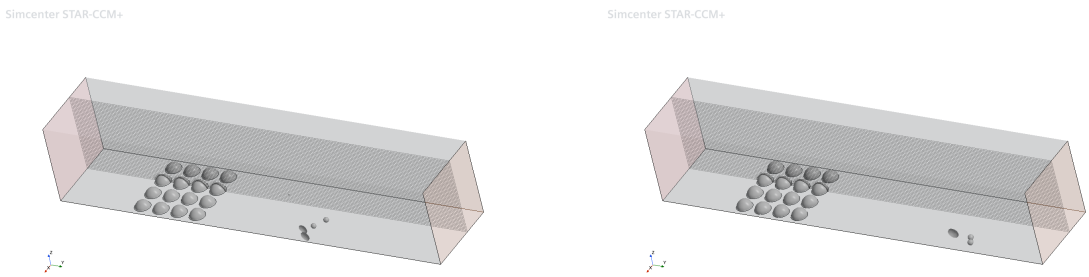

(a) Coalescence of droplets on the channel walls

(b) Coalescence of droplets on the GDL layer

Figure 25: Droplet coalescence at 40% RH - on the CW surface (L) ; on the GDL surface (R)

The standard deviation of the average water flow velocity between the various levels of relative humidity (see Table 13) is **0.243594**, shows the affect humidity has on the water transport behaviour across the domain.

The reduction of the average water film velocity at higher levels of relative humidity (above 20%) is in accordance with the physical laws surrounding humid air. In short, the longer transport times are due to the following factors:

1. Decrease in the gas phase density due to increase in humidity. The molecular weight of water (18 g/mol) is lower when compared to the molecular weight of water (29 g/mol). The reduction in density reduces the support from the gas phase to the droplet flowing across the channel.
2. There is also a slight increase in viscosity due to higher levels of humidity due to collisions between the air and water vapour molecules, leading to a higher drag force on the droplets, slowing down the droplet.
3. Coalescence of water droplets, aided by the condensation effects due to higher levels of humidity, results in larger water droplets being formed, adding on mass leading to a greater drag force on the droplet.
4. Interference from air molecules, due to an increase in the number of molecules, due to higher levels of humidity, the frequency of collisions between the gas phase and the droplets leads to higher resistance slowing down the droplet movement.

4.1.7 Extended domain:

To replicate the serpentine channels as close as possible, the domain from Figure 13 had to be extended to include the turns that are present in a serpentine channel. The number of pores in this domain was taken to be sixteen to include the effects of multiple pores as well. Humidity was not included to reduce the computational resources and lower the run time. The extended domain has been shown in the figure below (Fig):

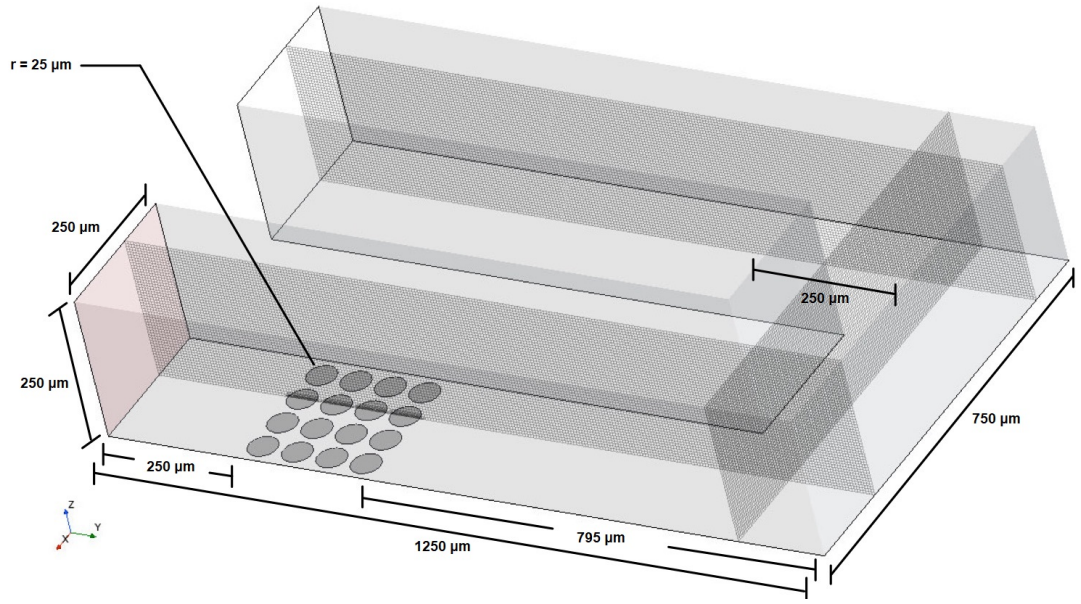

Figure 26: Extended computational domain with labelled dimensions

The simulation setup for this domain is the same as in Simulation 4 (see Table 5) with 16 pores and the pore radius (r_{pore}) of 25 μm. The water flow behaviour has been simulated with the extended domain and can be seen in the following figure (see Figure 27):

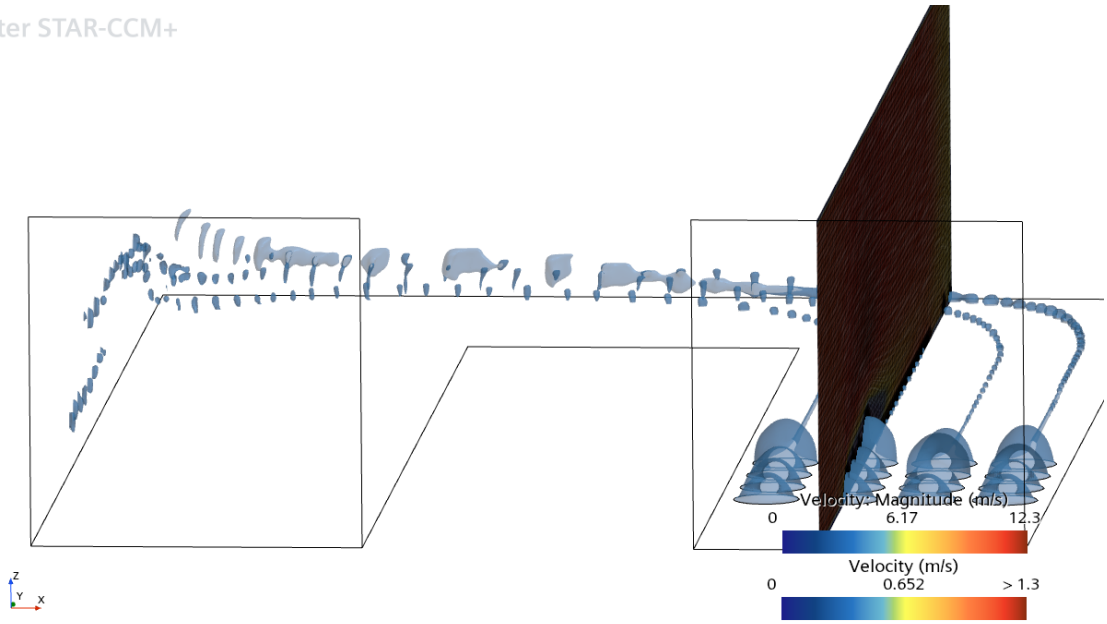

Figure 27: Water flow pattern of the extended domain

From Figure 27, it can be seen that due to the bend present in the domain and the lag in the momentum of the water droplets, results in the droplets moving up the channel walls. In addition to this, the droplets from the individual streams from the pores coalesce due

to the turn resulting in larger and heavier droplets and can be seen in the figure below (see Figure 28):

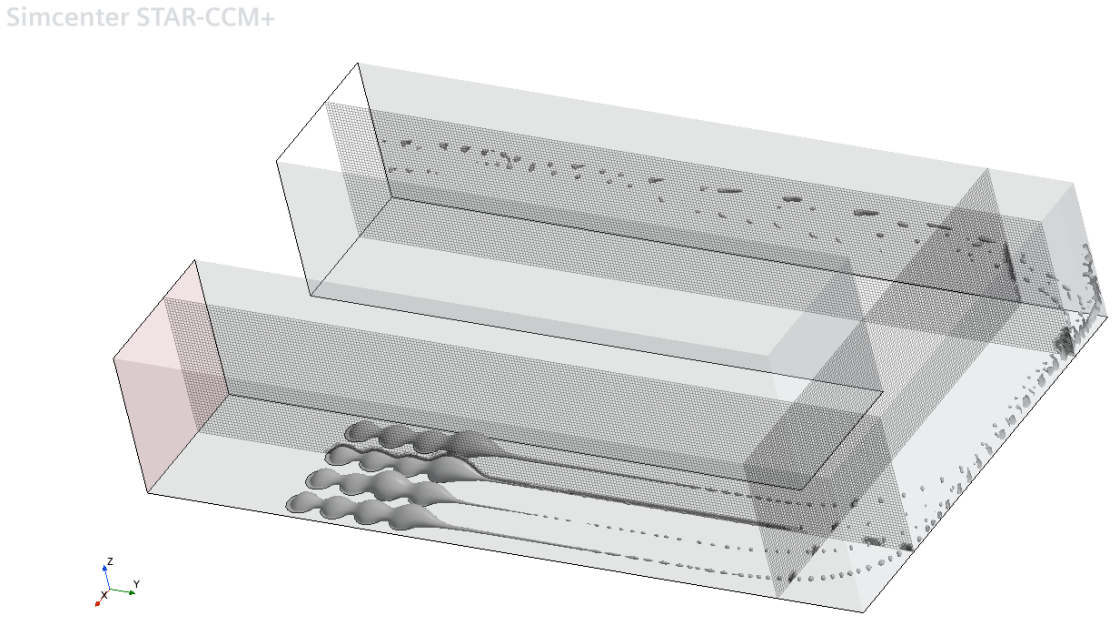

Figure 28: Water droplet stream coalescence due to bend in domain

The velocity vector field of the domain has also been included to show the development of the flow profile at the pore inlets and subsequent transport in the figure below (see Figure 29):

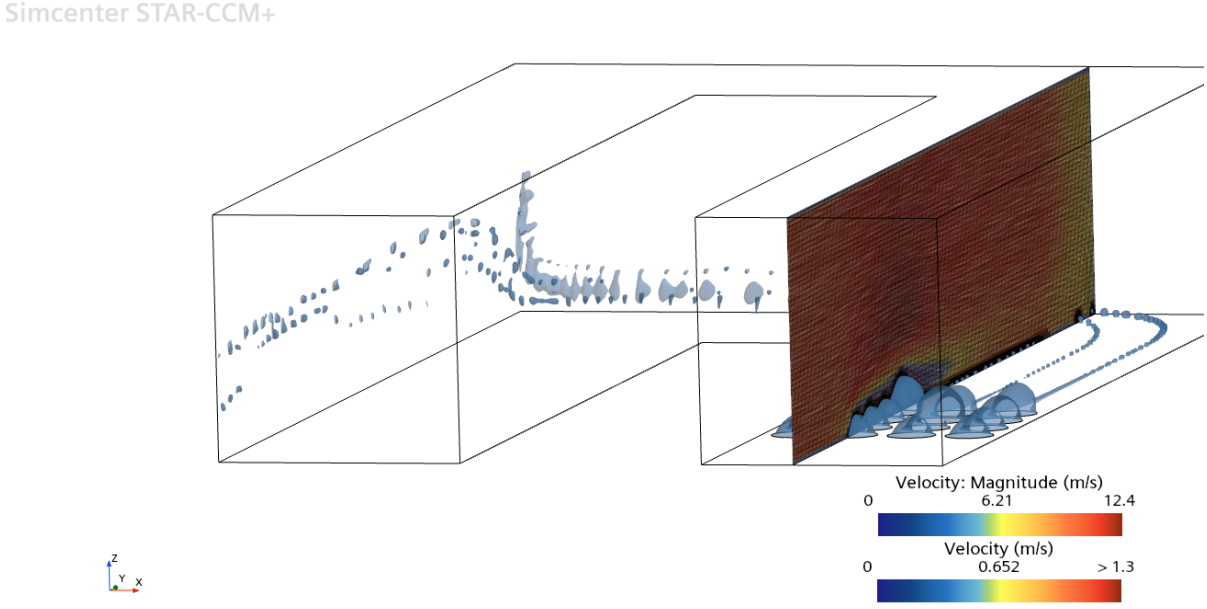

Figure 29: Velocity vector field of the water droplets in the extended domain

It can be seen that the velocity of the air encounters a break at the beginning of the

pore system leading to a higher magnitude in the region above the pore inlet showing the compensation of the velocity due to reduction in area. The boundary layer flow formation due to the droplet emergence can also be noted in the figure. The model is able to accurately demonstrate the air flow patterns in the domain in accordance to the flow physics theory.

The droplet profile of the water droplets along the hydrophilic channel walls and the hydrophobic GDL surface has been shown in the figure below (see Figure 30). The profile of the water droplets present on the walls is in line with the droplet profile shown in Figure 12, proving that the profile and behaviour of the water droplet is in line with the physics of a hydrophilic surface.

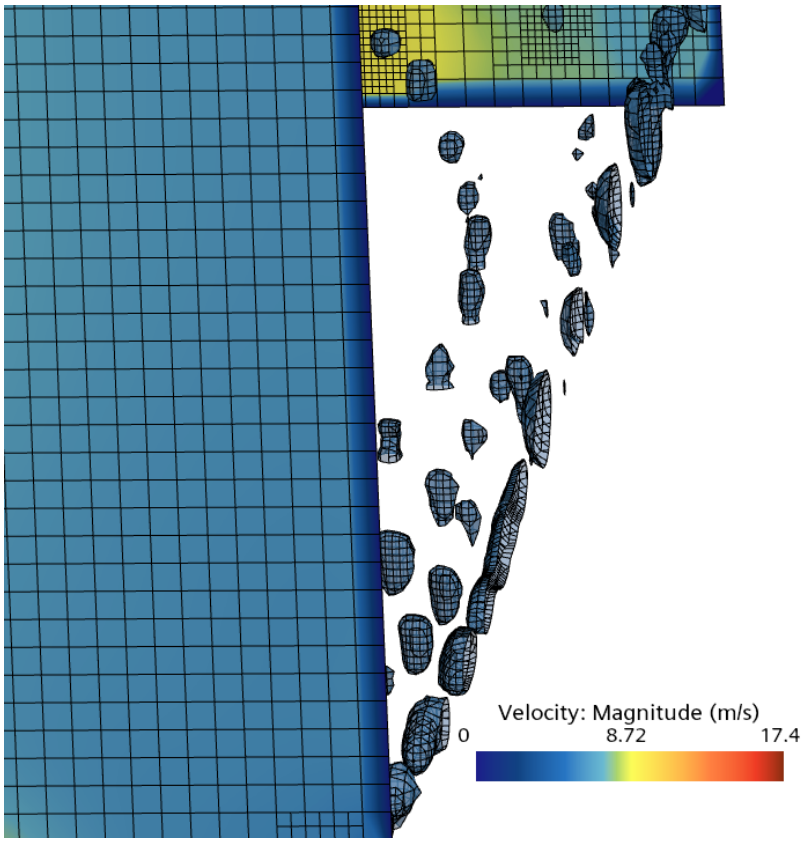

Figure 30: Hydrophilic & Hydrophobic surface effect on the droplet profile

To calculate the average water film velocity, the distance travelled by the water droplet had to be assumed to based on the center-line of the domain components. This can be seen in the following equation (see Equation 36):

$$D_{w,total} = D_{w,1} + D_{w,2} + D_{w,3} \tag{36}$$

where $D_{w,total}$ is the total distance travelled by the water film. $D_{w,1}$ is the distance travelled by the water from the last row of the pores to the center-line of the section perpendicular to the first section. $D_{w,2}$ is the distance travelled by the water from the center-line of the first section to the center-line of the third section (section after the turn). $D_{w,3}$ is the distance travelled by the water from the center-line of the second section to the exit of

the domain. The value for the total distance travelled based on the aforementioned sum of distances (from Equation 36) comes up to **2295** μm (see Equation 37):

$$D_{w,total} = (795 - 125) + (750 - 250) + (1250 - 125) = 2295\mu m \tag{37}$$

Based on this distance travelled, the average water film velocity ($v_{wf,avg}$) has been calculated and shown below in the table below (see Table 14):

Transport time (τ_t)	**Avg. water velocity ($v_{wf,avg}$)**
4.814697×10^{-4} s	4.7666551 ms^{-1}

Table 14: Transport time and the average water film velocity in the extended domain

4.2 Discussion, limitations and future work

4.2.1 Discussion of the results

In Section 3.5.5, the factors that were identified to have the most impact on the water transport rates were identified and were investigated with the help of simulation tools. The impact of the factors on the simulation results have also been discussed in previous sections. The variations in the factors has been tested out and the results - the time taken for the transport of the water from the first row of the pore inlets (from the exit) (τ_t) and the average water film velocity ($v_{wf,avg}$) of the water droplets (stream in certain cases) were calculated.

Based on the calculated average water film velocities, the **standard deviation** for each of the simulation configurations (see Table 5) have been calculated to show the variations of the factor under study had on the water velocity. The higher the standard deviation, the more the variations in the velocity of the configuration. This indirectly translates to the impact the said factor has on the velocity of the water film. **Higher the standard deviation (σ), higher the impact**.

In the table below (see Table 15), the standard deviation from the factors under investigation has been arranged in decreasing order, from the factor that has the most impact to the factor with the least impact. This indicates the factors that play a major role and that can be optimized for better water transport rates across the channel.

Ranking	Factor under investigation	Standard Deviation (σ)
1	Air inlet velocity (v_a)	1.883831
2	Pore number (N_{pore})	1.286027
3	Pore radius (r_{pore})	0.403200
4	Relative Humidity (ϕ)	0.243594
5	Wall Roughness	0.160064
6	Static contact angles ($\theta_{C,CW}, \theta_{C,GDL}$)	0.081633

Table 15: Impact of various factors investigated based on the standard deviation (σ)

It can be seen that the **maximum impact on average film velocity ($v_{wf,avg}$) is by the inlet air velocity (v_a)** as the gas phase is the primary driving force behind the movement of the water droplets across the domain. The higher the air velocity is, the faster the water droplets are pushed across the channel.

After the air inlet velocity, the next major impact on the average water film velocity is due to the number of pores (N_{pore}). The larger number of pores mean that with the mass flow rate of the system being constant, the larger area due to the larger number of pores, imply a smaller water inlet velocity. So, the larger number of pores indirectly, indicate that the major impact of the water inlet velocity (v_W) at the pores of the domain.

The pore radius (r_{pore}) also plays a major role on the water film velocities in a similar fashion to the factor above. The larger the pore radius (r_{pore}), the larger the area of the inlet, the slower the water inlet velocity (v_w). This factor also implicitly ties into the impact of the water inlet velocity (v_w) has on the water transport rates across the domain.

In short, the **water inlet velocity (v_w) exerts its influence via the pores - through the number of pores (N_{pore}) and the pore radius (r_{pore})**.

Then, the operating conditions of the system, i.e. the relative humidity (ϕ) of the gas phase plays a major role because the **humidity dictates the density of the air present, which in turn dictates the momentum and the force** with which the air is flowing. As seen from the impact of the air velocity, the primary driving force behind water movement, the force exerted by the air is fundamental to the water movement when the inlet velocity is the same in both the cases.

Finally, the materials involved in the construction of the domain exercise their influence in the water transport behaviour. The roughness of the surfaces and the hydrophobicity/hydrophilicity of the gas diffusion layer (GDL) and the channel walls (CW) respectively **alter the water droplet behaviour by influencing the surface tension forces** acting on the interface between the droplet and the surface it flows on.

Based on the above factors, one could identify ways to optimize the water droplet behaviour and transport rates across the flow channels of the gas diffusion layer of the PEM fuel cell. The factors of importance to optimize (in the order of priority) are **the air inlet velocity (v_a), the water inlet geometry (N_{pore}) and (r_{pore}), and the relative humidity (ϕ) of the inlet air**.

The average film velocity ($v_{wf,avg}$) of all the simulations has been **summarized** in the graph below (see Figure 31) for ease of visualization. It can be observed that the highest average water film velocity ($v_{wf,avg} = 8.163265\ ms^{-1}$) occurs when the inlet air velocity (v_a) is $10\ ms^{-1}$, the wall surfaces are smooth and the static contact angles ($\theta_{C,GDL}, \theta_{C,CW}$) are neutral. This has been shown at three instances on the graph as it was the idealistic base case.

The lowest average water film velocity ($v_{wf,avg} = 2.455598\ ms^{-1}$) when the relative humidity (ϕ) of the gas phase at the air inlet was 100 %RH.

The drastic decrease in the velocity of dry air at 16 pores and the humid air with 1% RH is due to the incorporation of several additional parameters to ascertain the effect of humidity as close to reality as possible. The temperature of the gas phase and of the domain was modified to be 85 $^{\circ}C$ (or 358K) to simulate the higher end of the operating temperature of a working fuel cell. In addition to this, the gas phase was changed from a single phase gas to a multi-component gas with air and water vapour as the constituent phases. The vapour pressure and the relative humidity levels were used to calculate the mass fraction to define the content of the multi-component gas. Due to this, the forces acting on the water droplet were markedly different. The water emergence profile also was drastically different (compare Figures 15 and 24) and the droplet detachment being discontinued after the formation of limited number of droplets.

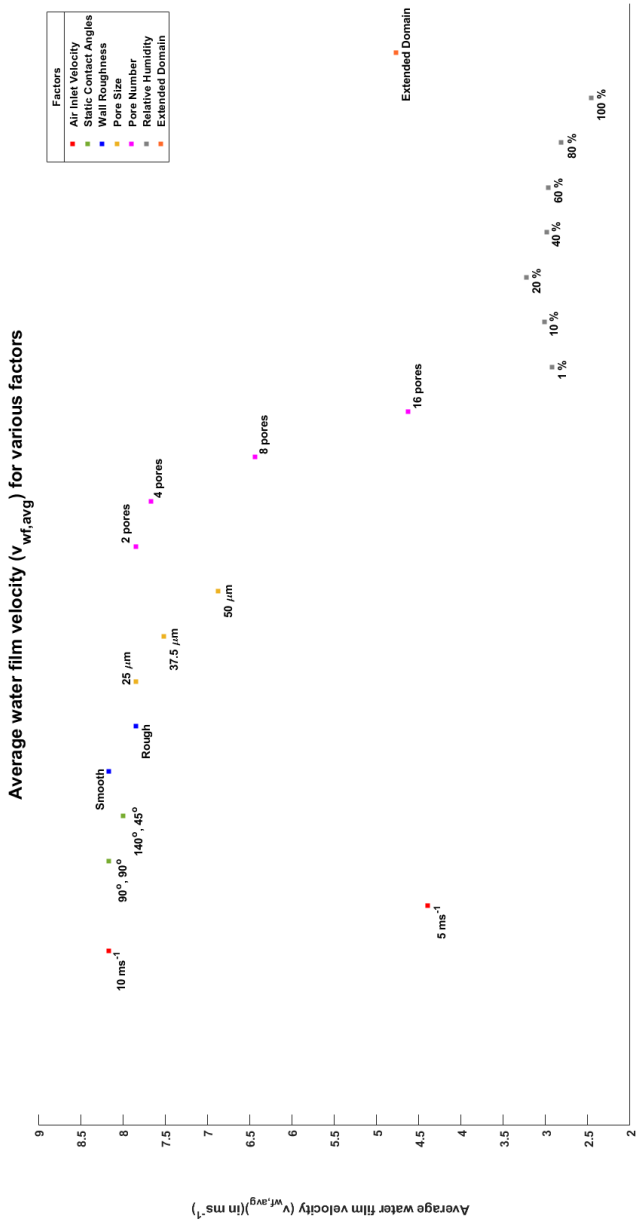

Figure 31: Summary of the individual average water film velocities for various factors and variations

Note: The angles for the Static Contact Angles data set in the graph are of the GDL and the channel walls respectively ($\theta_{C,GDL}$, $\theta_{C,CW}$).

4.2.2 Limitations of the results

As seen previously in Section 2.7, it is impossible to simulate the entirety of the flow channels with real-life descriptions of the materials used in the simulation. The concessions

made to study the simulation have a undeniable effect on the accuracy of the simulation. Since, a simulation model itself is based on several approximations, the accuracy of the results is heavily reliant on how close the assumptions made with respect to the factors under study. This section reiterates the assumptions taken in accordance to each aspect of the factor tested and how the simplification limits the results when compared to its real-life counterpart.

1. **Water inlet distribution:** In the simulation, the water inlets were placed at a location along the channel length, where the air flow would be well-developed and the distance to the channel exit would allow for the water film to be well-developed and undergo all the phenomenon that are possible. However, in reality, the water originates across the entire GDL, so some droplets would emerge near the exit, some would emerge next to the inlet and so on. The droplets from these locations would also interact with the droplets emerging from other randomized locations. These pores also have different diameters and different shapes across different orders of magnitude. Therefore, this would be extremely hard to simulate all the locations, number and sizes of the water inlets across the GDL. Even if this was managed, the effects of each individual factors could not be identified readily due the overlapping of the effects of each factor.

   So, the effects of the pore sizes, the number of pores and the location of the pores has been simulated individually to assess their importance in terms of water transport rate. Also, the shape of the pores has been simplified to be a circle for ease of simulating the droplet formation and emergence. This division of the factors into simplified versions affects the accuracy of the simulation compared to real-life functioning of a fuel cell. But, it does provide an insight into which factors affect the transport of water the most, providing a starting point from which complex simulations involving multiple factors being considered simultaneously could be undertaken in the future.

2. **GDL surface and Channel Walls:** In the simulation, the GDL and the Channel Walls surfaces were simulated to be non-porous surface and to be simulated based on the static contact angle to monitor the effects of the surface tension of the interface across its surface. In reality, the presence of pores along the GDL and the channel walls due to the use of carbon fibre based components has a definitive effect on the surface tension forces acting with varying contact angles on the droplet of water. The difficulty in accurately simulating a porous surface has already been mentioned. In addition to this, surface tension forces are hard to simulate due to a break in continuum of the particles near the boundary of the surface and the interface between the phases. If the boundary of the surface is not planar and has geometric features like pores and extrusions, then it becomes downright impossible to simulate the surface tension effects.

   In order to compute the effects of surface tension, the surfaces have to be taken as planar surfaces with limited roughness and a static contact angle to simplify these complex parameters into manageable and controllable factors. The static contact angle is sufficient to simplify the varying contact angles of the actual GDL and channel walls and implicitly factoring in the hydrophobicity and the hydrophilicity of the components accurately compared to their real-life counterparts.

   Since, all the minutiae of the GDL surface and channel walls cannot be replicated,

the simplifications are capable of simulating the major phenomenon of the surfaces accurately without complications.

3. **Constant density of the gas phase:** The gases that have been simulated possess constant density, i.e. they are incompressible. This is to facilitate the ease of calculating the relative humidity of the dry air and the partial pressure of water to identify the amount of mass of water that needs to be added to the dry air to assess the effects of humidity on water emergence and transport behaviour across the channels.

   However, in reality, the gas passing across the channel would have varying density based on the extent to which the water phase occupies the domain space, which was previously occupied by the gas phase. This would ensure higher density in regions where the cross-section area of the gas phase passing through would be lesser. In the simulation, the effect of the gas phase incompressibility can be seen when the velocity compensates for the reduction in the cross-section area by increasing proportionally to maintain the constant mass flow rate.

   This approximation helps us assess the mass conservation of the air and therefore calculate the mass transfer of the water phase accurately. If the density was not assumed to be constant, the density would be the factor compensating for the reduction in cross-section area. This would hinder us in our study of seeing the changes in velocity of the air due to the water present and this loss of information would make it harder to identify bottlenecks (regions of low velocity - dead zones) of the mass flow of the water as it is highly dependent of the velocity of the air flowing over it. (see results from air inlet velocity)

   The simplification eases the identifying of the bottlenecks to the water flow, it can help point the way to fixing the design issues that would later be useful in handling varying density of the gas flow when flowing across the upgraded domain.

4. **Humidity:** Additional simulation models to handle multiple complex phenomenon like evaporation and condensation was also tested, but was unsuccessful due to the simulation limits on the time scale of the evaporation process. The time steps to study these effects would have to be minimized, in addition to creating extremely fine meshes to capture the interaction between the water vapour phase and the liquid phase. Phase interaction models would be required to capture the involvement of not only three phases (including water vapour) individually but also the exponential increase in the number of inter-phase reactions with addition of every new phase. Due to these reasons, the simulation requirements in terms of computational resources would be very expensive and would result in extremely long simulation times.

   So, to circumvent this problem, the evaporation and the condensation models had to be turned off and was assumed to be non-existent to simplify the simulations.

4.2.3 Validity of the results

The problems associated with using simulation tools is that despite the results appearing impressive, it may not be physically valid. In other words, the behaviour appearing to be right but is in violation of the physical laws that govern the behaviour of said body in reality. Therefore, there is a need for the results from the simulation to be validated to

ensure that the model constructed by assuming valid assumptions are in fact producing tangible results that can be used in optimizing real world components.

This is done experimentally. It is impractical to optimize a certain phenomenon when one does not know the effect of the parameters set up for the experiments for said phenomenon. The drawbacks of studying the impact of the parameters in a working fuel cell with current generation of observational technology has already been discussed. In addition to this, it is uneconomical and time consuming to construct a set up every single time to study the variations of each factor and interactions between multiple factors. Therefore, the only pathway to validate the results is to compare it with the theory of the phenomenon based on observed physical laws. This grounds the results from the simulation in reality and therefore, can lead to further iterations of simulations with increasingly complex sub-models to build on the base models when the results obtained from the latter are in line with the theory. It would be wasteful to build models with additive complexity when the simple models are not in accordance with the physical laws.

The validity of the results from the simulations performed would be compared to the theoretical behaviour and assessed. The results from each of the factors investigated will be cross-checked with the theory to validate the findings from the said simulations. If the results are found to be valid, this can lead to the employment of complex sub models to assess each and every sub factor of the studied factors to further research avenues for optimization. If the results are not valid, then the model criteria would be re-evaluated to identify the source of the discrepancy and employ corrective measures if possible. If no corrective measures can be employed, then that also provides a starting point to research methodologies and techniques to minimize the discrepancy.

The results of the individual factor focus simulations has been assessed against the working theory as follows:

1. **Air Inlet Velocity:** As from the results of the standard deviation (ϕ) assessment (see Table 15) it can be seen that this factor is the most prominent parameter that drives the water transport behaviour. The water flow velocity was heavily dependent on the air inlet velocity, since the water inlet velocity is kept constant, owing to the fixed mass transport rates, the amount of water flowing through the domain is dependent on the force from the air pushing the droplet.

   The results from simulation 1 show this phenomenon exactly and therefore is in obvious agreement with the laws of momentum - Higher the driving force, faster the droplet of certain mass moves, or larger the quantity of water can be moved at the same velocity.

2. **Number of pores:** The mass flow rate of the water entering the domain is constant, so with an increase in number of pores which implies an increase in the area of the inlet, the velocity of the water at the inlet is lesser, This means that there is a heavier dependence of the air pushing the water droplets than when the water droplets have their own innate momentum from the inlet velocity. This means that the total momentum acting on the droplet is reduced with the air flow driving the momentum. So, the lesser the inlet water flow, lesser the total momentum. Therefore, the water droplets would move across the channel slower (see Figure 32).

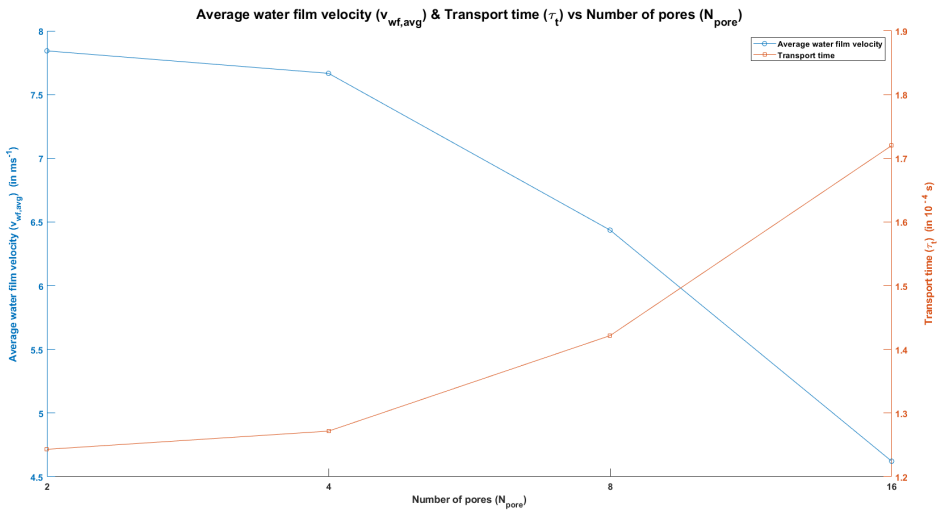

Figure 32: Plot of Average water film velocity and Transport time v Pore number

In addition to the slower velocities with increase in pore number (N_{pore}), the tendency to form droplets also increases since the droplets do not have innate momentum in the domains with higher pore numbers, the air flow tends to drag away the water droplets with the surface tension acting in the opposite direction. This would lead to an instability down the line causing the droplets to breakup easily and also be smaller in size. This physical phenomenon called Rayleigh instability lead to the formation of droplets in the model that required additional correction in the form of transforming the Eulerian phase into Lagrangian particles as the mesh was not fine enough to resolve the small size particles without causing smearing.

The need for this extra correction would indicate that the model is functioning as per the physical laws and producing small sized droplets that would need additional models to capture accurately.

3. **Pore radius:** This factor also as seen previously is dependent on the size of the inlet air, and subsequently the water inlet velocity. However, the reduction in the water inlet velocity is not as severe as compared to the simulation with varying pore size. This is reflected in the average water film velocity that can be seen in Figure 31, where the film velocities of both the groups of simulations can be observed. Since, the water inlet velocity and subsequently, the average water film velocity of the pore size simulations is higher than the pore number simulations, the droplet formation phenomenon is less pronounced and therefore, does not necessitate the use of Lagrangian Particle Tracking (LPT).

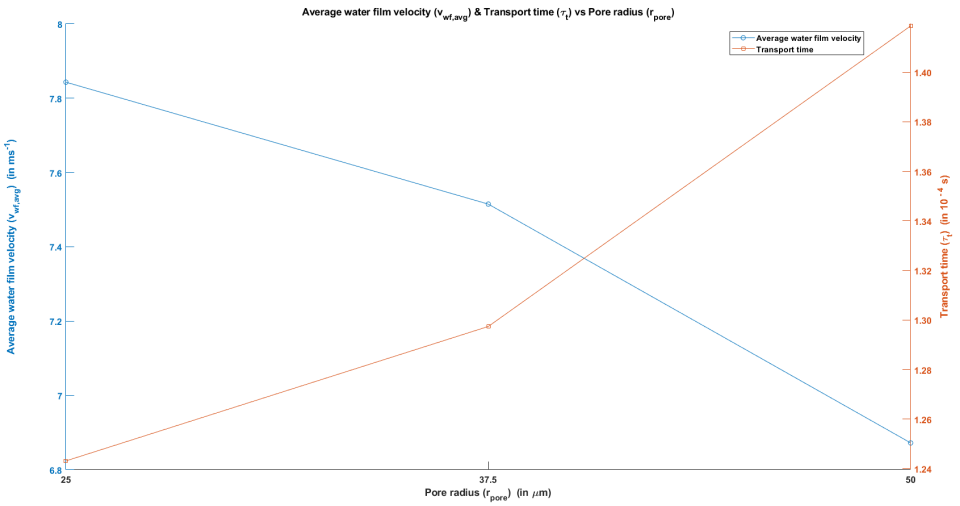

Figure 33: Plot of Average water film velocity and Transport time v Pore radius

Since there is no requirement of utilizing the LPT models, this shows that the base model does not create any untoward discrepancy in simulating the reduction in the film velocity. The model still obeys the physical laws - decrease in water film velocity with increase in pore radius (see Figure 33) and captures the droplet formation behaviour of the larger pore size accurately.

4. **Relative Humidity:** The simulation for the assessment of the impact of humidity on the water transfer rates requires a deviation from the base simulation models assessed so far. Since the gas phase contains an additional phase - water vapour in addition to the dry air, the increase in the number of phase interactions warrants the use of additional models to capture all the interactions accurately.

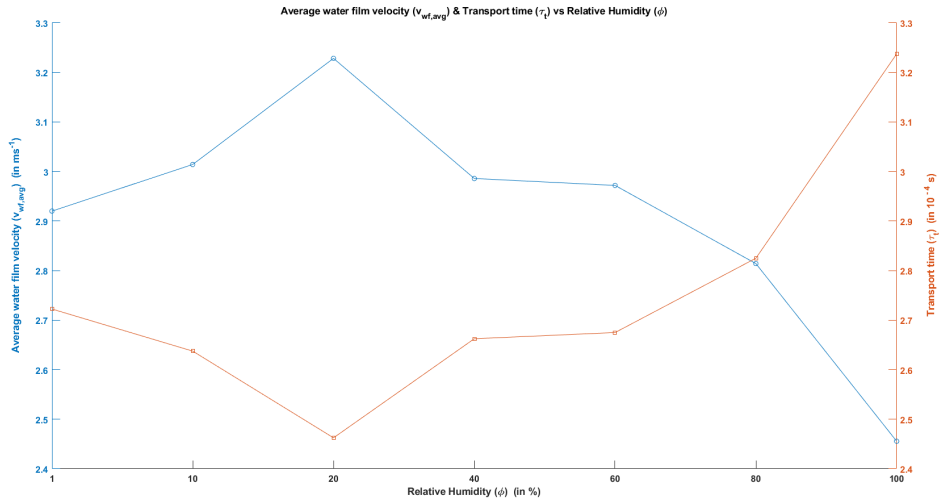

Figure 34: Plot of Average water film velocity and Transport time v Relative Humidity

The reduction in the average water film velocity with the increase in relative humidity is due to the drop in momentum of the gas phase. This is due to the drop in

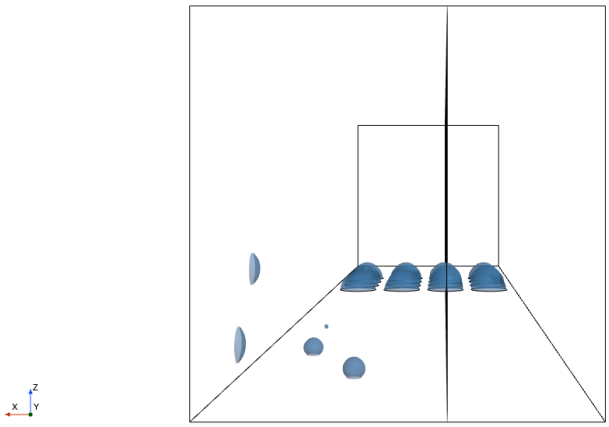

Figure 35: Droplet profile on both hydrophilic (CW) and hydrophobic (GDL) surfaces

the density of the gas phase due to increase in humidity - as the molecular weight of water molecules is lower than the molecular weight of air (18 g/mol compared to 29 g/mol), this results in a smaller force pushing the water droplets across the surface. In addition to this drop in density, the coalescence of droplets and condensation effects at the higher operating temperature lead to an increase in viscosity and drag force on the droplet further reducing the velocity with which it travels across the domain. This has been validated (see Figures 34 and 31) by the simulation models thereby proving the accuracy of the results obtained.

5. **Wall Roughness:** The results from this simulation with higher velocity of the water film ($v_{(wf,avg)smooth} = 8.163265\ ms^{-1}$) when the walls are smooth compared to when the walls are rough ($v_{(wf,avg)rough} = 7.843137\ ms^{-1}$) is straightforward enough to indicate the resistance of the rough surface to the flow of water droplets. The model captures this phenomenon with sufficient accuracy. The idealistic case of the smooth walls maybe favourable to producing higher velocities, however, in reality, this is not possible due to the nature of the materials used for the construction of the channel walls and the gas diffusion layer (GDL).

   However, the model accurately captures the effect of the roughness of the droplet velocity across the flow channels.

6. **Static Contact Angles:** The impact of the static contact angle (θ_C) on the behaviour of the droplet is primarily restricted to the amount of area covered by the droplet due to its profile that is derived on the basis of the static contact angle the droplet forms with the surface it is flowing on. The droplet occupies a minimal surface area on a hydrophobic surface due to the repelling nature of the material, and occupies a larger surface area on a hydrophilic surface. This has been accurately captured by all the models in several instances (see Figures 30 and 35).

   The effect of this phenomenon plays a role in the amount of area occupied by the droplet on the GDL surface as the existing water droplet would provide an obstruction to the air and the water that would emerge out of the pores present on a working GDL. This is the reason why the GDL is preferred to be hydrophobic

and since the water droplets have to be moved off the GDL as soon as possible, the channel walls are made to be hydrophilic to assist this transference.

The droplet profile in the simulation matches with the theoretical profile of the water droplets (see Figure 12) proving the validity of the contact angle models in the simulations used.

So, to **summarize**, the results obtained from the simulation models have been in complete accordance with the theory of the phenomenon, and the important factors that impact the water behaviour of the system have been captured with sufficient accuracy proving the validity of both the simulation models and the assumptions undertaken to simplify the design complexities.

4.2.4 Future Work

As previously discussed, the importance of managing the water levels in the fuel cell cannot be understated. The PEM fuel cell functions on the conductivity of the ions of the electrolyte membrane and this is directly dependent on how hydrated the electrolyte membrane is. To state plainly, the water levels are a make or break criteria affecting the performance of the fuel cell. In addition to this, the complex movement mechanisms across the fuel cell as seen in Figure 7 hints towards the complexities involved in managing the ideal water levels across the entire fuel cell stack. The stack cannot get flooded as this would cause mechanical stresses and affects the structural integrity of the fuel cell. Cannot dry out as this would reduce the current density of the fuel cell stack. The water cannot flow backwards as this would create resistance to the flow of the ions across the electrolyte. These requirements make it tricky to find a balance, which in turn is necessary for optimization of the water management problem.

It is impossible to find balance, therefore, the optimum, if the factors that affect the water flow rates are unknown. If the behaviour of the water flowing through the channel configurations is unknown. So, therefore, the complexities, the minutiae of the behaviour of the water droplets across the channel flow must be studied with precision to identify all of the underlying factors critical to the water flow behaviour.

So, this primary objective to identify the most important factors affecting the water flow has been investigated in this study and a deeper understanding regarding the physics governing the droplet behaviour was obtained.

The top factors influencing the water transport the most and the ones that would provide the most significant improvement to the cell performance on optimization have been identified. It has been found that (in order of significance) the air inlet velocity, the pore geometry - both the pore radius and the number of pores and the humidity of the air flowing through the domain were the main driving parameters that affected the major aspects of water behaviour across the domain.

Now that the main factors have been identified, this would provide a good starting point to continue work on further understanding the behaviour based on these influences and identify the pathway for the most significant improvement in cell performance.

As with any modelling, the assumptions undertaken to simplify the problem - therefore causing an inevitable loss of information strongly determine the accuracy of the results. The simplifications made due to the assumptions undertaken in this thesis study were

valid. But, they were restricted on the basis of the available computational resources and simulation times.

In future work, the simplifications made , especially in order to simplify the effects of humidity, electro-chemistry and operating temperature across a larger and more complex domain would bridge the gap between the model and the working fuel cell to a large extent.

The influence of evaporation and condensation effects on the water droplets due to the presence of humidity determined by the stoichiometric requirements would be a good starting point to start modelling from.

Then, a thermal study of the air and the water droplets across the elaborate serpentine channel configuration could be studied to identify potential hot zones and velocity dead zones that could be improved on.

The electro-chemistry aspect, the effect of changes in the oxygen reaction rates leading to inclusion of oxygen production from the pore inlets could also be incorporated to identify the interactions between the oxygen produced from the GDL with the water vapour and air mixture and see how that affects the droplet emergence would be very interesting to simulate and observe.

In short, the future work would require minimizing the number of assumptions taken in modelling the problem.

5 Conclusions

The summary of the entire thesis report can be split into the factors that were investigated to quantify their impact on the water transport rates for ease of concluding. They have been presented as follows:

1. **Air Inlet velocity (v_a):** The importance of the velocity with which the air flows into the channel domain and pushes the water droplets across said domain **cannot be understated**. This along with the water inlet velocity (v_w) are the sources of the momentum which induce the motion of the water droplets across the domain. So, it is not surprising that the average velocity of the water film/droplet ($v_{wf,avg}$) is highly dependent on the velocity of the air supplied at the inlet. Since, the air velocity at the inlet can be easily adjusted, this control extends to the velocity with the water droplet can move.

2. **Pore geometry - number (N_{pore}) and size (r_{pore}):** The size and the number of pores from which the water phase is introduced into the domain is also one of the key factors that influence the water movement behaviour. The fact that the inlet velocity of the water is dependent on the total area of the pore inlet (conservation of mass flow rate), the water inlet velocity being a source of momentum for the droplet to move. Since, the density of liquid water being three magnitudes higher than the density of air, the velocity of the water film (average) owes its magnitude to the water inlet velocity as well. In addition to this, the pore geometry plays a role in determining the profile of the water droplet after emergence, and also the tendency to form droplets, and also their probability of coalescence. These behavioral phenomenon significantly influence the water mass flow rates.

   Despite the overwhelming influence of pore geometry, it is one of the factors that is the most difficult to control. The randomness of the pore location, size and number in a working GDL warrants extensive study into designing materials with better pore geometry that is required for optimum water transport.

3. **Operating conditions - Relative Humidity (ϕ):** The level of humidity of the incoming air is not just important but also a determining factor affecting the velocity of the water droplets. The inlet air momentum being one of the sources behind the motion of the water droplet, as previously mentioned is dependent on the density of the gas. On humidification, the density reduces due to lower molecular weight of the water vapour. This, reduces the average molecular weight of the gas phase, causing a drop in the momentum behind the water droplet movement. If the water inlet velocity is also lowered, as is the case with large pore area (16 pore case), the average water film velocity is drastically reduced.

   We know that the number and pores size of the GDL layer in a working cell cannot be controlled without significant overhaul in material properties. However, the relative humidity of the inlet air can be controlled by calculating the exact of water that is required to be added at the operating temperatures of the fuel cell stack, adding to the repertoire of the factors that can be optimized for better water transport conditions.

4. **Material conditions - Wall surface roughness and Static Contact Angles (θ_C):** It is obvious that rougher the walls, the more friction involved in opposing the motion of

the droplet across the surface. In addition to this, the static contact angle also affects the velocity of the droplet by either repelling or holding onto the water droplet as it moves across the surface. However, the hydrophilic and the hydrophobic nature of the wall material plays a lesser role compared to the wall roughness.

But, out of these two factors, the wall roughness cannot be adjusted as easily as the static contact angles of the domain walls. The roughness depends on the properties of the material, which unfortunately, cannot be controlled without extensive testing of available materials to find an optimized material. However, the level of hydrophobicity or the hydrophilicity of the material can be controlled with the addition of coatings to the surface. The angles can be confirmed with the use of microscopes and can be varied based on the strength of the coatings. However, the effect of the coatings on the electrochemical reaction rates and water emergence would need to be studied.

So, to reiterate, the factors that affect the water transport rates **and** can be controlled **without** drastic changes are the air inlet velocity (v_a), the relative humidity (ϕ), and the static contact angle (θ_C). Since, the way these factors affect the transport rates is known and are controllable, it becomes easy to calibrate the right amount of water transport rates to maintain uniform and optimal humidity level across the membrane electrolyte and the fuel cell stack.

References

[1] Page 45, Berger, C. *Handbook of fuel cell technology*, (1968).

[2] Figure 1.3, Electrode reactions and charge flow for fuel cell with an acid electrolyte, Page 8, *Fuel Cell Systems Explained*, Third Edition. Andrew L. Dicks and David A. J. Rand. [ISBN: 978-1-118-61352-8].

[3] Figure 4.9, Basic structure of a low-temperature PEMFC with a simple configuration of bipolar plate, Page 82, *Fuel Cell Systems Explained*, Third Edition. Andrew L. Dicks and David A. J. Rand. [ISBN: 978-1-118-61352-8].

[4] Figure 4.3, Chemical structure of polyethylene, Page 72, *Fuel Cell Systems Explained*, Third Edition. Andrew L. Dicks and David A. J. Rand. [ISBN: 978-1-118-61352-8].

[5] Figure 4.4, Chemical structure of PTFE, Page 72, *Fuel Cell Systems Explained*, Third Edition. Andrew L. Dicks and David A. J. Rand. [ISBN: 978-1-118-61352-8].

[6] Figure 4.5, Chemical structure of a sulfonated fluoroethylene, also called 'perfluorosulfonic acid PTFE copolymer', Page 73, *Fuel Cell Systems Explained*, Third Edition. Andrew L. Dicks and David A. J. Rand. [ISBN: 978-1-118-61352-8].

[7] Figure 4.14, Simplified structure of a PEMFC electrode, Page 89, *Fuel Cell Systems Explained*, Third Edition. Andrew L. Dicks and David A. J. Rand. [ISBN: 978-1-118-61352-8].

[8] Figure 4.17, Schematic illustration of the different water movements to, within and from the electrolyte of a PEMFC, Page 93, *Fuel Cell Systems Explained*, Third Edition. Andrew L. Dicks and David A. J. Rand. [ISBN: 978-1-118-61352-8].

[9] Figure 4.24 (a-d) Main flow-field patterns used in PEMFC bipolar plates: (a) pin or grid type, (b) parallel channels, (c) interdigitated, (d) single serpentine channel, Page 111, *Fuel Cell Systems Explained*, Third Edition. Andrew L. Dicks and David A. J. Rand. [ISBN: 978-1-118-61352-8].

[10] VOF Discretization, Page 19, *Multiphase flows Lecture 7 - 2022*, TME160 Multiphase Flow, Chalmers University of Technology, Prof. Srdjan Sasic.

[11] Visualisation of the Courant number and the CFL condition on a computational grid, *Courant number in CFD - IdealSimulations* Available at URL: `https://www.idealsimulations.com/resources/courant-number-cfd/`.

[12] Contact Angle Hysteresis, Page 39, *Multiphase flows Lecture 7 - 2022*, TME160 Multiphase Flow, Chalmers University of Technology, Prof. Srdjan Sasic.

[13] Fig. 9, The contact angle of a liquid with a hydrophobic and a hydrophilic surface, *Electrospinning of Scaffolds from the Polycaprolactone/Polyurethane Composite with Graphene Oxide for Skin Tissue Engineering*, Sadeghianmaryan, A., Karimi, Y., Naghieh, S. et al., Applied Biochem Biotechnology (191), 567–578 (2020), Available at URL: `https://doi.org/10.1007/s12010-019-03192-x`.

[14] Section 4.2.1, Page 74, *Fuel Cell Systems Explained*, Third Edition. Andrew L. Dicks and David A. J. Rand. [ISBN: 978-1-118-61352-8].

[15] *Numerical simulations of two-phase flow in proton exchange membrane fuel cells using the volume of fluid method - A review*, Rui B. Ferreira, D.S. Falcao, V.B. Oliveira, A.M.F.R. Pinto, J. Power Sources 277 (2015), Pages 329 - 342, Available at URL: https://doi.org/10.1016/j.jpowsour.2014.11.124.

[16] *Water behavior in serpentine micro-channel for proton exchange membrane fuel cell cathode*, P. Quan, B. Zhou, A. Sobiesiak, Z. Liu, J. Power Sources 152 (2005), Pages 131 - 145, Available at URL: https://doi.org/10.1016/j.jpowsour.2005.02.075.

[17] *Liquid water transport in parallel serpentine channels with manifolds on cathode side of a PEM fuel cell stack*, K. Jiao, B. Zhao, P. Quan, J. Power Sources 154 (2006), Pages 124 - 137, Available at URL: https://doi.org/10.1016/j.jpowsour.2005.04.003.

[18] *Liquid water transport in straight micro-parallel-channels with manifolds for PEM fuel cell cathode*, K. Jiao, B. Zhao, P. Quan, J. Power Sources 157 (2006), Pages 226 - 243, Available at URL: https://doi.org/10.1016/j.jpowsour.2005.06.041.

[19] *A numerical study on liquid water exhaust capabilities of flow channels in polymer electrolyte membrane fuel cells*, H.I. Kim, J.H. Nam, D. Shin, T.Y. Chung, Y.G. Kim, CAP 10 (2010), Pages - S91 - S96, Available at URL: https://doi.org/10.1016/j.cap.2009.11.050.

[20] *Effects of hydrophilic/hydrophobic properties on the water behavior in the micro-channels of a proton exchange membrane fuel cell*, Y.H. Cai, J. Hu, H.P. Ma, B.L. Yi, H.M. Zhang, J. Power Sources 161 (2006), Pages 843 - 848, Available at URL: https://doi.org/10.1016/j.jpowsour.2006.04.110.

[21] *Characteristics of droplet and film water motion in the flow channels of polymer electrolyte membrane fuel cells*, Z. Zhan, J. Xiao, M. Pan, R. Yuan, J. Power Sources 160 (2006), Pages 1 - 9, Available at URL: https://doi.org/10.1016/j.jpowsour.2005.12.081.

[22] *Numerical study of water management in the air flow channel of a PEM fuel cell cathode*, P. Quan, M.C. Lai, J. Fuel Cell Science Technology 7 (2010), Pages 0110171 - 01101714, Available at URL: https://doi.org/10.1016/j.jpowsour.2006.09.110.

[23] *Dynamics of water droplets detached from porous surfaces of relevance to PEM fuel cells*, A. Theodorakakos, T. Ous, M. Gavaises, J. Nouri, N. Nikolopoulos, H. Yanagihara, J. Colloid INterface Sci. 300 (2006), Pages 673 - 687, Available at URL: https://doi.org/10.1016/j.jcis.2006.04.021.

[24] *Dynamic water transport and droplet emergence in PEMFC gas diffusion layers*, A. Bazylak, D. Sinton, N. Djilali, J. Power Sources 176 (2008), Pages 240 - 246, Available at URL: https://doi.org/10.1016/j.jpowsour.2007.10.066.

[25] *3-D numerical simulation of contact angle hysteresis for microscale two phase flow*, C. Fang, C. Hidrovo, F. Wang, J. Eaton, K. Goodson, Int. J. Multiph. Flow 34 (2008), Pages 690 - 705, Available at URL: https://doi.org/10.1016/j.ijmultiphaseflow.2007.08.008.

[26] *Multiphase flow model to study channel flow dynamics of PEM fuel cells: deformation and detachment of water droplets*, A. Golpaygan, N. Ashgriz, Int. J. Comput. Fluid D. 22 (2008), Pages 85 - 95, Available at URL: https://doi.org/10.1080/10618560701733707.

[27] *Effects of hydrophilic/hydrophobic properties on the water behavior in the microchannels of a proton exchange membrane fuel cell*, A. Golpaygan, N. Ashgriz, Int. J. Energy Res. 29 (2005), Pages 1027 - 1040, Available at URL: https://doi.org/10.1016/j.jpowsour.2006.04.110.

[28] *Three-dimensional multiphase flow model to study channel flow dynamics of PEM fuel cells*, A. Golpaygan, A. Sarchami, N. Ashgriz, Int. J. Energy Res. 35 (2011), Pages 118 - 1199, Available at URL: https://doi.org/10.1002/er.1775.

[29] *Deformation of a droplet in a channel flow*, E. Shirani, S. Masoomi, J. Fuel Cell Sci. Technol. 5 (2008), 041008, Available at URL: https://doi.org/10.1115/1.2930774.

[30] *2-D VOF numerical study on the two-phase flow*, X. Zhu, P. Sui, N. Djilali, Microfluid. Nanofluid. 4 (2007), Pages 543 - 555, Available at URL: http://refhub.elsevier.com/S0378-7753(14)01981-8/sref54.

[31] *Dynamic behaviour of liquid water emerging from a GDL pore into a PEMFC gas flow channel*, X. Zhu, P. Sui, N. Djilali, J. Power Sources 172 (2007), Pages 287 - 295, Available at URL: https://doi.org/10.1016/j.jpowsour.2007.07.024.

[32] *Three-dimensional numerical simulations of water droplet dynamics in a PEMFC gas channel*, X. Zhu, P. Sui, N. Djilali, J. Power Sources 181 (2008), Pages 101 - 115, Available at URL: https://doi.org/10.1016/j.jpowsour.2008.03.005.

[33] *Numerical investigation of water droplet dynamics in a low-temperature fuel cell microchannel: Effect of channel geometry*, X. Zhu, Q. Liao, P.C. Sui, N. Djilali, J. Power Sources 195 (2010), Pages 801 - 812, Available at URL: https://doi.org/10.1016/j.jpowsour.2009.08.021.

[34] *Three-dimensional simulation of water droplet movement in PEM fuel cell flow channels with hydrophilic surfaces*, B. Mondal, K. Jiao, X. Li, Int. J. Energy Res. 35 (2011), Pages 1200 - 1212, Available at URL: https://doi.org/10.1002/er.1776.

[35] *Effect of Channel Walls on droplet removal time*, K.A. Raman, B. Mondal, X. Li, Int. J. Adv. Therm. Sci. Eng. 2 (2011), Pages 27 - 33, Available at URL: http://refhub.elsevier.com/S0378-7753(14)01981-8/sref78.

[36] *Analysis of inter-droplet interaction in a PEM fuel cell cathode channel*, H. Kim, S. Jeon, M. Song, K. Kim, J. Power Sources 246 (2013), Pages 679 - 695, Available at URL: http://refhub.elsevier.com/S0378-7753(14)01981-8/sref95.

[37] Sections 4.4.2 - 4.4.5, Pages 94 - 102,*Fuel Cell Systems Explained*, Third Edition. Andrew L. Dicks and David A. J. Rand. [ISBN: 978-1-118-61352-8].

[38] Section 3.3, Page 46, *Fuel Cell Systems Explained*, Third Edition. Andrew L. Dicks and David A. J. Rand. [ISBN: 978-1-118-61352-8].

[39] *Effect of Gas Diffusion Layer Deformation on Liquid Water Transport in Proton Exchange Membrane Fuel Cell*, N. Bao, Y. Zhou, K. Jiao, Y. Yin, Q. Du, J. Chen, Eng. Appl. Comp. Fluid 8 (2014), Pages 26 - 43, Available at URL: https://doi.org/10.1080/19942060.2014.11015495.

[40] *Effect of air flow on liquid water transport through a hydrophobic gas diffusion layer of a polymer electrolyte membrane fuel cell*, P.V. Suresh, S. Jayanti, Int. J. Hydrog.

Energy 35 (2010), Pages 6872 - 6886, Available at URL: https://doi.org/10.1016/j.ijhydene.2010.04.052.

[41] *Three-dimensional numerical simulation of water droplet emerging from a gas diffusion layer surface in micro-channels*, Y. Ding, H. Bi, D. Wilkinson, J. Power Sources 195 (2010), Pages 7278 - 7288, Available at URL: https://doi.org/10.1016/j.jpowsour.2010.05.059.

[42] *GasLiquid Two-Phase Flow in Minichannels with Liquid Side Introduction*, W. Du, L. Zhang, X.T. Bi, D.P. Wilkinson, J. Stumper, H. Wang, Ind. Eng. Chem. Res. 49 (2010), Pages 6709 - 6721, Available at URL: https://doi.org/10.1021/ie901120n.

[43] *Water dynamics inside a cathode channel of a polymer electrolyte membrane fuel cell*, M. Hossain, S.Z. Islam, A. Colley-Davies, E. Adom, Renew. Energ. 50 (2013), Pages 763 - 779, Available at URL: https://doi.org/10.1016/j.renene.2012.08.041.

[44] *The effect of wall roughness on the liquid removal in micro-channels related to a proton exchange membrane fuel cell(PEMFC)*, G. He, Y. Yamazaki, A. Abudula, J. Power Sources 195 (2010), Pages 1561 - 1568, Available at URL: https://doi.org/10.1016/j.jpowsour.2009.09.052.

[45] *Effects of Roughness of Gas Diffusion Layer Surface on Liquid Water Transport in Micro Gas Channels of a Proton Exchange Membrane Fuel Cell*, L. Chen, H. Luan, Y. He, W. Tao, Numer. Heat. A-Appl. 62 (2012), Pages 295 - 318, Available at URL: https://doi.org/10.1080/10407782.2012.670586.

[46] *Effects of surface microstructures of gas diffusion layer on water droplet dynamic behaviors in a micro gas channel of proton exchange membrane fuel cells*, L. Chen, Y. He, W. Tao, Int. J. Heat. Mass Transf. 60 (2013), Pages 252 - 262, Available at URL: https://doi.org/10.1016/j.ijheatmasstransfer.2012.11.024.

[47] *A general model of proton exchange membrane fuel cell*, A.D. Le, B. Zhou, J. Power Sources 182 (2008), Pages 197 - 222, Available at URL: https://doi.org/10.1016/j.jpowsour.2008.03.047.

[48] *A generalized numerical model for liquid water in a proton exchange membrane fuel cell with interdigitated design*, A.D. Le, B. Zhou, J. Power Sources 193 (2009), Pages 665 - 683, Available at URL: https://doi.org/10.1016/j.jpowsour.2009.04.011.

[49] *Fundamental understanding of liquid water effects on the performance of a PEMFC with serpentine-parallel channels*, A.D. Le, B. Zhou, Electrochim. Acta 54 (2009), Pages 2137 - 2154, Available at URL: https://doi.org/10.1016/j.electacta.2008.10.029.

The materials used for reference in understanding the theoretical concepts and writing this report are as follows:

1. *Fuel Cell Systems Explained*, Third Edition. Andrew L. Dicks and David A. J. Rand. [ISBN: 978-1-118-61352-8].
2. *Multiphase flows Lecture 7 - 2022*, TME160 Multiphase Flow, Chalmers University of Technology, Prof. Srdjan Sasic.
3. *Simcenter STAR-CCM+ Documentation*, Version 2302, Siemens Digital Industries Software (2023).

I, Charan Kamal Vedula, hereby declare that this thesis report is the product of my own work and have referenced the sources of information to the best of my ability. I apologize for any unintentional discrepancies present and inconvenience caused.